AN INVESTIGATION OF AKR1B1 AND AKR1B10 IN GASTROINTESTINAL CANCERS

A THESIS SUBMITTED TO
THE GRADUATE SCHOOL OF NATURAL AND APPLIED SCIENCES
OF
MIDDLE EAST TECHNICAL UNIVERSITY

BY

ESİN GÜLCE SEZA

IN PARTIAL FULFILLMENT OF THE REQUIREMENTS
FOR
THE DEGREE OF DOCTOR OF PHILOSOPHY
IN
MOLECULAR BIOLOGY AND GENETICS

SEPTEMBER 2023

Approval of the thesis:

AN INVESTIGATION OF AKR1B1 AND AKR1B10 IN GASTROINTESTINAL CANCERS

submitted by **ESİN GÜLCE SEZA** in partial fulfillment of the requirements for the degree of **Doctor of Philosophy** i**n Molecular Biology and Genetics, Middle East Technical University** by,

Prof. Dr. Halil Kalıpçılar
Dean, Graduate School of **Natural and Applied Sciences** _____

Prof. Dr. Mesut Muyan
Head of the Department, **Biological Sciences** _____

Prof. Dr. Sreeparna Banerjee
Supervisor, **Biological Sciences, METU** _____

Examining Committee Members:

Prof. Dr. Nülüfer Tülün Güray
Biological Sciences, METU _____

Prof. Dr. Sreeparna Banerjee
Biological Sciences, METU _____

Prof. Dr. Emirhan Nemutlu
Pharmaceutical Basic Sciences, Hacettepe University _____

Assoc. Prof. Dr. Çağdaş Devrim Son
Biological Sciences, METU _____

Assist. Prof. Dr. Onur Çizmecioğlu
Molecular Biology and Genetics,
İhsan Doğramacı Bilkent University _____

Date: 07.09.2023

I hereby declare that all information in this document has been obtained and presented in accordance with academic rules and ethical conduct. I also declare that, as required by these rules and conduct, I have fully cited and referenced all material and results that are not original to this work.

Name Last name : Esin Gülce Seza

Signature :

ABSTRACT

AN INVESTIGATION OF AKR1B1 AND AKR1B10 IN GASTROINTESTINAL CANCERS

Seza, Esin Gülce
Doctor of Philosophy, Molecular Biology and Genetics
Supervisor: Prof. Dr. Sreeparna Banerjee

September 2023, 137 pages

Aldo-keto reductases (AKRs) are a large family of oxidoreductases that can utilize electrons from NADPH to reduce many substrates. AKR1B1 and AKR1B10 are among the extensively studied human AKRs due to their roles in the polyol pathway and detoxification reactions, respectively.

Our previous research has shown that AKR1B1 and AKR1B10 have diverse effects on colorectal cancer. Using *ex vivo* samples from colon and rectal tumor patients, I have shown that AKR1B1 expression was associated with a stronger mesenchymal phenotype and worse prognosis, while AKR1B10 expression was associated with the activation of metabolic pathways. Next, using hepatocellular carcinoma (HCC) cell lines with differing metabolic characteristics and low endogenous AKR1B10 expression, I aimed to understand the effect of AKR1B10 on metabolic reprogramming. Forced expression of AKR1B10 in the glycolytic cell line SNU423 activated signaling suggesting enhanced fatty acid synthesis and generation of reactive oxygen species. Overexpression of AKR1B10 in the oxidative cell line HuH-7 resulted in low viability and activation of the nutrient

sensor AMPK, especially when glucose and glutamine were withdrawn. Untargeted metabolomics of glucose/glutamine starved AKR1B10 expressing HuH-7 revealed for the first time enhanced gluconeogenesis, most likely for biomass generation and a slower TCA cycle, reflecting poor energetics.

Metabolic reprogramming and activation of invasion and metastasis are considered among the major hallmarks of cancer. Overall, my data suggests that AKRs may play critical roles in enhancing both metastatic spread and deregulated metabolism, providing a mechanistic basis for their association with poor prognosis in gastrointestinal cancers.

Keywords: Colorectal Cancer, Hepatocellular Carcinoma, AKR1B1, AKR1B10

ÖZ

GASTROİNTESTİNAL KANSERLERDE AKR1B1'İN VE AKR1B10'UN İNCELENMESİ

Seza, Esin Gülce
Doktora, Moleküler Biyoloji ve Genetik
Tez Yöneticisi: Prof. Dr. Sreeparna Banerjee

Eylül 2023, 137 sayfa

Aldo-keto redüktazlar (AKR'ler), NADPH'den gelen elektronları kullanarak birçok substratı indirgeyebilen geniş bir oksidoredüktaz ailesidir. AKR1B1 ve AKR1B10, sırasıyla poliol yolundaki ve detoksifikasyon reaksiyonlarındaki rolleri nedeniyle kapsamlı olarak incelenen insan AKR'leri arasındadır.

Önceki çalışmamız, AKR1B1'in ve AKR1B10'un kolorektal kanserde farklı etkilere sahip olduğunu göstermiştir. Bu çalışmada, hastalardan alınan kolon ve rektum kanser örnekleri kullanılarak, AKR1B1 ifadesinin mezenkimal fenotip ve kötü prognoz ile ilişkili olduğu gösterilmiştir. AKR1B10 ifadesinin ise metabolik yolakların aktivasyonu ile ilişkili olduğu gösterilmiştir. Ayrıca birbirinden farklı metabolik özelliklere ve düşük endojen ifadesine sahip hepatosellüler karsinom (HCC) hücre hatları kullanılarak, AKR1B10'un metabolik olarak yeniden programlanma üzerindeki etkisi gözlemlenmiştir. Glikolize bağımlı bir hücre hattı olan SNU423, AKR1B10 ifadesi ile yağ asiti sentez sinyalleri ve reaktif oksijen türlerinde artış göstermiştir. Oksidatif olan HuH-7 hücre hattı ise, AKR1B10 ifadesi ile özellikle glikoz ve glutamin çekildiğinde, hücre ölümü ve besin sensörü

olan AMPK aktivasyonu göstermiştir. AKR1B10 ifadeleyen HuH-7 hücreleri, glikoz ve glutamin açlığında, ilk defa yapılan metabolomiks çalışmasında hücre devamlılığı için olası bir şekilde artan glukoneogenez göstermiştir. Ayrıca zayıf enerji durumunun bir göstergesi olarak yavaş bir trikarboksilik asit döngüsü göstermiştir.

Metabolik olarak yeniden programlama ve invazyon ile metastazın aktivasyonu kanserin başlıca özellikleri arasında nitelendirilmiştir. Genel olarak bu veriler, AKR'lerin hem metastatik yayılım artışında hem de metabolik yolakların düzensizleşmesinde kritik roller üstlenebiliceğini gösterirken, gastrointestinal kanserlerde kötü prognoz ilişkisi için mekanistik bir temel sağlayabilir.

Anahtar Kelimeler: Kolorektal Kanser, Hepatosellüler Karsinom, AKR1B1, AKR1B10

This thesis is dedicated to my beloved family.

ACKNOWLEDGMENTS

First and foremost, I would like to express my deepest gratitude to my esteemed mentor, Prof. Dr. Sreeparna Banerjee. Her unwavering support, invaluable guidance, endless patience, constructive feedback and continuous encouragement have been the cornerstone of my research journey.

I would like to thank my thesis monitoring committee members, Prof. Dr. N. Tülün Güray and Assist. Prof. Dr. Onur Çizmecioğlu, for their kind and valuable contributions to my thesis. I would like to thank jury members Prof. Dr. Emirhan Nemutlu and Assoc. Prof. Dr. Çağdaş Devrim Son for their contributions to my thesis.

I am also indebted to Dr. Seçil Demirkol Canlı, Prof. Dr. Ali Osmay Güre, Prof. Dr. Emirhan Nemutlu and Dr. Cemil Can Eylem for their collaboration in this work.

I extend my heartfelt appreciation to Prof. Dr. Mesut Muyan for his endless support and generous sharing of his profound scientific insights and experiences during my Ph.D. journey.

My whole life has been enriched by the enduring legacy of Mustafa Kemal Atatürk. His ideals of secularism, democracy and revolutionism have always inspired me as a proud woman scientist and I am deeply indebted to his visionary leadership of this 100-year-old Republic.

I extend my gratitude to my colleagues, referred to as the “Downstair Zombies” for their ever-present willingness to assist and support. I also wish to express my appreciation to Alexandra Elbakyan for her commitment to open science.

To the Lab B-59 family, both past and present members, your support is invaluable. I would like to extend my thanks to Dr. Melis Çolakoğlu Ülgen for her humor and friendship, Burak C. Kızıl for bridging the distance no matter how with

our video calls, Sinem Ulusan for her cheerful jokes, Aydan Torun for her kindness and unwavering support and the “Nutrient Restriction” team. Dr. Hepşen Hazal Hüsnügil’s calming presence, Dr. Aliye Ezgi Güleç’s culinary talents, Göksu Oral’s sense of fun, Nazlı Şevval Menemenli’s exceptional kindness and İrem Yücel’s genuine friendship have brought immeasurable joy to the lab.

I would like to thank the incredible “The AKR Team” members for being a constant source of companionship and laughter during the most challenging times. Adventurous spirit Çağdaş Ermiş, kind heart İsmail Güderer, wonderful friend Hoşnaz Tuğral and Nutella lover Nisan Korkmaz have collectively made for an incredible journey throughout the years.

I offer my sincerest gratitude to all those who have contributed to my academic and personal growth. B. Kağan Yıldız, thank you for being there and listening every single day; your friendship has been invaluable.

Efe Boyacıgiller, your love and constant belief in my abilities, even during the most demanding times, gave me the strength to pursue. Your endless patience has been a constant source of support.

I am deeply thankful to my family. Hasan and Sevda Seza, your love, patience, support, sacrifices and encouragement have shaped me into the I am today. It was truly impossible to achieve this degree without your unwavering presence in my life.

This work is partially funded by the Scientific and Technological Research Council of Turkey (TÜBİTAK) as a part of the COST action CA17118 under grant numbers TUBİTAK 118Z688 and 219Z213, by METU Scientific Research Projects Coordination Unit (BAP) number ÇDAP-108-2020-10197, GAP-108-2023-11067 and TEZ-D-108-2023-11069. I would like to thank YÖK for the financial support from the 100/2000 PhD scholarship.

TABLE OF CONTENTS

LIST OF TABLES

TABLES

LIST OF FIGURES

FIGURES

LIST OF ABBREVIATIONS

ABBREVIATIONS

AKR	Aldo-Keto Reductase
CRC	Colorectal Cancer
HCC	Hepatocellular Carcinoma
PPP	Pentose Phosphate Pathway
EMT	Epithelial to Mesenchymal Transition
TCA	Tricarboxylic Acid
FAS	Fatty Acid Synthesis
FAO	Fatty Acid Oxidation
ROS	Reactive Oxygen Species
AMPK	AMP-Activated Protein Kinase
mTOR	Mammalian Target of Rapamycin
NAD(P)H	Nicotinamide adenine dinucleotide phosphate
NAD(H)	Nicotinamide adenine dinucleotide
OXPHOS	Oxidative Phosphorylation

CHAPTER 1

INTRODUCTION

1.1 Aldo-Keto Reductases (AKRs)

Aldo-keto reductases (AKRs) are a superfamily of enzymes that catalyze an extensive range of oxidation-reduction reactions. They are mainly cytosolic, monomeric (34-37 kDa), nicotinamide adenine dinucleotide phosphate (NADPH) dependent oxidoreductases and are involved in many critical metabolic events in health and disease (Penning, 2015). AKRs are grouped into 16 families and named AKR1 to AKR16 in various species of prokaryotes to animals. Around 200 members were identified as sharing similar three-dimensional structures (Penning, 2015; AKR website https://akrsuperfamily.org/). The AKRs are classified according to sequence similarity, common protein fold, and highly conserved a (β/α) 8-barrel presence with a highly similar sequence of pyridine nucleotide-binding site (Mindnich & Penning, 2009). They can reduce aldehydes and ketones (carbonyl groups) to their corresponding primary and secondary alcohols and common substrates include sugar aldehydes (e.g., glucose), reactive lipid aldehydes, prostaglandins, ketosteroids, xenobiotics, chemical carcinogens, carcinogen metabolites, and aflatoxin aldehyde (Penning & Drury, 2007).

The nomenclature system of AKRs starts with the family name and continues with the subfamily (Jez et al., 1997). Next, the Arabic numeral represents the family and a letter indicates the subfamily when the subfamily exists (e.g., AKR**1A**). The last Arabic number designates the unique protein structures changing their substrates and kinetics (e.g., AKR1A**1**). In other words, the enzyme AKR1A1 is a human aldehyde reductase indicating AKR in family 1, subfamily A and unique protein

number 1. A broad overview of AKR superfamily members is available at the website: https://akrsuperfamily.org/.

There are 15 defined human AKRs (Penning, 2015) listed as AKR1A1 (aldehyde reductase), AKR1B family members AKR1B1 (aldose reductase), AKR1B10 (small intestine reductase) and AKR1B15 (3-Keto-acyl CoA reductase), AKR1C1–C4 (hydroxysteroid dehydrogenases), AKR1D1 (steroid 5β-reductase), AKR1E2 (1,5-Andyro-D-fructose reductase), AKR6 family (Potassium voltage-gated channel) AKR6A3 (β subunit 1), AKR6A5 (β subunit 2) and AKR6A9 (β subunit 3) and the AKR7 family (AKR7A2 and AKR7A3 aflatoxin aldehyde reductases).

The human AKRs are involved in a wide range of metabolic reactions, including different substrates such as glucose, ketosteroids, lipid aldehydes, xenobiotics, prostaglandins and carcinogens or their derivatives (Banerjee, 2021; W. D. Chen & Zhang, 2012; Penning, 2015). Aberrant activation of these proteins has been implicated in the pathogenesis of several inflammatory human diseases (W. D. Chen & Zhang, 2012). The AKR1B and AKR1C family members have been strongly implicated in cancer (Banerjee, 2021). Several studies have shown that AKR1B10 and AKR1C family members were associated with tobacco-induced carcinogenesis (Hsu et al., 2001; Penning, 2005; L. Zhang et al., 2008). In addition, AKR1B1 has been implicated in retinopathy, neuropathy and nephropathy (diabetic complications), sepsis and colon cancer (Penning, 2015; Ramana, 2011). Mutations in AKR1D1 have been linked to liver failure in a pediatric population (Lemonde et al., 2003). In contrast, AKR7A is associated with enhanced hepatocellular antioxidant defense and protection against acetaminophen-induced hepatoxicity (M. M. E. Ahmed et al., 2011). Human AKRs' contribution to various diseases and understanding the underlying mechanism may help develop novel therapeutic strategies.

1.2 AKRs and Oxidative Stress

NRF2 (nuclear factor erythroid-related factor), the Cap'n'Collar basic leucine zipper transcription factor, is a crucial transcription factor mediating protection against oxidants (Kovac et al., 2015). NRF2 allows cells to survive short exposure to electrophilic, oxidative, and inflammatory stress (Macleod et al., 2016). A cytosolic protein kelch-like ECH-associates protein 1 (KEAP1) primarily provides the activity of NRF2. KEAP1 targets NRF2 as a homodimeric substrate adaptor that recruits the Cullin3/Ring-box-1 (CUL3/RBX1) E3 ubiquitin ligase. Under homeostatic conditions, KEAP-1 binds tightly to NRF2 proteins. In the presence of oxidative stress, cysteine residues in KEAP1 are oxidized and form adducts with stress molecules (Penning, 2017). This event allows free or newly transcribed NRF2 to evade KEAP1-mediated ubiquitination, allowing it to translocate to the nucleus and start gene expression (Kovac et al., 2015). Translocated NRF2 activates the antioxidant response element (ARE), including genes responsible for xenobiotic detoxification, such as NQO1 (NADPH Quinone Dehydrogenase 1), SOD1 (Superoxide Dismutase 1), CAT (Catalase) and HMOX (Heme Oxygenase). Of note, AKR1B1, AKR1B10, AKR1C1-3 and AKR7A2/3 are all regulated by KEAP1/NRF2 system and have ARE elements in their promoters (Penning, 2017). AKRs are Phase I drug metabolism enzymes implicated in the detoxification of chemotherapeutic drugs (Penning & Drury, 2007). Upregulation of AKRs by NRF2 decreases cellular toxicity. AKR1C family especially helps in the survival of cells from toxicity and can affect the efficacy of many drugs, such as cisplatin, mitomycin, and doxorubicin (Penning, 2017).

1.3 AKR1B1

AKR1B1 (aldose reductase) is one of the most studied human AKRs (W. D. Chen & Zhang, 2012) and is a rate-limiting enzyme in the polyol pathway **(Figure 1.1)**, catalyzing the conversion of excess glucose to sorbitol. In healthy cells, the enzyme

hexokinase phosphorylates glucose as soon as it enters the cell. In the presence of excess glucose (such as in diabetes), the polyol pathway gains importance in removing glucose when hexokinase is saturated. Excess glucose is converted to sorbitol, which cannot cross the cell membrane and the excess sorbitol is converted to fructose by the enzyme sorbitol dehydrogenase (SDH), along with the reduction of NAD to NADH. When the NADH/NAD ratio is high, aberrant reactive oxygen species (ROS) production exceeds the ROS scavenging capacity of the cellular antioxidant systems, such as glutathione and thioredoxin (Korge et al., 2015). Under homeostatic conditions, only less than 3% of the glucose enters the polyol pathway; on the other hand, in hyperglycemia up to 25-30% of the glucose flux may occur through the polyol pathway (Ramana, 2011).

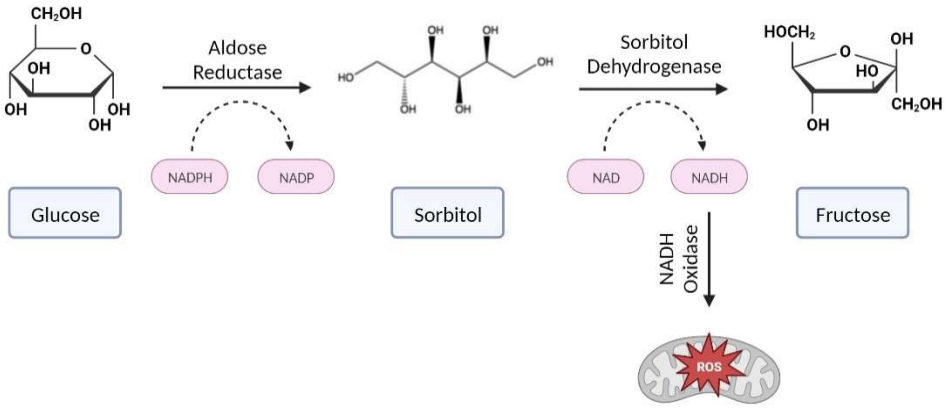

Figure 1.1 The Polyol Pathway showing the conversion of glucose to sorbitol and then to fructose.

The figure was created by BioRender and adapted from Banerjee, 2021. ROS: Reactive Oxygen Species.

AKR1B1 is expressed in most human tissues, and its aberrant expression has become a research interest in many inflammatory diseases such as diabetes, cataractogenesis, retinopathy and nephropathy, atherosclerosis, sepsis, uveitis and asthma (Penning, 2015; Ramana, 2011; Srivastava et al., 2011). Aldose reductase

inhibitors have been reported to reduce inflammation in several diseases (Srivastava et al., 2011). In animal cancer models, chemical inhibition of AKR1B1 showed significant mitigation of the disease (Srivastava et al., 2011).

A pan-cancer AKR1B1 mRNA expression analysis in 20 different cancer types from RNA sequencing data of cancer and matched normal tissue from The Cancer Genome Atlas (TCGA) showed that AKR1B1 is broadly expressed in human cancers. The AKR1B1 expression was upregulated in BLCA (bladder urothelial carcinoma), KIRP (kidney renal papillary cell carcinoma) and CHOL (cholangiocarcinoma) compared to the matched normal tissue expression. (Banerjee, 2021). In addition, the expression of AKR1B1 was significantly downregulated in breast invasive carcinoma (BRCA), cervical squamous cell carcinoma (CESC), pancreatic adenocarcinoma (PAAD), prostate adenocarcinoma (PRAD), pheochromocytoma and paraganglioma (PCPG), colon adenocarcinoma (COAD) and rectal adenocarcinoma (READ) compared to normal tissues (Banerjee, 2021).

Several studies have pointed out the role of AKR1B1 in colon carcinogenesis. *In vitro* and *in vivo* RNA interference (RNAi) and chemical AKR inhibitor studies with drugs such as Sorbinil or Fiderestat showed decreased cell proliferation or colonic polyp formation via the inhibition of mitogenic signaling as well as growth factor and cytokine-induced cancer cell growth (Ramana et al., 2010; Saxena et al., 2013; Tammali et al., 2011). Moreover, chemical inhibition of aldose reductases in SW480, HCT-116, and HT-29 colon cancer cell lines prevented tumor growth in nude mice xenografts by inhibiting G1-S transition in the cell cycle (Ramana et al., 2010). Interestingly, one study showed higher AKR1B1 expression in the cells that were classified as mesenchymal in the NCI-60 Human Tumor Cell Lines dataset (Schwab et al., 2018). We have extensively analyzed pathway enrichment from RNA sequencing data of human colon cancers from The Cancer Genome Atlas (TCGA) and publicly available microarray data and observed significant enrichment of gene ontology (GO) terms associated with motility, mesenchymal phenotype and synthesis of extracellular matrix (Demirkol-Canlı et al., 2020). *In*

vitro experiments carried out with colon cancer cell lines silenced for AKR1B1 also confirmed decreased motility in cells expressing low AKR1B1 (Taskoparan et al., 2017).

1.4 Epithelial to Mesenchymal Transition (EMT)

Epithelial to mesenchymal transition (EMT) is an important biological process that transforms polarized epithelial cells that are typically connected to the basal membrane and neighboring cells (**Figure 1.2**). During this transition, the cell undergoes multiple biochemical changes, allowing it to gain mesenchymal characteristics. These changes include loss of cell to cell junction and apical-basal polarity, decreased expression of epithelial markers along with enhanced migratory capacity and invasiveness, resistance to apoptosis and production of extracellular matrix (ECM) components (Lai et al., 2020). During normal embryogenesis and wound healing, the cell gains a mesenchymal phenotype; however, this process is reversible and called mesenchymal-epithelial transition (MET). It is also known that cancer cells may undergo either full EMT where the cells become entirely mesenchymal, or, more commonly, partial EMT where they retain some epithelial properties along with mesenchymal characteristics to gain invasive and metastatic phenotype as a cluster of cells with an invasion front. These cells are also frequently resistant to chemotherapeutics (Chaffer et al., 2016).

The tumor microenvironment affects the phenotype of epithelial cancer cells and initiates the transition process of EMT via the deregulation of Wnt signaling, TGFβ (transforming growth factor-beta) signaling, and Notch signaling pathways (Chaffer et al., 2016). Several studies have revealed that glucose and glutamine intake and cellular metabolism are altered in cancer cells during EMT progression. For example, glucose metabolism is critical for tumor aggressiveness. Glucose uptake, glycolysis flux, mitochondrial dysfunction, and acidity of the tumor environment increase during EMT (Kang et al., 2019). Another study has reported that Snail (SNAI1), a key regulator of EMT, represses phosphofructokinase-1

(PFK-1), a key regulator enzyme in glycolysis, and elevates glucose flux towards the pentose phosphate pathway (Kim et al., 2017).

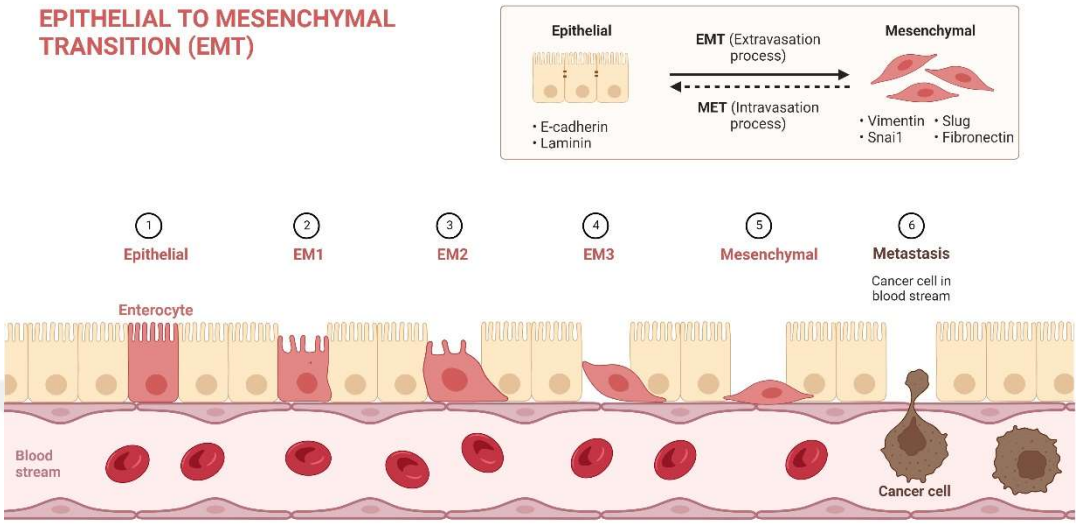

Figure 1.2 Epithelial to mesenchymal transition (EMT) progression in enterocytes.

The figure was created by BioRender by using a template generated by David Camell (creator) and Erin Marshall and adapted by Nieto et al., 2016.

1.5 AKR1B10

AKR1B10, human small intestine aldose reductase, is the second well-defined AKR1B family enzyme. It is mainly expressed in the gastrointestinal tract (colon, small intestine, liver, kidney and gallbladder) and adrenal gland (Chung et al., 2012). Unlike AKR1B1, AKR1B10 is a poor reductant of glucose, xylose and prostaglandin H_2, but it can reduce retinals, isoprenyl aldehydes (farnesal and geranylgeranial) and cytotoxic aldehydes such as acrolein and 4-hydroxy-2nonenal (Matsunaga et al., 2011). In brief, AKR1B10 detoxifies carbonyl compounds, maintains retinoic acid homeostasis, and affects lipid metabolism (Matsunaga et al., 2012).

AKR1B10 was reported to be significantly upregulated in squamous lung cell carcinoma and lung adenocarcinomas associated with tobacco smoking (Fukumoto et al., 2005). An analysis of publicly available data by our group showed that the expression of AKR1B10 was increased at a very early stage in the transformation of liver cells during carcinogenesis, starting from cirrhosis, followed by liver cell dysplasia, and then hepatocellular carcinoma (HCC) (Sheraj et al., 2021). Kaplan-Meier analysis revealed that high AKR1B10-expressing tumors were significantly associated with worse overall survival (OS) in HCC patients (Shi et al., 2019). AKR1B10 has been suggested as a tumor biomarker in several cancer types (W. D. Chen & Zhang, 2012). Thus, silencing of AKR1B10 in HCT-8, an ileocecal colorectal adenocarcinoma cell line, led to less clonogenic growth compared to control cells (Yan et al., 2007). However, the role of AKR1B10 in cancer is controversial. In HCC cells, knockdown of AKR1B10 by shRNA was shown to reduce cellular proliferation and cell cycle arrest (J. Wang et al., 2018). However, we showed that the expression of AKR1B10 in colon cancer cell lines did not affect cancer progression by altering cellular proliferation or cell cycle, while the migration capacity of the AKR1B10-expressing cells was decreased significantly (Taskoparan et al., 2017).

High expression of AKR1B10 has been shown in many different studies to predict poor prognosis in HCC; however, the signaling pathways mediating this have not been adequately evaluated (Distefano & Davis, 2019). Serum alpha-fetoprotein (AFP) levels are a widely used screening test for HCC (Zhou et al., 2006). AKR1B10 upregulation was shown to be associated with viral hepatitis C infection (Sato et al., 2012). Elevated serum AFP levels was correlated with high AKR1B10 expression in chronic hepatitis C patients (Sato et al., 2012). It was also reported that hepatitis C or hepatitis B patients with high AKR1B10 expression might be at high risk of HCC incidence (Junfei Jin et al., 2016; Mori et al., 2017; Murata et al., 2016).

In addition to detoxification reactions, AKR1B10 was shown to promote fatty acid and lipid synthesis by blocking the ubiquitin-dependent degradation of acetyl CoA

carboxylase (ACC) α (C. Wang et al., 2009), a rate-limiting enzyme of fatty acid biosynthesis. The role of AKR1B10 in enhancing fatty acid synthesis via direct interaction and stabilization of ACC has been reported in breast cancer cells (Ma et al., 2008). Additionally, the same research group showed that siRNA-mediated silencing of AKR1B10 in a lung and colon cancer cell line could reduce the phospholipid amount by 50% and enhance the amount of lipid peroxides (C. Wang et al., 2009). Lastly, AKR1B10 expression was shown to enhance fatty acid oxidation in breast cancer cells to enhance metastatic spread (van Weverwijk et al., 2019). A role of AKR1B10 in carcinogenesis can be envisaged since retinoids play essential roles in proliferation, differentiation, and morphogenesis (Matsunaga et al., 2012). Retinoids are natural derivatives of vitamin A, which has many regulatory functions in the cells, such as proliferation, apoptosis and differentiation (S. Chen et al., 2022). AKR1B10 regulates retinoic acid homeostasis by reducing retinals to retinols and inhibits the cellular differentiation caused by retinoic acids (Penning, 2005).

Bioinformatics analyses carried out by our group using publicly available RNA sequencing or microarray data indicated significant enrichment of GO terms associated with metabolism in CRC tumors expressing high AKR1B10 (Taskoparan et al., 2017). Additionally, based on the fact that AKR1B10 can use a wide variety of metabolites as its substrate and the limited amount of wet lab data available showing a role of AKR1B10 in fatty acid metabolism, a role of this enzyme in modulating cancer cell metabolism is highly feasible.

1.6 Cancer Cell Metabolism

Deregulated metabolism has been appreciated as one of the hallmarks of cancer cells in the last decade (Hanahan, 2022; Hanahan & Weinberg, 2011). Cancer cells generally prefer rapid energy production pathways to enable unlimited survival and growth, provided adequate biomass generation pathways are also active. Survival and biosynthesis in mammalian cells are mainly supported by glucose and

glutamine. The Warburg effect, suggesting enhanced glucose uptake by tumor cells compared to non-proliferating healthy cells, was proposed more than 100 years ago. After this, however, the focus of cancer research shifted to a better understanding of the genetic basis of cancer. Nonetheless, with the advancement of omics technologies such as proteomics and metabolomics in the last two decades, the role of the proteome and metabolome, in addition to the transcriptome, has gained momentum.

Glucose is the primary carbon source of glycolysis and the tricarboxylic acid (TCA) cycle to generate ATP and carbon intermediates for biosynthetic reactions. Oncogenic mutations in cancer cells provide an enhanced ability to take up glucose from the extracellular matrix. High glucose uptake is provided by the upregulation of class I transporter GLUT1 (glucose transporter) to generate metabolic intermediates for anabolic reactions (Pavlova & Thompson, 2016). TCA cycle intermediates have a role as precursors in metabolically active cells. Stimulated glucose uptake may cause elevated pyruvate production, which enters the TCA cycle to generate metabolic intermediates to be consumed in various biosynthesis reactions or biomass generation (Pavlova et al., 2022). Citrate generated in the TCA cycle can be exported out of the mitochondria and used to generate building blocks for the synthesis of fatty acids in metabolically active cells (Pavlova et al., 2022).

Cancer cells generally favor a switch from ATP generation via oxidative phosphorylation in the mitochondria to glycolysis in the cytosol, despite the presence of oxygen, functional mitochondria and the fact that glycolysis generates a lot less ATP. The preferred activation of glycolysis results in lactate accumulation, thereby reducing the pH in the tumor microenvironment (Cairns et al., 2011). An alternative energy-providing mechanism is that glycolysis-derived pyruvate can be reduced to lactate under low oxygen availability (Pavlova et al., 2022). However, cancer cells may preferentially convert pyruvate to lactate instead of oxidizing in mitochondria and this phenomenon was discovered by Otto Warburg (Warburg et al., 1927).

Secondly, cancer cells are highly dependent on non-essential amino acids, such as glutamine, which can enhance cellular proliferation by supporting nitrogen metabolism (biosynthesis of nucleotides) (Pavlova et al., 2022). Demand for nitrogen is uniquely associated with cellular proliferation. Glutamine is preferred in cancer cells as a nitrogen source for nucleotide synthesis and a carbon source in the TCA cycle and lipid biosynthesis (Jonghwa Jin et al., 2023). The TCA cycle metabolite, α-ketoglutarate, can be derived from glutamine for energy generation or a source of citrate to support *de novo* lipogenesis (Pavlova et al., 2022). Reactive oxygen species (ROS) are elevated in rapidly proliferating cells. Glutamine also plays a critical role in cellular oxidative defense mechanisms via the synthesis of endogenous antioxidant glutathione (Jonghwa Jin et al., 2023).

1.6.1 Pentose Phosphate Pathway (PPP)

Metabolic intermediates generated during glycolysis and the Pentose Phosphate Pathway (PPP) provide building blocks for the synthesis of nucleic acids, amino acids, and fatty acids (Pavlova & Thompson, 2016). The PPP, also known as the hexose monophosphate shunt, utilizes glucose-6-phosphate to generate NADPH and ribose in the cells. Glucose-6-phosphate dehydrogenase (G6PD) is the rate-limiting step of the Pathway. G6PD and 6-phosphogluconate dehydrogenase (6PGD) are the two dehydrogenases that catalyze the formation of NADPH (**Figure 1.3**). Upregulation of PPP has been reported in many cancer types whereby the riboses are used for nucleic acid generation, and reducing electrons from NADPH are used for the reduction of reactive oxygen species (ROS) via the glutathione system or for anabolic reactions such as fatty acid synthesis (Patra & Hay, 2014).

The PPP has two branches: oxidative (oxPPP) and non-oxidative PPP (non-oxPPP). The oxidative PPP is an irreversible arm in which glucose-6-phosphate is converted to ribulose 5-P, NADPH, and carbon dioxide by G6PDH. Activation of the non-oxPPP branch provides a balance between the generation of NADPH and riboses.

The two key enzymes of the non-oxPPP branch are transaldolase (TALDO1) and transketolase (TKT), which catalyze reversible reactions to increase the generation of riboses (Figure 2). 80% of ribonucleotides in cancer cells are reported to be produced in non-oxidative PPP (Boros et al., 1998). Moreover, the expression and activity of TALDO1 and TKT have been shown they are dysregulated in several human cancer types (Patra & Hay, 2014).

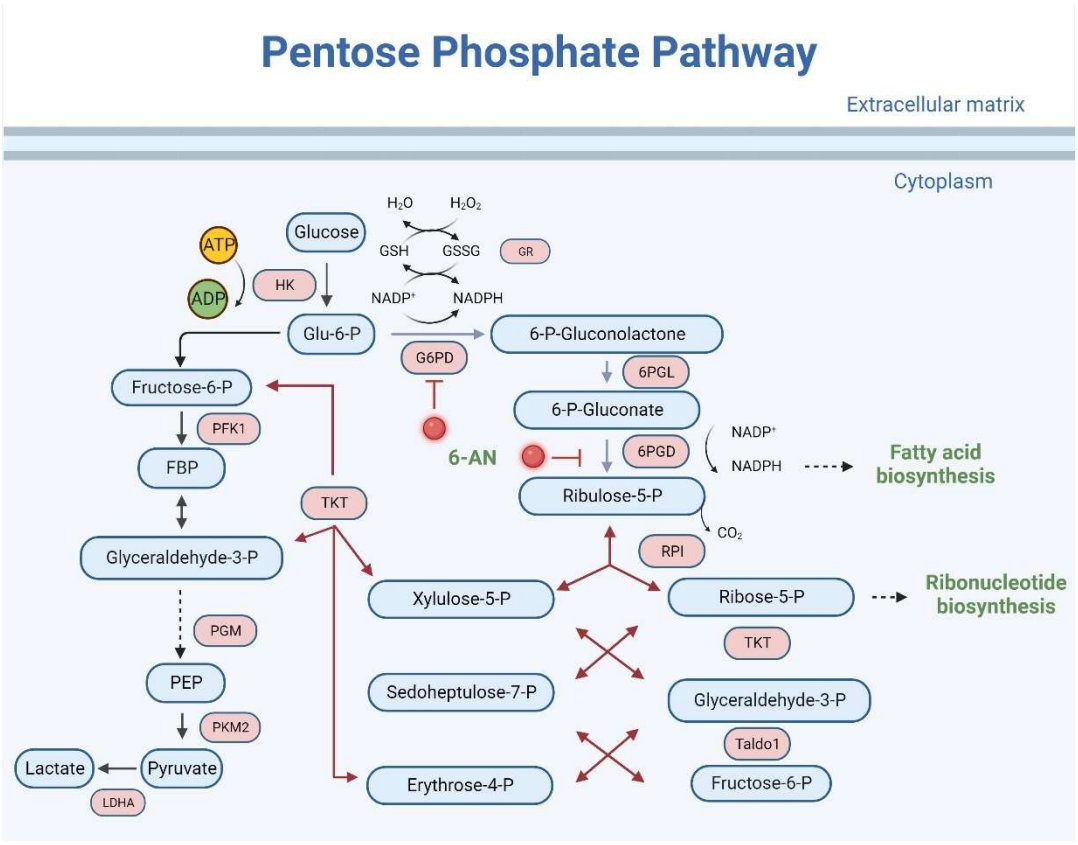

Figure 1.3 The pentose phosphate pathway.

Cross-talk with glycolysis is also shown. Blue arrows represent the oxidative reactions of PPP; red arrows represent the non-oxidative reactions of PPP. Image adapted from Jiang et al., 2014. G6PD: Glucose-6-phosphate dehydrogenase, 6PGL: 6-phosphogluconolactonase, 6PGD: 6-phosphogluconate dehydrogenase, RPI: Ribose phosphate isomerase, TKT: Transketolase, TALDO1: Transaldolase 1, HK: Hexokinase, GR: Glutathione reductase, PFK1: Phosphofructokinase 1, PGM: phosphoglyceratemutase, PKM2: Pyruvate kinase M2, LDHA: Lactate

dehydrogenase A, FBP: Fructose 1,6-bisphosphate, PEP: Phosphoenolpyruvate, 6-AN: 6-aminonicotinamide, specific PPP inhibitor. The figure was created by BioRender.

1.6.2 Fatty Acid Metabolism

Fatty acids are essential components of cellular metabolism; their synthesis is indispensable for membrane synthesis, in addition to their role in signal transduction and high synthesis of ATP when catabolized. Cancer cells have very high energy requirements for continual biomass generation and proliferation (DeBerardinis & Chandel, 2016). Fatty acid metabolism can differ considerably between normal and cancer cells. While normal cells obtain fatty acids from exogenous sources, cancer cells can also carry out *de novo* lipogenesis (Fhu & Ali, 2020). Additionally, cancer cells are known to be highly metabolically plastic, switching metabolic pathways when certain nutrients are limiting while alternative fuels are more abundant. Thus, when glucose is limited or consumed or when energy requirements are high (such as during the process of metastatic spread), cancer cells can utilize fatty acid stores for ATP generation in the presence of oxygen (Cassim et al., 2018). Fatty acid synthesis is a more widespread event in cancer cells that rely on lipid deposits to provide higher amounts of ATP when other nutrients are scarce or consumed (Koundouros & Poulogiannis, 2020). During fatty acid synthesis, acetyl CoA is carboxylated to malonyl CoA with the enzyme acetyl CoA carboxylase (ACC); this step is repeated several times whereby the malonyl CoA is condensed to generate palmitate catalyzed by the enzyme fatty acid synthase (FASN).

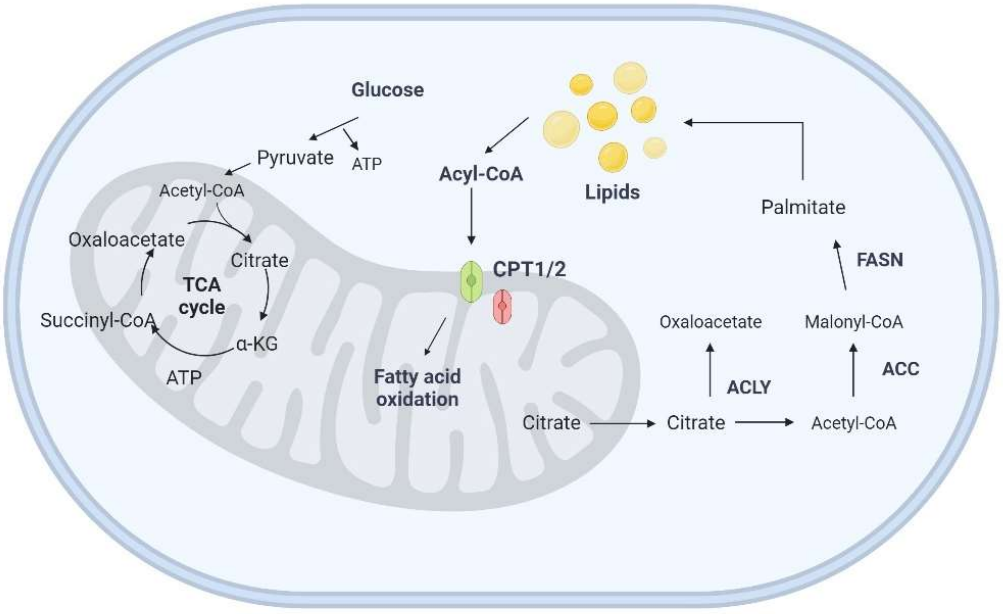

Figure 1.4 Fatty acid metabolism.

Overview of the metabolic pathways required for de novo fatty acid synthesis. Citrate is cleaved by ACLY (ATP Citrate Lyase) to acetyl CoA and oxaloacetate. Acetyl CoA is converted to malonyl CoA by ACC (Acetyl CoA Carboxylase) and condensed by FASN (Fatty Acid Synthase) to generate palmitate. CPT1/2: Carnitine palmitoyltransferases 1 and 2. α-KG:α-Ketoglutaric acid. The figure was created by BioRender.

1.6.3 Energy Sensing Pathways

Cellular metabolism is highly regulated by a number of proteins and signaling pathways that can exquisitely sense the requirement of cells for essential nutrients such as glucose and amino acids. Key among these pathways are the antagonistic 5' adenosine monophosphate-activated protein kinase (AMPK) pathway, which senses low energy levels and activates catabolism and the mechanistic target of Rapamycin (mTOR) pathway, which senses the presence of adequate nutrients and activates anabolic pathways.

1.6.3.1 AMP-Activated Protein Kinase (AMPK) Pathway

AMP-activated protein kinase (AMPK) is an important regulator of cellular energy homeostasis (Herzig & Shaw, 2018). Activation of AMPK (phosphorylation) leads to the inhibition of anabolic pathways and activation of catabolic processes, producing ATP and restoring homeostasis of energy mechanisms. A high ADP:ATP or AMP:ATP ratio, glucose and oxygen deprivation can activate the cellular sensor AMPK (Steinberg & Carling, 2019). The binding of AMP to the AMPKγ subunit enables the phosphorylation of AMPK at a conserved Threonine (Thr) 172 residue in the α subunit via liver kinase B1 (LKB1) an upstream kinase that has tumor-suppressive properties (Steinberg & Carling, 2019). Thirdly, AMPK can be activated by calmodulin-dependent kinase (CAMKKβ) in the presence of high cellular levels of calcium (Hardie, 2015). All anabolic pathways, including the synthesis of ribosomal RNA, phospholipids, proteins and fatty acids, are inhibited by the activation of AMPK (Hardie, 2015). In addition, glucose and fatty acid transport, fatty acid oxidation, autophagy, mitochondrial synthesis and oxidative metabolism are activated to generate ATP (Ke et al., 2018).

Downstream of AMPK, ACC1 and ACC2 (acetyl CoA carboxylase 1 and 2) are well-established downstream targets that can suppress fatty acid synthesis and increase fatty acid oxidation (Garcia & Shaw, 2017). AMPK inhibits the synthesis of fatty acids and promotes oxidation by phosphorylation of acetyl CoA carboxylase 1 (ACC1) at the Serine (Ser) 79 residue, which is an inhibitory phosphorylation for lipogenesis (Galic et al., 2018). ACC causes a decrease in malonyl-CoA, which inhibits carnitine palmitoyltransferase I (CPT1).

1.6.3.2 Mammalian Target of Rapamycin (mTOR) Pathway

The mammalian target of rapamycin (mTOR) is an evolutionarily conserved serine/threonine kinase and one the major regulators of cell growth and division. Unlike the AMPK pathway, activation of the mTOR pathway provides cell growth,

protein synthesis and biomass accumulation (G. Y. Liu & Sabatini, 2020). mTOR complex 1 (mTORC1) and complex 2 (mTORC2) are two biochemically distinct complexes of mTOR, which contain different subunits (Laplante & Sabatini, 2012). mTORC1 activates downstream targets related to protein, lipid, nucleotide and ATP synthesis while repressing autophagy (G. Y. Liu & Sabatini, 2020). mTORC1 drives lipid synthesis via sterol regulatory element binding protein 1/2 (SREBP1/2) and proliferator-activated receptor γ (PPARγ). SREBP1/2 upregulate genes that are responsible for *de novo* lipid synthesis and cholesterol synthesis (Laplante & Sabatini, 2012), such as ACC and FASN (Soliman, 2011). PPARγ is the regulator of scavenger receptor CD36 (Chawla et al., 2001). Of note, mTORC1 also phosphorylates S6K (p70S6K) and eukaryotic initiation factor 4E-binding proteins (4E-BPs) to activate protein synthesis. Serendipitously discovered mTORC2 phosphorylates protein kinase C (PKC), Akt and serum/glucocorticoid regulated kinase 1 (SGK1) (G. Y. Liu & Sabatini, 2020; Yoon, 2017). Its role in protein translation or cell growth is currently undefined.

1.7 Aims and the Novelty of This Study

The study was designed to evaluate a role of AKRs in gastrointestinal cancers. We have previously reported (as a part of my Master's thesis) that the functional consequences of AKR1B1 and AKR1B10 expression in colon cancer were highly divergent (Taskoparan et al., 2017). Expression of AKR1B1 in CRC cell lines enhanced proliferation, motility, and inflammation, while expression of AKR1B10 mediated the opposite. Moreover, we observed that a combined signature of high AKR1B1 ($AKR1B1^{HIGH}$) and low AKR1B10 ($AKR1B10^{LOW}$) (AKR signature) expression was associated with a significantly worse prognosis of CRC patients independent of confounding factors. In other words, tumors expressing the AKR signature were associated with worse disease-free survival (DFS) independent of age, gender, KRAS or BRAF mutations, and TNM stage (Taskoparan et al., 2017). Based on these previous data, I hypothesized that AKR1B1 and AKR1B10

expression in CRC tumor specimens could be associated with EMT. In addition, *in silico* analyses carried out in our lab indicated an important role of AKR1B10 in metabolism. The liver is the center of primary metabolic activities, such as the metabolism of lipid, glucose, and cholesterol. Therefore, it is highly likely that aberrant metabolic pathways contribute to cancer development in HCC (Zarrinpar, 2017). High expression of AKR1B10 has been shown in many different studies to predict poor prognosis in HCC while having tumor suppressive roles in CRC. Therefore, I aimed to establish whether nutrient sensing pathways and the metabolome was altered in liver cancer cells expressing AKR1B10. More details on the specific aims are shown below.

1.7.1 EMT and Colorectal Cancer

To better address how the AKR signature contributes to tumorigenesis, we evaluated the AKR gene signature with prognostic significance in CRC via activation of EMT (Demirkol-Canlı et al., 2020). Using publicly available datasets as well as *ex vivo* gene expression analysis using the patient colon and rectal tumor specimens (Ankara cohort), we aimed to validate our previous *in silico* finding that the AKR signature was associated with a worse prognosis. I observed that, confirming our *in silico* findings, *ex vivo* tumor samples showed a high positive correlation between AKR1B1 expression and mesenchymal markers and a negative correlation with epithelial markers. The opposite was observed with AKR1B10. Patients in the Ankara cohort expressing high AKR1B1 also showed significantly worse prognosis.

1.7.2 Liver Cancer

Screening and early diagnosis of HCC are essential to reduce its mortality. Current guidelines mostly recommend the detection of serum alpha-fetoprotein (AFP) levels every six months and ultrasound examination in patients with

cirrhosis (Yilmaz et al., 2018). However, AFP levels are intermittently changed in cirrhosis and are not always predictive of cancer. Non-cirrhotic patients are primarily screened by ultrasound (Yilmaz et al., 2018). The poor prognosis associated with the expression of AKR1B10 is primarily observational, showing that tumor samples that express high levels of AKR1B10 protein or RNA were associated with worse survival. However, the pathways that can lead to such poor prognosis have not been addressed in any detail. The AKR1B10 protein can be secreted and has been detected in the blood. Serum levels of AFP and AKR1B10 together was reported to predict the incidence of HCC better than AFP alone (Zhu et al., 2019), indicating the importance of AKR1B10 in the liver. A very recent study has shown that serum AKR1B10 was a better prognostic marker, particularly for early-stage HCC patients with good liver function compared to serum AFP (Xie vd., 2023).

The primary hypothesis of my thesis was to establish the signaling pathways that are mediated in HCC cells expressing AKR1B10. For this, I selected two different liver cancer cell lines, SNU423 and HuH-7, neither of which express any AKR1B10 and yet have highly divergent metabolic phenotypes. Bioinformatics studies suggest that SNU423 cells are glycolytic and can activate the PPP, while HuH-7 cells are more oxidative and rely primarily on fatty acid oxidation as their source of energy (Ye et al., 2023). I have overexpressed AKR1B10 in these cell lines and evaluated the activation of energy sensing pathways. Using untargeted metabolomics in HuH-7 cells, I have evaluated the metabolic pathways that are altered with the expression of AKR1B10 in comparison to controls. Overall, this study is the first to show a comprehensive analysis of the metabolome associated with the expression of AKR1B10 and point towards a major deregulation in bioenergetics, primarily through a slowing down of the TCA cycle, activation of gluconeogenesis and aberrant activation of the shunts that carry reducing electrons from the cytosol to the mitochondria.

CHAPTER 2

MATERIALS AND METHODS

2.1 Cell Culture

Low levels of endogenous AKR1B1 and AKR1B10 expressing human colon cancer cell lines (Taskoparan et al., 2017) RKO and SW480 cells were selected for the study. Both cell lines were purchased from ATCC (American Type Culture Collection). RKO cells were cultured in EMEM supplemented with 10% FBS (fetal bovine serum), 2 mM L-glutamine, 1 mM sodium pyruvate, 1% non-essential amino acids solution, and 1% Penicillin and Streptomycin solution. SW480 cells were grown in Leibovitz L-15 medium supplemented with 10% FBS and 1% Penicillin and Streptomycin solution. The SW480 cells were grown in a humidified incubator at 37°C and 100% air. The human embryonic kidney cell line HEK293FT cell line was a kind gift from Dr. Mayda Gürsel (İzmir Biomedicine and Genome Center, Türkiye). HEK293FT cells were grown in DMEM (high glucose: 4.5 g/l) supplemented with 10% FBS, 6 mM L-glutamine, 1 mM sodium pyruvate, 1% non-essential amino acids solution and 1% Penicillin and Streptomycin solution. Both RKO and HEK293FT cells were cultured in a humidified atmosphere at 37°C and 5% CO_2. All cell culture consumables were purchased from Biological Industries.

The human hepatocellular carcinoma cell lines; SNU423 and HuH-7 cells were a kind gift from Dr. Rengül Çetin Atalay (University of Chicago, USA). SNU423 cells were cultured in RPMI medium supplemented with 10% FBS (Capricorn Scientific), 2 mM L-glutamine and 1% Penicillin and Streptomycin solution. HuH-7 cells were cultured in DMEM (low glucose: 1 g/l) supplemented with 10% FBS

(Capricorn Scientific), 4 mM L-glutamine and 1% Penicillin and Streptomycin solution. SNU423 and HuH-7 cells were incubated at 37°C and 5% CO_2 in a humidified incubator. All cell culture consumables were purchased from Biological Industries except FBS, which was obtained from Capricorn Scientific.

Mycoplasma testing was conducted regularly for each cell line (Young et al., 2010). Genomic DNA was isolated from cell lines to perform a PCR reaction (See Table 2 for primer sequence labeled as MGSO and GPO-3). All cell lines were grown in a prophylactic dose of plasmocin (Invivogen, 2.5 µg/ml).

2.2 Cloning of AKR1B1 and AKR1B10

AKR1B1 (NM_001628) pCMV-XL5 and AKR1B10 (NM_020299) pcDNA 3.1(-) vectors were available in Banerjee Lab. AKR1B1 pCMV-XL5 vector was cut with two restriction enzymes: EcoRI-HF (NEB) and XbaI (NEB). AKR1B10 pcDNA 3.1(-) vector was amplified with the high-efficiency polymerase enzyme NEB Phusion (NEB) with a primer pair containing the restriction cut sites (See Table 2). The PCR product was cleaned with MN Nucleospin Gel and PCR Clean-up kit (Macherey-Nagel) and quantified with Biodrop (Biochrom). The PCR product was cut with EcoRI-HF (NEB) and XbaI (NEB) restriction enzymes. The cut DNA fragments for AKR1B1 and AKR1B10 were loaded on 1% agarose gel, isolated from the gel with MN Nucleospin Gel and PCR Clean-up kit, and quantified by the spectrophotometer.

Restriction digestion of the vector pLenti-puro (Addgene, Plasmid #39481) was optimized by cutting with EcoRI-HF alone, XbaI alone and the two enzymes together at various time intervals; 2 hours, 4 hours, 6 hours and 16 hours (data not shown). The most suitable time point was 4 hours for both restriction enzymes. A high concentration of vector was cut and the linear vector was confirmed for the correct size by agarose gel electrophoresis, cut from the agarose gel, and isolated with the MN Nucleospin Gel and PCR Clean-up kit. The amount of isolated vector

was determined by Biodrop and reconfirmed by running on an agarose gel. AKR1B1 or AKR1B10 cDNA fragments were ligated with precut pLenti-puro vector at three different vector:insert ratios. Ligation was carried out with T4 DNA ligase (NEB) for 16 hours at 16°C. The heat-inactivated ligation products of AKR1B1 and AKR1B10 were transformed into *Escherichia coli* (*E.coli*) Stbl3 bacterial strain (A kind gift from Dr. Urartu Şeker, Bilkent University). Ampicillin-resistant colonies were first tested with a colony PCR. AKR1B1 pLenti-puro and AKR1B10 pLenti-puro plasmids were isolated from randomly selected positive colonies with MN Nucleospin Plasmid kit (Macherey-Nagel) and confirmed by Sanger sequencing (BMLabosis).

2.3 Generation of Viral Particles for Transduction

HEK293FT cells were co-transfected with the AKR1B1 pLenti-puro or AKR1B10 pLenti-puro plasmids (transfer plasmids), envelop plasmid pCMV-VSV-G (Addgene, Plasmid #8454) and packaging plasmid psPAX2 (Addgene, Plasmid #12260). HEK293FT cells were seeded in 10 cm tissue culture dishes for transfection with the transfection agent Polyethyleneimine (PEI, Sigma-Aldrich). An empty pLenti-puro vector (no coding sequence) was also transfected to generate control (empty vector) cells. The ratio of the plasmids had been optimized in the lab previously according to which 5 µg transfer vector, 2.5 µg envelope vector and 2.5 µg packaging vector were used (Chu et al., 2013). A total 10 µg DNA and 30 µl PEI (1 mg/ml) transfection agent was used at a ratio of 1:3 [DNA: PEI (w/v)]. After 24 hours of transfection, the media were changed with a fresh complete medium. Viral particles containing media were collected at 48 and 72 hours post-transfection for each transfer vector and centrifuged at 500 x g for 5 minutes to remove cell debris. Supernatants containing viral particles were collected and filtered with a 0.45 µm pore size syringe filter before snap-freezing in liquid nitrogen (Güderer, 2021). İsmail Güderer from the Banerjee lab generated the viral particles.

2.4 Transduction and Generating Stable Cell Lines

50,000 cells were seeded in 12-well plates for colon cell lines. After 24 hours of attachment, infections were carried out 1:1 ratio of viral particles containing media and proper antibiotic-free media or no dilution (full virus). The liver cell lines SNU423 and HuH-7 were reverse-transduced with 50,000 cells. The viral particles were added at 1:1 ratio of dilution with culture medium or no dilution (100% medium containing viral particles). The transduction medium was supplemented with polybrene (Merck Millipore) at a 1:1000 (v/v) ratio to enhance infection efficiency.

72 hours post-transduction, RKO and SW480 polyclones were selected with 1 µg/ml puromycin. HuH-7 and SNU423 cells were selected with 3 µg/ml and 2 µg/ml of puromycin, respectively. Within a week, untransduced cells were completely dead for each cell line. Puromycin selection pressure was always continued with 0.5 µg/ml for RKO and SW480 and 1 µg/ml for HuH-7 and SNU423 cells (maintenance dose). The ectopic expression of AKR1B1 and AKR1B10 in colon cancer cell lines and the ectopic expression of AKR1B10 in liver cancer cell lines were confirmed by western blot and PCR. İsmail Güderer generated the polyclonal RKO and SW480 cell lines overexpressing AKR1B1 and AKR1B10 (Güderer, 2021), while Hoşnaz Tuğral generated polyclonal HuH-7 cell lines expressing AKR1B10 (Tuğral, 2022). Puromycin kill curves were generated for each cell line by İsmail Güderer, Hoşnaz Tuğral and Esin Gülce Seza (data not shown).

2.5 Chemicals

HCC cells were treated with the pentose phosphate pathway inhibitor 6-Aminonicotinamide (6-AN, Sigma-Aldrich A68203) and the fatty acid oxidation inhibitor (+)-Etomoxir (Cayman 11969). 6-AN was dissolved in DMSO and

etomoxir was dissolved in nuclease-free water. The aliquoted chemicals were stored at -80 °C.

2.6 RNA Isolation From Colorectal Cancer Patient Samples

2.6.1 Patient Characteristics

Tumor samples from 32 patients diagnosed with colon cancer and 19 patients diagnosed with rectal cancer were collected at the Department of Gastroenterological Surgery, Yüksek İhtisas Training and Research Hospital, Ankara. Informed consent was obtained from all patients. Overall survival (OS) time, age, follow-up status, gender, grade, TNM (Tumor Node Metastasis) stage, perineural invasion and vascular invasion information were available for 46-49 patients, as detailed in **Table 1**. A Univariate Cox regression analysis was carried out by Dr. Seçil Demirkol Canlı (Hacettepe University). The Bilkent University Ethics Committee approved the study. The total number of 51 colon and rectal cancer patient samples will be mentioned as the "Ankara Cohort".

Table 1. Univariate analysis for survival in Ankara Cohort (n=51).

Characteristics	**Number of patients**	**Hazard ratio****	**p-value****
Location			
Colon*	32	3.855	0.001
Rectum	19		
Age			
<=60*	23	1.427	0.347
>60	26		
Other/unknown	2		

Table 1. (cont'd)

Characteristics	Number of patients	Hazard ratio**	p-value**
Gender			
Female*	23	1.090	0.820
Male	28		
TNM Stage***			
1	5	1.652	0.217
2	0		
3	41		
4	3		
Other/unknown	2		
Grade*****			
Well-differentiated	22	1.235	0.579
Moderately differentiated	24		
Poorly differentiated	0		
Other/unknown	5		
Perineural invasion			
No*	34	1.987	0.077
Yes	15		
Other/unknown	2		
Vascular invasion			
No*	27	1.532	0.262
Yes	22		
Other/unknown	2		

*Univariate analysis was carried out by Dr. Seçil Demirkol Canlı. *represents reference data for the calculation of the hazard ratio. ** Univariate Cox regression analysis was carried out. *** TNM stage calculation was treated as a continuous variable. **** Tumor grading was calculated as a continuous variable.*

2.6.2 RNA Isolation From Tumor Samples

Total RNA from colon and rectal cancer patient samples was extracted from frozen tumor tissues using Trizol reagent (Ambion) with a tissue homogenizer. The well-established phenol-chloroform extraction was followed as described by Demirkol et al., 2017. After adding an appropriate amount of chloroform (500 µl for 1 ml Trizol reagent), tissue samples were incubated for 10 minutes at room temperature. They were centrifuged at 4°C and 12,000 x *g* for 15 minutes. The separated upper phase was transferred to a new nuclease-free Eppendorf tube and mixed with 500 µl isopropanol for 1 ml Trizol reagent. After 10 minutes of room temperature incubation, samples were centrifuged at 4°C and 12,000 x *g* for 15 minutes. The samples separated from the supernatants were mixed with 75% ethanol and centrifuged again. Ethanol was removed from each sample and the RNA pellets were air-dried. The pellets were dissolved in nuclease-free water at 55°C for 15 minutes.

2.7 RNA Isolation From Cell Lines

Total RNA from control (empty vector: EV), AKR1B1 and AKR1B10 ectopically expressing RKO and SW480 cells and control (EV) and AKR1B10 ectopically expressing SNU423 cells were extracted by using NucleoSpin RNA kit (Macherey Nagel) according to manufacturer's instructions.

2.8 RNA Quantification and cDNA Synthesis

RNA concentration was determined by BioDrop (Biochrom). An A260/230 ratio of 2.0 or slightly above and an A260/280 ratio between 1.8 and 2.1 were considered for further applications. After quantification, patient samples were treated with DNase I (Thermo Fisher Scientific) and incubated at 37°C for 30 minutes. The reaction was inhibited by adding 1 µl 50 mM EDTA and incubating at 65°C for 10

minutes. Cell line samples were treated on-column Dnase during the total RNA extraction process. All RNA samples were stored at -80 °C.

500 ng RNA for patient samples and 1 µg RNA from cell lines were converted to cDNA using a RevertAid First Strand cDNA Synthesis Kit (Thermo Fisher Scientific). Random hexamer primers were used according to the manufacturer's instructions in all reactions, including cell line samples. cDNA libraries were stored at -20 °C.

2.9 RT-PCR and RT-qPCR

Reverse transcription-polymerase chain reaction (RT-PCR) was used to obtain the optimum annealing temperature for each primer pair or mycoplasma testing. Reactions were performed in a 20 µl final volume containing 2 µl (50-100 ng) of cDNA and 18 µl reaction mixture, including 0.2 mM dNTP mix (Thermo Scientific), 1.5 mM $MgCl_2$, 10X ammonium buffer, 1 U of Taq polymerase (Ampliqon), 0.5 µM forward and reverse primers and PCR grade nuclease-free water. The samples were placed in a T100 thermal cycler with a gradient mode (Bio-Rad). After 40 cycles of the reaction, samples were mixed with 6X DNA loading dye (Thermo Scientific) and run on a 1% agarose (Sigma-Aldrich) gel containing ethidium bromide solution (PanReac AppliChem). The gel was visualized under UV light.

Quantitative reverse transcription-polymerase chain reaction (RT-qPCR) for patient samples and CRC cell lines were carried out in a CFX Connect Real-Time PCR Detection System (BIO-RAD) and for HCC cell lines were carried out in a Rotor-Gene Q (Qiagen) machine using MIQE Guidelines. cDNA from patient samples and cell line samples were synthesized as described above. Each primer pair was generated with a standard curve with 1:10, 1:50, 1:100, 1:250, 1:500, 1:1000 and 1:10000 dilutions of 1000 ng cDNA. Primers with related genes and melting temperatures are shown in **Table 2**. Reaction conditions were initial denaturation

(3 minutes) at 95°C, denaturation (30 seconds) at 95°C, annealing (30 seconds) at optimized temperature (°C), extension (30 seconds) at 72°C and final extension (3 minutes) at 72°C with 40 cycles.

ACTB and *GAPDH* genes were used as internal controls for patient cDNA samples. Fold changes for patient samples were calculated with respect to the geometric mean of *ACTB* and *GAPDH* expression using the Pfaffl method (Pfaffl, 2001). BT-20, an epithelial breast carcinoma cell line, was included in each PCR run using patient samples to assess batch differences. Ct (cycle threshold) values for *AKR1B1*, *AKR1B10*, *CDH1*, *VIM*, *GAPDH* and *ACTB* were observed below 33 for the BT-20 cell line. The patient sample expression data for each gene were normalized to the expression of each gene in BT-20; however, the BT-20 expression data were not used for statistical analysis (Demirkol-Canlı et al., 2020). Gene expression in cell lines were calculated with respect to the mean of *ACTB* expression using the Pfaffl method (Pfaffl, 2001).

Table 2. Primer pairs used in this study.

Target Gene	**Forward Primer (5'→3')**	**Reverse Primer (5'→3')**	**Tm (°C)**
Mycoplasma Detection	(MGSO)TGCACCATCTGTCACTCTGTTAACCTC	(GPO3)GGGAGCAAACAGGATTAGATACCCT	55
AKR1B10 Cloning	(EcoRI)GCCGGGAATTCGCCACCATGGCCACGTTTGTGGAG	(XbaI)GTTCTAGAACCTCAATATTCTGCATTGAAGGG	72
AKR1B10 NM_020299	CAGAATGAACATGAAGTGGGG	GCTTTTCCACCGATGGC	55
AKR1B1 NM_001628.4	AAGCCGTCTCCTGCTCA	TTGCTGACGATGAAGAGC	55
CDH1 NM_004360.5, NM_001317184.2, NM_001317185.2	TACACTGCCCAGGAGCCAGA	TGGCACCAGTGTCCGGATTA	59

Table 2. (cont'd)

Target Gene	Forward Primer (5'→3')	Reverse Primer (5'→3')	Tm (°C)
VIM NM_003380.5	CCAGCCGGAGCTACGTGACTA	GTGCGGGTGTTCTTGAACTCG	59
TALDO1 NM_006755.2	GTCATCAACCTGGGAAGGAA	CAACAAATGGGGAGATGAGG	60
TKT NM_001064.4, NM_001135055.3, NM_001258028.2	GAAGATCAGCTCCGACTTGG	GTCGAAGTATTTGCCGGTGT	60
G6PD NM_000402.4, NM_001042351.3, NM_001360016.2	TGACCTGGCCAAGAAGAAGA	CAAAGAAGTCCTCCAGCTTG	56
ACTB NM_001101.5	CAGCCATGTACGTTGCTATCCAGG	AGGTCCAGACGCAGGATGGCATG	55-60
GAPDH NM_002046.7, NM_001256799.3, NM_001289745.3, NM_001289746.2, NM_001357943.2	CGACCACTTTGTCAAGCTCA	CCCCTCTTCAAGGGGTCTAC	55-60

2.10 Protein Isolation

A protein isolation mixture was prepared by mixing M-PER Mammalian Protein Extraction Reagent (Thermo Fisher Scientific) with phosphatase inhibitors (PhosSTOP, Roche) and protease inhibitor cocktail (cOmplete, Mini, EDTA-free Protease Inhibitor Cocktail, Roche). Both phosphatase and protease inhibitors were prepared as 10X solution in 1X PBS (Phosphate-Buffered Saline) and diluted to 1X in a protein lysis buffer. Samples from cell culture were washed with PBS and

scraped with the protein lysis buffer. The lysed cell mixture was collected into a 1.5 ml test tube and incubated on ice for 30 minutes and then vortexed every 10 minutes. Then, the protein samples were centrifuged for 10 minutes at 14,000 x *g* and 4°C. The supernatants were separated from cell debris and collected into clean and pre-chilled 1.5 ml Eppendorf tubes and stored at -80°C.

The Bradford method was used to quantify the total protein amount of the M-PER mixture extracted samples. Pierce Bradford Protein Assay Kit (Thermo Scientific) was used with a standard curve generated with bovine serum albumin (supplied by the kit) according to the manufacturer's instructions. The absorbance values at 595 nm were determined with a spectrophotometer (Thermo Scientific Multiskan GO). Measured proteins were mixed with 6X reducing protein loading dye and boiled for 6 minutes at 95°C. The boiled proteins were stored at -20°C.

2.11 Western Blotting

Total proteins were separated in 10% or 12% SDS-PAGE gels prepared with 37.5:1 Acrylamide/Bis solution (30% w/v, Serva) according to the manufacturer's protocol. 15-30 µg protein was loaded into gels and transferred to PVDF (polyvinylidene difluoride, Roche) membranes with a pore size of 0.2 µm. PageRuler Plus Prestained protein ladder (Thermo Scientific) was used as a 10-250 kDa marker. According to the established protocol, the transfer was performed at 115 volts (V) for 90 minutes. 5% nonfat dried milk (PanReac AppliChem) in 1X TBS-T (Tris-buffered saline containing 0.1% Tween 20) was used for blocking at room temperature. After blocking, primary antibodies were incubated overnight at 4°C and secondary antibodies were incubated for 1 hour at room temperature. The antibodies used in the study are shown in **Table 3**. After washing the secondary antibodies with 1X TBS-T, bands were visualized with Clarity Western ECL Substrate (BIO-RAD) and ChemiDoc MP Imaging System (BIO-RAD). α-Tubulin or β-actin was used as a loading and normalization control.

Table 3. Antibodies used in this study.

Protein Name	Vendor	Catalog No	Host	Dilution
AKR1B1	Invitrogen	PA5-29718	Rabbit	1:1000
AKR1B10	Invitrogen	PA5-23017	Rabbit	1:1000
G6PD	Cell Signaling	CST12263	Rabbit	1:1000
TKT	Cell Signaling	CST64414	Rabbit	1:1000
p-AMPK	Cell Signaling	CST2535	Rabbit	1:1000
p-ACC (S79)	Cell Signaling	CST3661	Rabbit	1:1000
p-Akt (T308)	Cell Signaling	CST4056	Rabbit	1:1000
Akt	Cell Signaling	CST9272	Rabbit	1:1000
p-GSK3β	Cell Signaling	CST9323	Rabbit	1:1000
GSK3β	Cell Signaling	CST9315	Rabbit	1:1000
p-p70S6K (T389, T412)	Cell Signaling	CST9234	Rabbit	1:1000
p70S6K	Cell Signaling	CST2708	Rabbit	1:1000
p-mTOR (S2448)	Cell Signaling	CST5536	Rabbit	1:1000
p-4E-BP1	Cell Signaling	CST9451	Rabbit	1:1000
PDCD4	Santa Cruz	376430	Mouse	1:500
α-Tubulin	Proteintech	HRP-66031	Mouse	1:5000
β-Actin	Santa Cruz	47778	Mouse	1:4000

2.12 Proliferation Assay

An MTT (3-(4,5-Dimethylthiazol-2-yl)-2,5-Diphenyltetrazolium Bromide) assay was carried out to observe cellular proliferation and viability. 10,000 cells for CRC cell lines and 5,000 cells for HCC cell lines per well were seeded for a 96-well plate in a complete medium. After 24 hours of attachment of the cell, drug treatment or nutrient withdrawal were carried out for indicated time points. MTT (Invitrogen) powder was dissolved in PBS at a concentration of 12 mM or 5mg/ml. At the end of the incubation period, the medium was discarded and 100 µl of MTT

containing fresh medium (the final concentration is 1.2 mM) was added to each well. Metabolically active cells (proliferative cells) enable the formation of formazan crystals from MTT. After 4 hours of incubation at 37°C, 100 µl of 0.1% SDS-0.01 M HCl solution was added to each sample and incubated for 16 hours at 37°C. The formazan salts became soluble in the SDS-HCl solution. The absorbance values at 570 nm were measured with a spectrophotometer (Thermo Scientific Multiskan GO). Proliferation or viability was normalized to control cells.

2.13 Colony Formation Assay

A colony formation assay was carried out to determine long-term proliferation according to published protocols (Feoktistova et al., 2016). AKR1B10 expressing or control (EV) SNU423 cells were seeded at a density of 1000 cells/well in a 6-well plate. The cells were treated with the complete culture medium or culture medium containing drugs or indicated starvation medium for 8 days in a humidified incubator with 5% CO_2 at 37°C. The culture medium was renewed every two days. When the colonies became visible with the naked eye, the cells were washed with PBS once and fixed with 4% paraformaldehyde (PFA, Sigma-Aldrich) solution in PBS for 15 minutes at room temperature. Then, the fixation solution was removed from the wells and rewashed with PBS once. 1 ml of 0.5% crystal violet (Sigma-Aldrich) solution (dissolved in 80% ddH_2O and 20% methanol) was added and incubated for 20 minutes at room temperature on a bench-type rocker. Afterward, plates were carefully washed with a gentle stream of tap water four times and air-dried overnight without a lid. The next day, the stained colonies were visualized in the ChemiDoc MP Imaging System (BIO-RAD). The images were analyzed with Java-based ImageJ (National Institute of Health, USA) software using the Threshold/Subtract method (Güderer, 2021).

2.14 Induction of Hypoxia

Hypoxic conditions was provided with a Hypoxia Incubator Chamber (Stemcell Technologies). The hypoxia chamber was connected and filled with a premixed gas containing 1% O_2, 5% CO_2 and 94% N_2. A tightly sealed hypoxia chamber was monitored by an oxygen sensor connected to Arduino interfaced with a computer for real-time oxygen concentration inside the chamber. Prior to the experiment, the cell culture medium was incubated for 16 hours for degassing as described previously (Tunçer et al., 2017). The medium was replaced with a degassed medium and cells were incubated for 24 hours in the hypoxia chamber.

2.15 NADP/NADPH Assay

AKR1B10 expressing SNU423 cells were seeded on 15 cm cell culture dishes at 3,000,000 cells/dish density and treated with 6-AN to determine NADPH levels. Empty vector cells were used for control in the experiment. A fluorometric NADP/NADPH Assay Kit (ab176724, Abcam) was used and followed the protocol as described. After incubating with 10 μM 6-AN for 24 hours, SNU423 cells were trypsinized and counted. 4,000,000 cells were centrifuged at 1500 rpm for 5 minutes at room temperature. The cells were resuspended in NADP/NADPH lysis buffer and incubated for 15 minutes at room temperature. Lysates from cells were transferred into a 96-well black sterile opaque plate. NADPH, NADP extraction solution or NADP/NADPH control solution was added to the labeled wells and incubated for 15 minutes at room temperature. NADP solution was added to the NADPH test sample or NADPH solution was added to the NADP test sample. NADP/NADPH control solution added group was incubated with the same solution. Next, the NADPH reaction mixture was added to each well and incubated in the dark for 1.5 hours at room temperature. All treatments were carried out in duplicate. A standard curve was generated with 1 mM NADPH stock solution diluted with PBS according to the manufacturer's protocol. The change in

fluorescence for each treatment was measured with a Spectramax iD3 Microplate Reader (Molecular Devices) at 540 nm excitation and 590 nm emission wavelengths.

2.16 Citrate Synthase Assay

AKR1B10 expressing or control (EV) transfected SNU423 and HuH7 cells were plated in a T25 flask and grown until 80-90% confluency. Where indicated, the cells were incubated in glucose and glutamine free medium for 72h prior to the start of the experiment. 1,000,000 cells per sample were collected in eppendorf tubes. 100 µl of ice-cold lysis buffer containing 20 mM HEPES, 1mM EDTA and 0.1% Triton X-100 (pH=8.0) was added to each sample and incubated for 30 minutes. A probe sonicator was used for 10 seconds at 30 kHz to lyse the cells followed by centrifugation at 10,000 x g for 15 minutes. The supernatant was collected in fresh eppendorf tubes and the protein content was determined.

A reaction mixture was prepared in 20 mM Tris-HCl (pH=8.0) buffer containing 1 mM oxaloacetic acid (Sigma-Aldrich), 1 mM DTNB [Ellman's Reagent; 5,5-dithio-bis-(2-nitrobenzoic acid), Sigma-Aldrich] and 9.4 µg/ml Citrate Synthase (Sigma-Aldrich). At the time of the experiment, the lysate (10µl) was added to the wells of a 96-well plate. The reaction mixture (90µl) was added to the lysates prior to the measurement at 412 nm. The absorbance was measured every 30 seconds for 40 minutes at 37°C in a plate reader (Thermo Scientific Multiskan GO). Blank (no cell lysate) readings were subtracted from each measurement. An absorbance versus time graph was generated in Excel (Microsoft).

Enzyme activity was determined as kcat (s-1) (Vmax/molar concentration of the enzyme) described previously (Ulusan et al., 2022). The change in absorbance was determined with the equation A=(A2-A1)/(t2-t1) where A2 and t2 were the final absorbance and time while A1 and t1 were the initial absorbance and time.

2.17 Intracellular Reactive Oxygen Species Detection Assay

ROS levels in the cells were measured with dihydroethidium (DHE, Invitrogen), a cell permeable fluorescent probe. The DHE probe is highly selective for $O_2\bullet^-$. 10,000 cells/well were seeded in a 96-well sterile black plate and incubated for 18 hours at 37°C and 5% CO_2. At the end of the incubation, the medium was discarded and the cells were washed with PBS. They were then evaluated for ROS production with the addition and incubation of 5 μM DHE for 90 minutes at 37°C %5 CO_2 in the dark. The fluorescence intensity of the probe at 518 nm excitation and 605 nm emission wavelength was quantified in a Spectramax iD3 Microplate Reader (Molecular Devices). The data were normalized to cell numbers using an MTT assay.

2.18 Oxygen Consumption Rate Assay

AKR1B10 expressing HuH-7 cells were seeded an opaque 96-well cell culture plate at 30,000 cells per well density. A fluorometric Extracellular Oxygen Consumption Assay (ab197243) was used according to the protocol provided. The cells were incubated with glucose and glutamine free medium for 72 hours. Pre-warmed (37°C) fresh medium was added with the oxygen sensor and mineral oil was used to block the entry of oxygen from the surroundings. The OCR data was normalized to DAPI staining with the corresponding group of cells. 0.3 μM DAPI was incubated for 5 minutes after 15 minutes of 4% paraformaldehyde (PFA, Sigma-Aldrich) fixation. DAPI staining was measured at Ex/Em:364/454 wavelengths and the OCR was measured at Ex/Em:380/650 wavelengths with a Spectramax iD3 Microplate Reader (Molecular Devices). The cells were also treated with 1.5 μM Carbonyl cyanide-p-trifluoromethoxyphenylhydrazone (FCCP) for the calculation of spare reserve capacity (SRC). The OCR value of FCCP treated cells (maximal OCR) was divided by the OCR value of untreated

cells (basal OCR) at 10, 20 and 40 minutes. SRC was obtained by multiplying these values by 100 (Marchetti et al., 2020).

2.19 Metabolomics Assays

2.19.1 Sample Preparation

AKR1B10 expressing or control (EV) HuH-7 cells were seeded as 1,000,000 cells per T75. The cells underwent glucose and L-glutamine withdrawal for 72 hours, followed by treatment with the fatty acid oxidation inhibitor Etomoxir (5 µM) for 30 minutes. The concentration and duration of treatment were optimized using phosphorylation of ACC as a readout. Each group of cells were plated in five T75 flasks (five replicates) and incubated at 37°C. After each incubation, the cells were washed with isotonic (0.9%) sodium chloride (NaCl, Sigma-Aldrich) solution. 1 ml of ice-cold methanol:dH_2O (9:1) was added and the cells were quickly frozen in liquid nitrogen for 10-20 s. The cells were scraped in an extra 1 ml of ice-cold LC-MS grade methanol (Isolab) solution. A total 2 ml of cell lysate was collected into 2 ml Eppendorf tubes and centrifuged at 14,000 x *g* and 4°C for 30 minutes. 2 x 1 ml of clear supernatant was transferred into fresh Eppendorf tubes and the pellet was dissolved in RIPA buffer to measure the protein amounts (See the **Appendix B**). All samples were stored at -80°C.

2.19.2 Derivatization

1 ml supernatant from each sample was completely dried in a vacuum concentrator (Christ) at 4°C. 20 µl of 20 mg/ml methoxyamine hydrochloride (Sigma-Aldrich) in pyridine (Sigma-Aldrich) solution was added to each sample and incubated at 30°C for 90 minutes for methoximation. Next, 80 µl of N-Methyl-N-(trimethylsilyl)trifluoroacetamide (MSTFA) with 1% trimethylchlorosilane (1%

TMCS, Supelco) was added and incubated at 37°C for 30 minutes for silylation and derivatization as described previously (Eylem et al., 2021).

2.19.3 Gas Chromatography-Mass Spectrometer (GC-MS) Analysis

The derivatized samples were analyzed with a gas chromatography-mass spectrometer QP2010 Ultra system (Shimadzu) with a DB5-MS column (Agilent). The protocol was followed as described and optimized as previously (Eylem, 2022; Eylem et al., 2021). An autosampler (AOC-20, Shimadzu) was used for the sample injection. The column oven temperature was set to 60 °C and the injection temperature was set to 250 °C in a splitless injection mode. Helium was used a carrier gas in the experiment with a 1 ml/minute flow rate. Prior to the experiment, the flow of acetone (washing reagent) was tested. SIMCA (version 14.1) Multivariate Data Analysis Software (Umetrics AB) and Metaboanalyst (version 5.0, https://new.metaboanalyst.ca/MetaboAnalyst/home.xhtml) were used for the pathway analysis.

2.20 Statistical Analysis

All experiments were replicated at least twice independently unless otherwise indicated. Data analysis and graphing were carried out with GraphPad Prism version 8.0.1. $p<0.05$ was considered statistically significant. Student's t-test and ANOVA followed by Tukey's test were carried out according to the data.

CHAPTER 3

RESULTS

3.1 AKR Signature in Colorectal Cancer (CRC)

Colorectal cancer (CRC) is the third most common and second lethal cancer globally, according to Global Cancer Statistics 2020 (Sung et al., 2021). CRC develops from dysplastic adenomatous polyps in most cases. These polyps can lead to the development of adenocarcinoma after a multistep process, such as activation of oncogenes, inactivation of tumor suppressor genes, epigenetic changes, and alteration of DNA repair mechanisms (Ballinger & Anggiansah, 2007). The loss of genetic and epigenetic stability observed in most early neoplastic lesions accelerates the accumulation of mutations and clonal selection of most malignant cells (Kuipers et al., 2015). With the progression of CRC, alterations in EMT-related genes were observed *in silico*, along with shorter overall survival (OS) from publicly available databases (Busuioc et al., 2021).

We previously showed that high AKR1B1 and low AKR1B10 lead to increased cell motility and inflammation in CRC cells and that AKR1B1 and AKR1B10 can be used as potential biomarkers since they might be associated with poor prognosis in CRC (Taskoparan et al., 2017). Although AKR1B1 and AKR1B10 are both oxidoreductases, they differ in their preferred substrates. We reported that an AKR signature of high AKR1B1 expression and low AKR1B10 expression ($AKR1B1^{HIGH}$ and $AKR1B10^{LOW}$) was associated with poor overall survival (OS) (Demirkol-Canlı et al., 2020). The AKR signature ($AKR1B1^{HIGH}$ and $AKR1B10^{LOW}$) was also associated with worse recurrence-free survival in microsatellite stable (MSS) patients and patients with distal colon tumors compared to $AKR1B1^{LOW}$ and $AKR1B10^{HIGH}$ tumors. To address why the AKR signature

was associated with poor prognosis, we carried out a series of experiments using *ex vivo* colon and rectal tumor samples from patients with survival data.

Pathologically diagnosed tumor tissues from 32 colon cancer patients and 19 rectal cancer patients (Ankara cohort) were provided by Dr. İsmail Gömçeli and Dr. Nesrin Turhan and from the Department of Gastroenterological Surgery, Yüksek İhtisas Training and Research Hospital (Ankara, Türkiye) following informed consent from all patients. Total RNA was extracted from colon and rectal tissue specimens. The RNA was converted to cDNA and the expression of *AKR1B1* and *AKR1B10* was determined by RT-qPCR. The activation of EMT pathways is associated with poor prognosis; additionally, our previous data hinted at the activation of EMT pathways with the AKR signature (Taskoparan et al., 2017). Therefore, the expression of *CDH1* (E-Cadherin; epithelial marker) and *VIM* (Vimentin; mesenchymal marker) were determined and the geometric mean of internal controls *β-Actin* and *GAPDH* were calculated and used in fold change calculation using the Pfaffl method (Pfaffl, 2001).

We observed that the mRNA expression of *AKR1B1* in the colon and rectal tumor samples was significantly and positively correlated with the expression of *VIM* and negatively correlated (close to significance, p=0.058)) with the expression of *CDH1* (**Figure 3.1 A**). On the other hand, the expression of *AKR1B10* was significantly and negatively correlated with the expression of *VIM,* while it was significantly and positively correlated with *CDH1* expression (**Figure 3.1 B**).

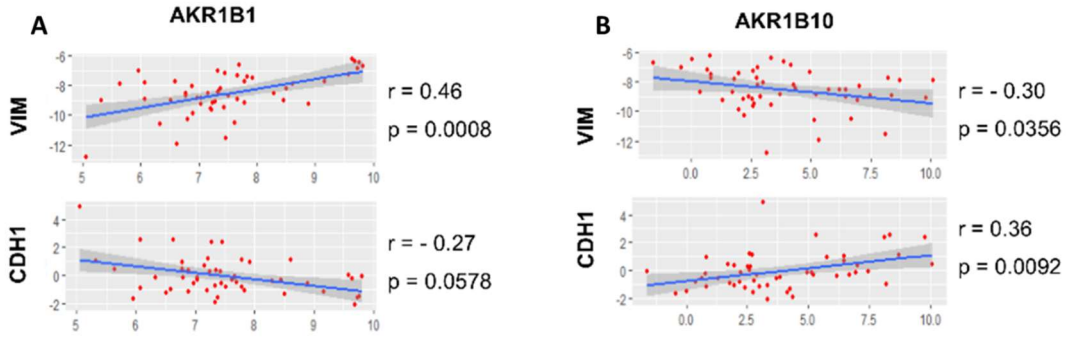

Figure 3.1 Correlation analysis of AKR1B1 and AKR1B10 with EMT markers.

AKR1B1, AKR1B10, CDH1 and VIM mRNA expression in Ankara Cohort (n=51) were determined by RT-qPCR. BT-20 cell line was included in each RT-qPCR to normalize the expression of each gene; however, the BT-20 expression data were not used for statistical analysis. ***A*** *and* ***B*** *present AKR1B1 and AKR1B10 correlation graphs, respectively. Spearman correlation r and p values were shown next to the respective graph.*

3.1.1 EMT Score Calculation in Ankara Cohort

EMT score is a quantitative mathematical scoring approach based on the expression levels of E-cadherin and Vimentin (Demirkol, 2018). The EMT score for the Ankara cohort was calculated according to expression values of *CDH1* and *VIM* levels and assigned between -2.0 to 0 range from the most epithelial to the most mesenchymal. Patient samples with higher EMT scores were categorized as mesenchymal and patients with lower EMT scores were correlated with more epithelial phenotype. The EMT score was generated by Dr. Seçil Demirkol-Canlı based on the mRNA expression of *CDH1* and *VIM* generated by qRT-PCR.

The EMT score of patients in the Ankara Cohort was positively correlated with AKR1B1 expression suggesting more mesenchymal (MES) phenotype in high AKR1B1 expressing tumors (**Figure 3.2 A**). On the other hand, AKR1B10^{HIGH} tumors showed lower EMT scores and a more epithelial (EPI) phenotype (**Figure 3.2 B**).

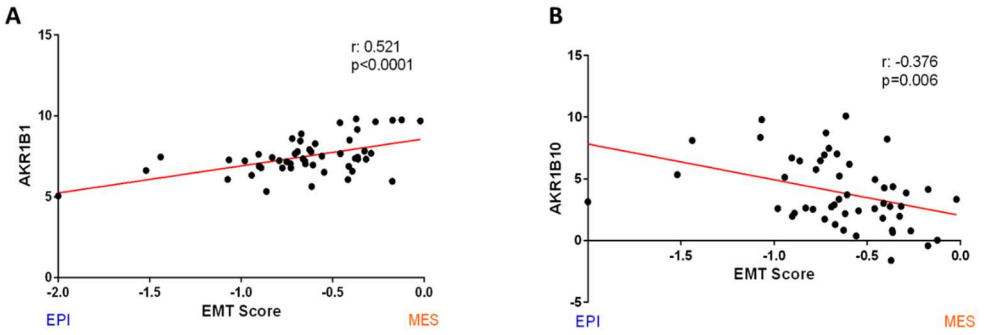

Figure 3.2 The EMT score of Ankara Cohort according to AKR1B1 and AKR1B10 expression.

*Linear correlation of log expression and EMT scores are shown for Ankara Cohort. Pearson r values and p values are indicated in respective graphs. Data for AKR1B1 and AKR1B10 are shown in **A** and **B**, respectively. EPI: Epithelial phenotype and MES: Mesenchymal phenotype.*

3.1.2 Ectopic Expression of AKRs in Colon Cancer Cell Lines

To delineate the signaling pathways associated with the EMT phenotype observed with the *ex vivo* analyses, we carried out a number of *in vitro* analyses. Colon cancer cell lines RKO and SW480 have a low endogenous expression of AKR1B1 and AKR1B10 (Taskoparan et al., 2017). A lentivirus mediated stable ectopic expression of AKR1B1 and AKR1B10 was carried out in these cell lines.

First, the expression of AKR1B1 and AKR1B10 in RKO and SW480 cell lines stably expressing either gene was confirmed at the RNA (**Figure 3.3**) and protein levels (**Figure 3.4**). Cycle threshold (Ct) values of AKR1B1, AKR1B10 and housekeeping *ACTB (β-Actin)* represented for RKO (**Figure 3.3A**) and SW480 (**Figure 3.3B**) colon cancer cell lines. Since there is high sequence similarity between AKR1B1 and AKR1B10, the expression of AKR1B1 in AKR1B10 expressing cells and AKR1B10 in AKR1B1 expressing cells was also determined. Based on the high Ct values, the gene specific primers were capable of successfully amplifying the target mRNA of interest.

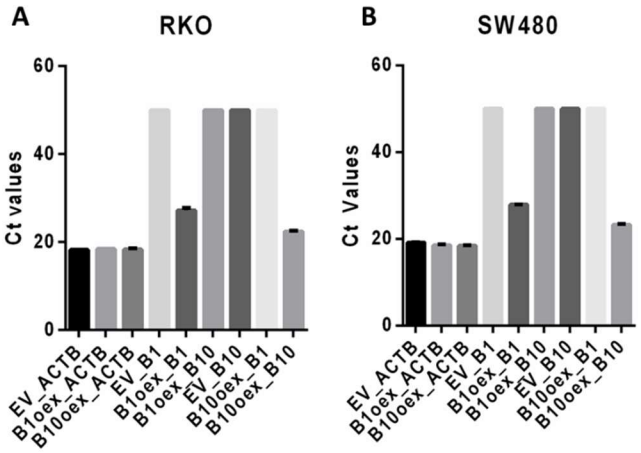

Figure 3.3 mRNA expression of *AKR1B1* and *AKR1B10* in ectopically AKR1B1 or AKR1B10 expressing RKO and SW480 cells.

*RT-qPCR was conducted with AKR1B1 and AKR1B10 primers in the RKO (**A**) and SW480 (**B**) cells ectopically expressing each gene. Ct values were depicted as a random value of 50 since the endogenous expression of each gene (reflected in EV_B1 and EV_B10) was beyond the detection limit (N/A). The samples are represented as EV (Empty Vector), B1oex (AKR1B1 expressing cells) and B10oex (AKR1B10 expressing cells).* ACTB *was used as an internal control.*

3.1.3 Signaling Pathways in AKR1B1 and AKR1B10 Expressing Colon Cancer Cell Lines

A Reverse Phase Protein Array (RPPA) carried out using protein samples from the tumors obtained from the Ankara Cohort indicated that $AKR1B1^{HIGH}$ and $AKR1B10^{LOW}$ (confirmed by RT-qPCR) showed aberrant activation of the metabolic AKT-GSK-3β pathway (Demirkol-Canlı et al., 2020). Evaluation of publicly available Reverse Phase Protein Array (RPPA) data from The Cancer Genome Atlas (TCGA) Colon Adenocarcinoma (COAD) and Rectal Adenocarcinoma (READ) cohort as well as CRC cell lines also indicated aberrant activation of nutrient sensing pathways (Demirkol-Canlı et al., 2020).

Gene expression-based consensus molecular subtypes (CMS) classification was conducted according to stratified AKR signature using publicly available microarray data from the dataset GSE39582 (Marisa et al., 2013). We observed that a majority of the AKR1B1^{LOW} and AKR1B10^{HIGH} tumors were categorized into CMS3, while AKR1B1^{HIGH} and AKR1B10^{LOW} tumors were associated with CMS4 (Demirkol-Canlı et al., 2020). The CMS3 class is associated with metabolic deregulation and the CMS4 class is characterized by EMT activation and mesenchymal phenotype (Guinney et al., 2015). In addition to the RPPA and western blot data shown below, these data strongly hinted at metabolic deregulation.

To further substantiate the *in silico* data, the expression and the activation (through phosphorylation) of several nutrient-sensing pathway proteins by western blot (**Figure 3.4**). p70S6K (ribosomal protein S6 kinase beta-1, or S6K1) is a serine-threonine kinase downstream mTOR (mammalian target of Rapamycin) protein. Phosphorylated p70S6K targets PDCD4 for ubiquitination and degradation. We observed a decrease in p70S6K phosphorylation at T389 and an increase in PDCD4 protein levels in AKR1B10 expressing cells, suggesting decreased signaling from p70S6K (**Figure 3.4 A and B**). Densitometric analysis indicating the high ratio of PDCD4/p-p70S6K reflecting the inhibition of p70S6K signaling with AKR1B10 expression is shown in **Figure 3.4 C** and **D** for RKO and SW480, respectively. In addition, AKR1B1 expressing cells also showed an increase in the PDCD4 protein expression, although the ratio of PDCD4/p-p70S6K was comparable to the EV cells. The high PDCD4 protein expression in the AKR1B1 expressing cells could have resulted from an increase in its mRNA expression rather than via post-translational regulation (Demirkol-Canlı et al., 2020). Of note, although the cells could successfully stably express AKR1B1 and AKR1B10, the AKR1B1 antibody could recognize another AKR1B1 member, possibly AKR1B10 (please see the AKR1B10 band with the AKR1B1 antibody in RKO cells).

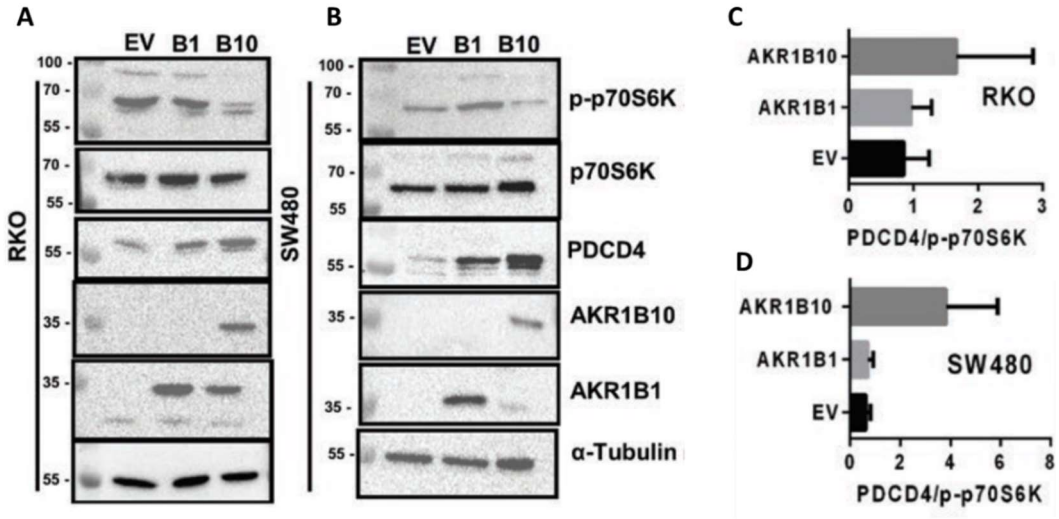

Figure 3.4 Western blot showing phosphorylation of p70S6K and PDCD4 levels in AKR1B1 and AKR1B10 expressing RKO and SW480 cells.

*Phosphorylation of p70S6K (at T389), total p70S6K, PDCD4, AKR1B10 and AKR1B1 levels were shown in **A** and **B** for RKO and SW480, respectively. EV represents empty vector cells and B1 and B10 represent ectopically AKR1B1 and AKR1B10 expressing corresponding colon cancer cell lines. α-Tubulin was used for loading control. 30 µg total protein was loaded for each cell line. **C** and **D** represent the densitometric analysis ratio of PDCD4 levels to phosphorylation levels of p70S6K. Data from three independent biological replicates were represented.*

I also examined the phosphorylation of AKT (T308), mTOR (S2481) and GSK-3β (S9) in RKO and SW480 cells ectopically expressing AKR1B1 and AKR1B10 (**Figure 3.5**). We observed modest and non-significant changes in the activation of AKT (T308) and GSK-3β (S9). The phosphorylation of mTOR was inhibited in RKO cells expressing AKR1B10 but activated in SW480 cells expressing AKR1B10. These data suggest that the tumor microenvironment may play a crucial role in the signaling mediated by AKR proteins, which cannot be taken into consideration *in vitro* experimental designs. Supporting this, our group has

observed remarkable expression of AKR1B1 in stromal cells, particularly cancer-associated fibroblasts and M2 macrophages (data not shown), which can strongly influence signaling via stromal-epithelial interactions.

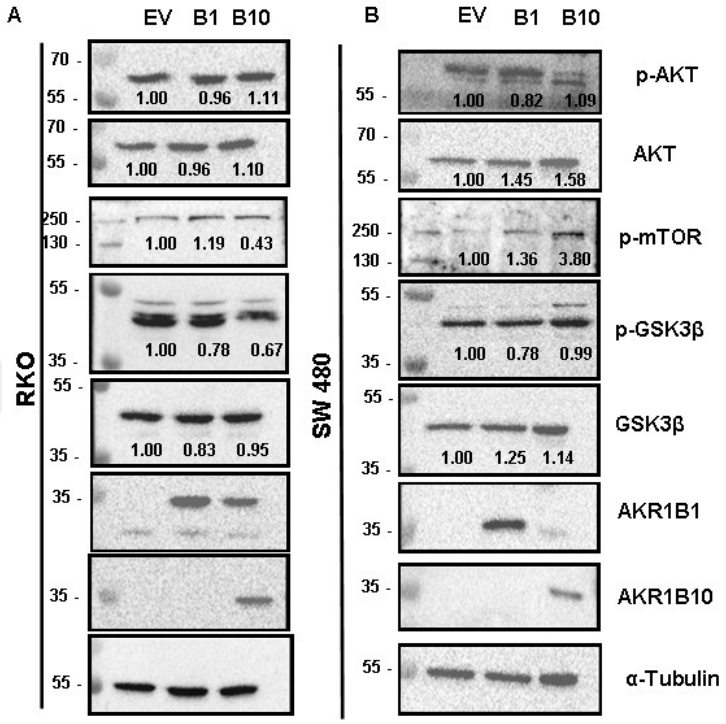

Figure 3.5 Western blot showing the AKT pathway proteins in AKR1B1 and AKR1B10 expressing CRC cell lines.

*Phosphorylation of AKT (at T308), mTOR (S2481), GSK-3β (S9) and total protein levels of AKT, GSK-3β, AKR1B1 and AKR1B10 were shown in **A** and **B** for RKO and SW480, respectively. EV represents empty vector cells and B1 and B10 represent ectopically AKR1B1 and AKR1B10 expressing corresponding colon cancer cell lines. α-Tubulin was used for loading control. 30 µg total protein was loaded for each cell line. Normalized densitometric analysis according to EV cells was shown under the corresponding samples.*

3.2 AKR1B10 Signaling and Metabolic Evaluation in Hepatocellular Carcinoma (HCC)

Data from *ex vivo* colon cancer samples (RPPA) as well as *in vitro* cell line data, along with our *in silico* analyses, strongly suggested a role of AKR1B10 in metabolism. The liver is the prime metabolic organ of the body; moreover, high AKR1B10 expression in liver hepatocellular carcinoma was shown to be associated with poor prognosis (Distefano & Davis, 2019). However, the signaling pathways that are activated in AKR1B10 expressing HCC cells have not been adequately evaluated (Banerjee, 2021; Distefano & Davis, 2019). Therefore, we aimed to examine mechanistically the metabolic pathways that are associated with AKR1B10 expression in HCC.

Liver cancer is the third leading cause of cancer death after lung and colorectal cancer (Sung et al., 2021). Primary liver cancer includes HCC, which is very common among primary hepatic malignancies (Clark et al., 2015), intrahepatic cholangiocarcinoma (iCCA) and other rare tumors (Sia et al., 2017). The worldwide incidence of HCC is estimated at 4.7% of all new cancer cases, contributing to 8.3% of all cancer-related deaths in 2020 (Pope et al., 2019; Sung et al., 2021). The liver is the center of primary metabolic activities such as lipid, glucose and cholesterol metabolism. Therefore, it is highly likely that aberrant metabolic pathways can contribute to cancer development in HCC (Zarrinpar, 2017).

To address my hypothesis that AKR1B10 expression in HCC may lead to aberrant metabolic signaling, I selected two HCC cell lines with low endogenous expression of AKR1B10 and distinctive metabolic properties. SNU423 cells are highly glycolytic and also rely on the Pentose Phosphate Pathway (PPP) for survival; in contrast, HuH-7 cells predominantly rely on fatty acid oxidation and glutaminolysis (Ye et al., 2023). We examined whether AKR1B10 expression in SNU423 cells was associated with the aberrant activation of the PPP and in HuH-7 cells was associated with enhanced fatty acid oxidation.

3.2.1 Evaluation of Pentose Phosphate Pathway and Metabolic Changes in SNU423 Cells

SNU423 cells rely on glycolysis and Pentose Phosphate Pathway (PPP) for survival and proliferation (Ye et al., 2023). I hypothesized that ectopic AKR1B10 expression in SNU423 cells was associated with the aberrant activation of PPP. This hypothesis stemmed from the ability of AKR1B10 to enzymatically use the reducing electrons from NADPH to sustain its oxidoreductase activity and the primary source of NADPH in the cell is the PPP. Moreover, *in silico* data generated from our lab suggested that the expression of AKR1B10 and the PPP enzyme Glucose-6-phosphate dehydrogenase (G6PD) were highly correlated (Sheraj, 2021).

3.2.1.1 Confirmation of Ectopic Expression of AKR1B10 in SNU423 Cells

SNU423 cells transduced with the EV (empty vector, control) or AKR1B10 lentiviruses and were selected for 72 hours with puromycin (2 µg/ml), by which time the wild-type (untransduced) cells were all dead. The surviving virus-transduced cells were collected as a polyclone, expanded in a maintenance dose of puromycin (1 µg/ml) and stored in the vapor phase of liquid nitrogen. The expression of AKR1B10 was confirmed with western blotting compared to EV and wild-type cells (**Figure 3.6**).

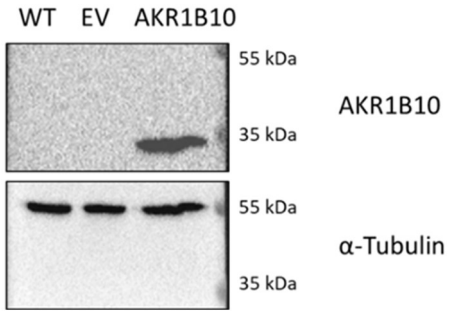

Figure 3.6 AKR1B10 expression in stably transduced polyclonal SNU423 cells compared to EV (control) and wild-type cells.

AKR1B10 protein level was evaluated in wild-type (WT), empty vector (EV) transduced and AKR1B10 transduced samples. α-Tubulin was used as a loading control. 15 µg total protein was loaded.

3.2.1.2 Evaluation of mRNA Levels of PPP Enzymes in AKR1B10 Expressing SNU423 Cells

mRNA expression of the PPP enzymes G6PD (Glucose-6-phosphate dehydrogenase), TKT (Transketolase) and TALDO1 (Transaldolase 1) were evaluated in EV (Empty Vector) transduced and AKR1B10 expressing SNU423 cells. No significant difference was observed in the transcript levels in both oxidative and non-oxidative branches of the PPP enzymes in AKR1B10 expressing SNU423 cells compared to EV cells (**Figure 3.7**).

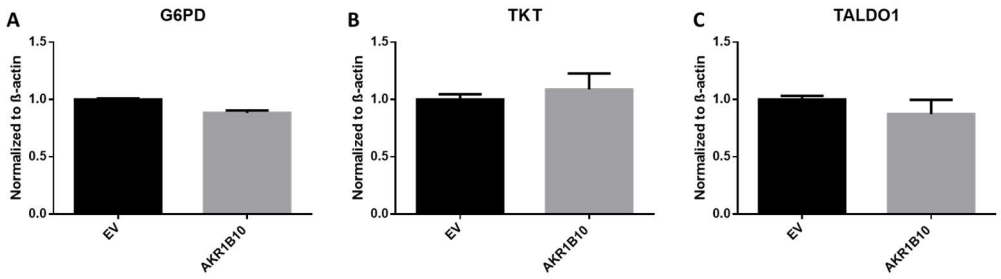

Figure 3.7 Transcript levels of the PPP enzymes in AKR1B10 expressing SNU423 cells compared to EV (control cells).

Results are represented as fold change with respect to control (EV) cells. β-actin was used as the housekeeping gene for normalization. 1 µg of cDNA was diluted to 1:10 for each replicate (5 ng in the reaction tubes). Data from two biological replicates are shown.

3.2.1.3 Evaluation of Protein Levels of PPP Enzymes in AKR1B10 Expressing SNU423 Cells

We next determined whether the expression of AKR1B10 can affect the protein expression of the PPP enzymes when the oxidative branch of the PPP, which generates NADPH, is inhibited. For this, SNU423 cells ectopically expressing AKR1B10 were treated with 6-aminonicotinamide (6-AN), which mainly inhibits the NADPH-generating enzymes, Glucose-6-Phosphate Dehydrogenase (G6PD) and 6-Phosphogluconate Dehydrogenase (GPGD). However, AKR1B10 expressing cells treated with increasing concentrations of the 6-AN (5 and 10 µM) did not significantly affect G6PD and TKT protein levels compared to EV cells (**Figure 3.8**).

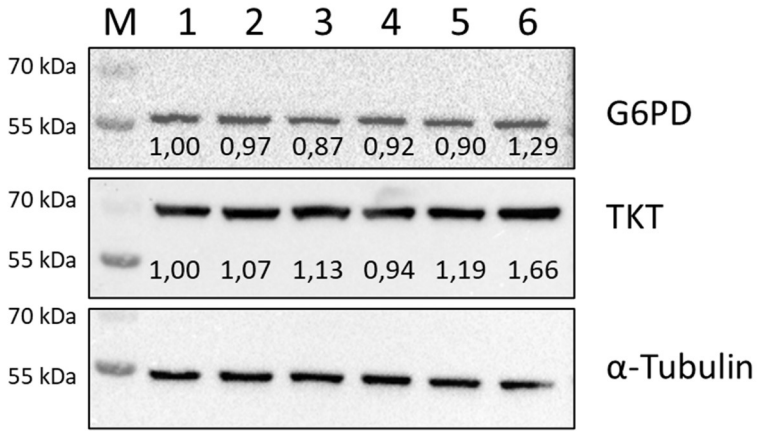

Figure 3.8 Evaluation of G6PD and TKT proteins in SNU423 cells stably expressing AKR1B10 in the presence of PPP inhibitor, 6-AN.

M represents the protein ladder. Lanes 1-6 correspond to: Empty Vector (EV) vehicle (DMSO) treated cells (1), EV cells treated with 5 µM 6-AN (2), EV cells treated with 10 µM 6-AN (3), AKR1B10 expressing vehicle-treated cells (4), AKR1B10 cells treated with 5 µM 6-AN (5), AKR1B10 expressing cells treated with 10 µM 6-AN (6). Densitometric analysis was carried out and written down for each sample. 30 µg protein was loaded and α-Tubulin was used as a loading control. Two biological replicates were carried out.

3.2.1.4 The Effect of PPP Inhibitor on Proliferation in AKR1B10 Expressing SNU423 Cells

The lack of any difference in the transcript and protein levels of the PPP enzymes with AKR1B10 expression in SNU423 cells suggested that AKR1B10 did not regulate the pathway at the expression level. However, we could not rule out whether AKR1B10 expression affected the enzymatic activities of the PPP proteins or whether the PPP was necessary for the survival of AKR1B10 expressing cells for NADPH generation.

We next evaluated whether inhibition of the PPP was a vulnerability in AKR1B10 expressing SNU423 cells. For this, a long-term clonogenic assay (colony formation assay) with AKR1B10 expressing SNU423 cells treated with 6-AN or vehicle (DMSO). We observed that SNU423 cells treated with 5μM 6-AN for the duration of the clonogenic assay (8 days) resulted in 100% cell death irrespective of the expression of AKR1B10 (data not shown). Treatment with 1 μM 6-AN did not lead to any cell death, suggesting that this drug concentration was ineffective. Treatment of the cells with 2 μM 6-AN resulted in a decrease in the number of colonies formed; however, contrary to our expectations, AKR1B10 expressing cells showed a significantly higher number of colonies when treated with 6-AN cells compared to the EV control cells (**Figure 3.9**). This suggests that although SNU423 cells were highly dependent on the PPP for survival (complete death with 5 μM 6-AN), the ectopic expression of AKR1B10 allowed the SNU423 cells to survive when the PPP was inhibited.

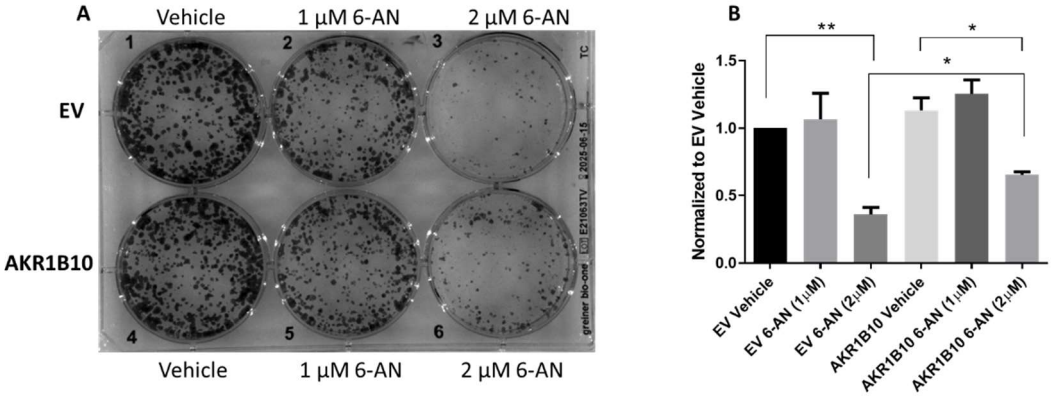

Figure 3.9 The colony formation ability of SNU423 stably expressing AKR1B10 in the presence of the PPP inhibitor 6-AN.

*(A) Fixed and stained colonies of SNU423 cells after colony formation assay for 8 days. The upper row corresponds to vehicle-treated EV cells (1), EV cells treated with 1 µM 6-AN (2) and EV cells treated with 2 µM 6-AN. The bottom row corresponds to vehicle-treated AKR1B10-expressing cells (4), AKR1B10-expressing cells treated with 1 µM 6-AN (5) and AKR1B10-expressing cells treated with 2 µM 6-AN (6), respectively. (B) Quantification of the colony formation data. The average of two independent biological replicates are shown. * $p<0.05$, t-test.*

3.2.1.5 Determination of AMPK Pathway in 6-AN Treated AKR1B10 Expressing SNU423 Cells

The AMP-activated Protein Kinase (AMPK) pathway is one of the key energy sensors in cells to maintain homeostasis by mediating decisions between the activation of anabolic and catabolic pathways in cells. NADPH is a co-factor that is primarily involved in anabolic pathways such as the synthesis of fatty acids. Therefore, the activation of AMPK was determined via phosphorylation at T172 in its α-subunit. AMPK is phosphorylated by an upstream kinase LKB1 primarily when the ATP/AMP ratio is low; however, activation is also known to occur via Ca^{2+}/calmodulin-dependent protein kinase kinase (CaMKK) (Herzig & Shaw, 2018). A major downstream target of AMPK is the protein Acetyl CoA

Carboxylase (ACC), which can get phosphorylated at S79 when AMPK is active. Of note, this is an inhibitory phosphorylation of ACC that inhibits lipid synthesis while activating fatty acid oxidation. We hypothesized that the inhibition of NADPH synthesis via the PPP leading to increased survival of AKR1B10 expressing cells could be related to the differential activation of the AMPK/ACC signaling axis. Therefore, we determined the phosphorylation of AMPK (T172) and ACC (S79) in AKR1B10 expressing SNU423 cells after 24 hours of 6-AN treatment (**Figure 3.10**). The phosphorylation of AMPK was high in both 6-AN treated and untreated cells and did not show any significant difference upon treatment. The phosphorylation of ACC was lower in AKR1B10 expressing cells compared to the control EV cells (**Figure 3.10**, please compare lanes 1 and 4); this low phosphorylation of ACC could be associated with high lipid synthesis in AKR1B10 expressing SNU423 cells. 6-AN treatment led to an increase in the phosphorylation of ACC in both EV and AKR1B10-expressing cells compared to the vehicle-treated cells. This suggests that the loss of NADPH synthesis (via the inhibition of PPP) could lead to a decrease in fatty acid synthesis in SNU423 cells. Of note, treatment of AKR1B10 expressing SNU423 cells with 10 μM 6-AN led to a significant increase in p-ACC compared to AKR1B10 vehicle cells (**Figure 3.10 Part B**). This suggested a stronger inhibition of fatty acid synthesis and activation of fatty acid oxidation when AKR1B10 expressing cells underwent an inhibition of the PPP, most likely due to the lower NADPH availability in the cytosol.

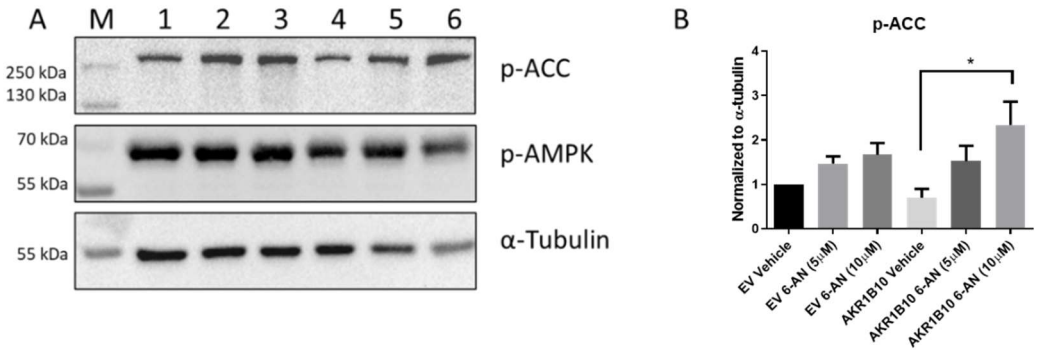

Figure 3.10 Determination of AMPK and ACC phosphorylation levels in 6-AN treated AKR1B10 transfected SNU423 cells.

*M represents the protein ladder. Part A: Lanes 1-6 correspond to: Empty Vector (EV) vehicle-treated cells (1), EV cells treated with 5 µM 6-AN (2), EV cells treated with 10 µM 6-AN (3), AKR1B10 expressing vehicle-treated cells (4), AKR1B10 cells treated with 5 µM 6-AN (5), AKR1B10 expressing cells treated with 10 µM 6-AN (6). All treatments were carried out for 24 hours. 30 µg protein was loaded and α-Tubulin was used as a loading control. Part B: Densitometric analysis for p-ACC (phosphorylation of ACC). The average of two biological replicates is shown. *p<0.05, one-way ANOVA followed by Tukey's multiple comparison test.*

3.2.1.6 NADPH/NADP Ratio in AKR1B10 Expressing SNU423 Cells

Since we observed a decrease in p-ACC in AKR1B10 expressing cells and a strong increase in p-ACC when the AKR1B10 expressing cells were treated with 6-AN, this suggested a role of AKR1B10 in lipid metabolism (synthesis or oxidation). We first determined the cellular NADPH/NADP ratio in AKR1B10 expressing cells compared to control EV, along with AKR1B10 expressing cells or control EV cells treated with 6-AN. We observed no major difference in the NADPH/NADP ratio between AKR1B10 and EV cells. However, the AKR1B10 expressing cells treated with 6-AN showed a consistent and replicable increase in NADPH/NADP ratio compared to the EV cells treated with 6-AN (**Figure 3.11**). This was unexpected; however, it needs to be remembered that there are multiple sources of NADPH in the cytosol (in addition to the PPP), such as the malic enzyme 1 (ME1) which catalyzes the reversible oxidative decarboxylation of malate to pyruvate, or isocitrate dehydrogenase 1 (IDH1) which catalyzes the reversible oxidative decarboxylation of isocitrate to yield α-ketoglutarate. It is feasible that HCC cells have high metabolic plasticity; therefore, inhibition of one pathway could lead to the activation of alternate NADPH-generating pathways. Additionally, the NADPH/NADP Assay kit measures both cytosolic and mitochondrial levels of the cofactor. Comparable levels of NADPH can also be synthesized in the

mitochondria via serine-driven one-carbon metabolism, in which methylene tetrahydrofolate is oxidized to 10-formyl-tetrahydrofolate and the electrons are accepted by NADP to generate NADPH (Fan et al., 2014). In fact, serine driven synthesis of NADPH was recently shown to be the predominant NADPH synthesizing pathway in the liver (Z. Zhang et al., 2021). The high NADPH/NADP ratio in the AKR1B10 expressing cells treated with 6-AN may be associated with higher mitochondrial synthesis of NADPH. A high cytosolic NADPH/NADP ratio may favor increased biosynthesis of fatty acids (via shuttling of electrons to the cytosol), while a high cytosolic and mitochondrial NADPH/NADP ratio can activate the GSH/GSSG (glutathione) endogenous antioxidant system that is found in both cytosol and mitochondria. The activation of both or either of these pathways may have led to an increase in the survival of AKR1B10 expressing SNU423 cells treated with 6-AN (**Figure 3.9**).

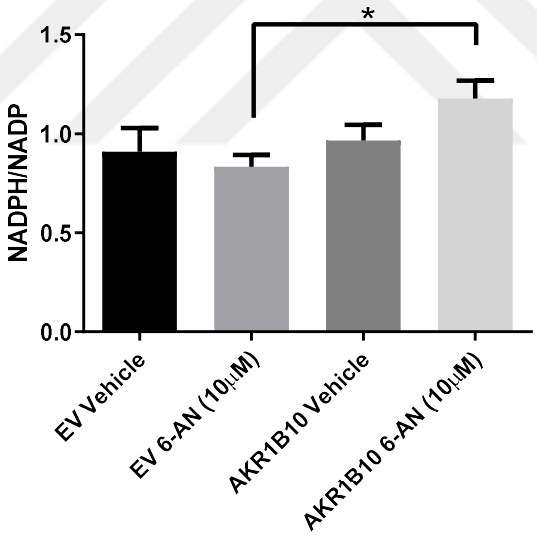

Figure 3.11 Determination of NADPH/NADP ratio in AKR1B10 expressing SNU423 cells.

AKR1B10 expressing or EV (Empty Vector) transfected cells were treated with 5 or 10 μM 6-AN for 24 hours and then processed for NADP/NADPH assay. The manufacturer's protocol was followed. Data were analyzed with two independent

*biological replicates. *p<0.05, one-way ANOVA followed by Tukey's multiple comparison test.*

3.2.1.7 Effect of Hypoxia on the Activation of ACC and AMPK in SNU423 Cells Expressing AKR1B10

Enhanced fatty acid synthesis in cancer cells has numerous functions, including the synthesis of phospholipids (biomass) for the generation of membranes in rapidly proliferating cells as well as second messengers (such as diacylglycerol) that are essential signaling molecules (Koundouros & Poulogiannis, 2020). Additionally, the synthesized lipids may provide an essential source of nutrients, particularly under hypoxic stress and/or glucose deficiency (Koundouros & Poulogiannis, 2020). We, therefore, incubated SNU423 cells expressing AKR1B10 or EV with 10 μM 6-AN or vehicle in hypoxia (1% oxygen) and normoxia (21% oxygen). We observed that SNU423 cells responded to the inhibition of PPP under hypoxic stress by remarkably increasing the phosphorylation of ACC in both EV and AKR1B10 cells; however, the increase in p-ACC in the EV cells was nearly twice that of the AKR1B10 expressing cells. Similarly, treatment of SNU423 cells with 6-AN under normoxia also led to an increase in p-ACC in both AKR1B10 expressing and control cells; however, the increase in p-ACC in control (EV) cells was, again, nearly twice that of the AKR1B10 expressing cells (**Figure 3.12**). A concomitant increase in phosphorylation of AMPK was also observed. Of note, AKR1B10 expressing cells showed decreased p-ACC levels under normoxia compared to the control EV cells. These data point suggest that synthesized lipids may indeed be used for energy purposes under hypoxic stress, particularly when cellular sources of NADPH are low. It has previously been shown that fatty acid oxidation is possible even with 1% oxygen (Frezza et al., 2011). Nonetheless, AKR1B10 expressing cells did not activate p-ACC to the same extent as the control cells, suggesting that these cells may have the metabolic plasticity to utilize alternative fuel sources such as glucose under both hypoxia and normoxia.

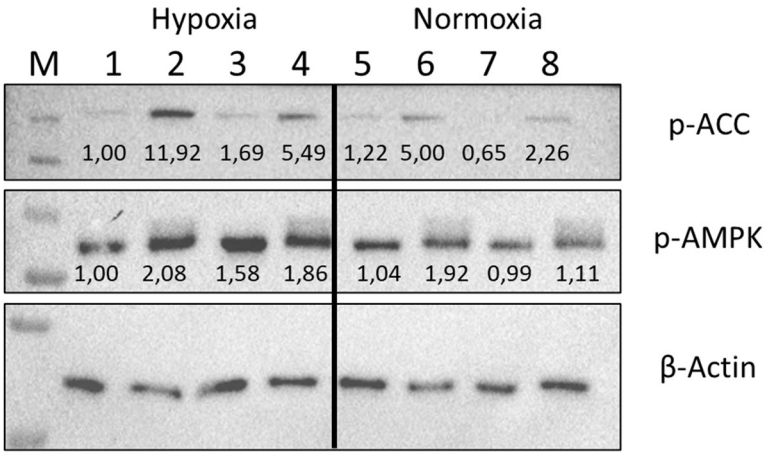

Figure 3.12 Determination of AMPK and ACC phosphorylation levels with 6-aminonicotinamide (6-AN) treatment under hypoxic conditions.

M represents the protein ladder. Lane 1 and 2 indicate vehicle (DMSO) and 10 μM 6-AN treated empty vector (EV) cells in hypoxia and lane 5 and 6 indicate vehicle (DMSO) and 10 μM 6-AN treated empty vector (EV) cells in normoxia, respectively. Lane 3 and 4 indicate the AKR1B10 expressing cells treated with vehicle (DMSO) and 10 μM 6-AN in hypoxic conditions. Lane 7 and 8 indicate the AKR1B10 expressing cells treated with vehicle (DMSO) and 10 μM 6-AN in normoxia, respectively. All treatments and hypoxia were carried out for 24 hours. 15 μg protein was loaded and β-actin was used as a loading control.

3.2.1.8 Effect of Glucose Deprivation on the Activation of ACC and AMPK in SNU423 Cells Expressing AKR1B10

We next evaluated whether the stress of glucose deprivation in a glycolytic cell line such as SNU423 could affect the p-ACC levels in AKR1B10 expressing SNU423 cells. In this experiment, we did not use the PPP inhibitor 6-AN since the lack of glucose in the culture medium was expected to prevent any shunting of glucose-6-phosphate into the PPP. Gluconeogenesis can occur in liver cells; however, most HCC cells undergo incomplete gluconeogenesis where the end product is not glucose; rather, it is the glycolytic intermediates that are used for biomass

generation (Grasmann et al., 2019). Cancer cells are also highly reliant on the non-essential amino acid glutamine, which can be used for the synthesis of α-ketoglutarate for anaplerosis into the TCA cycle for the synthesis of NADPH and glutathione (Jonghwa Jin et al., 2023). Therefore, we also examined whether glutamine deprivation could lead to the differential regulation of energetics in AKR1B10 versus control (EV) cells. As a readout of glucose and glutamine deprivation, we examined the mTOR pathway, which is known to be exquisitely sensitive to glucose and amino acid availability and can regulate fatty acid metabolism (Koundouros & Poulogiannis, 2020).

We observed that phosphorylation of ACC, AMPK and mTOR targets (p70S6K and 4EB-P1) did not show any significant difference in phosphorylation between EV and AKR1B10 expressing SNU423 cells grown in complete medium in both hypoxia and normoxia (**Figure 3.13**). L-glutamine starvation, however, resulted in a greater activation of the mTOR pathway (via phosphorylation of p70S6K and 4EBP1) in AKR1B10 expressing cells grown under hypoxia (compare Lane 2 and 5). More importantly, glucose starvation (compare Lane 3 and 6) resulted in a greater inhibition of the mTOR pathway in AKR1B10 expressing cells under both hypoxia and normoxia. These data suggest that the AKR1B10 cells are highly reliant on the availability of glucose in SNU423 cells, which can be used for both energy generation and biomass synthesis, such as fatty acids.

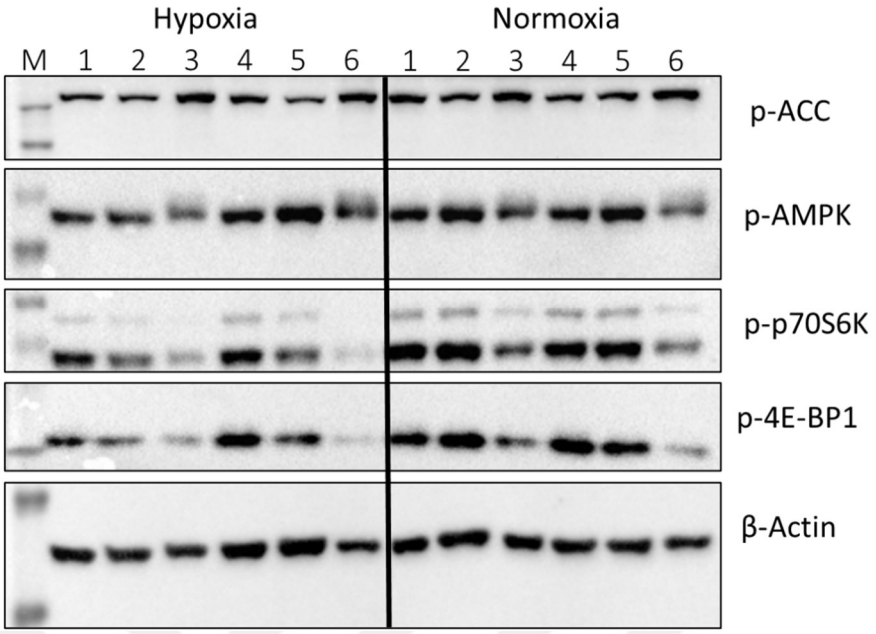

Figure 3.13 Determination of nutrient withdrawal effects on AMPK, ACC and p70S6K pathways under hypoxic conditions.

M represents the protein ladder. Lane 1 and lane 4 indicate the empty vector (EV) cells and AKR1B10 expressing cells incubated with complete medium, respectively. Lane 2 and lane 5 indicate the empty vector (EV) cells and AKR1B10 expressing cells incubated with no L-glutamine (0 mM), respectively. Lane 3 and lane 6 indicate the empty vector (EV) cells and AKR1B10 expressing cells incubated with no glucose (0 g/L), respectively. Hypoxic and normoxic conditions are indicated in the figure and the same loading order is valid for both conditions. All treatments and hypoxia were carried out for 24 hours. 15 µg protein was loaded and β-actin was used as a loading control.

3.2.1.9 Effect of AKR1B10 Expression on Citrate Synthase Activity in SNU423 Cells Expressing AKR1B10

Acetyl CoA levels are a robust indicator of fatty acid synthesis in cells (Xiao et al., 2018). Citrate synthase (CS) is an enzyme of the TCA cycle that catalyzes the aldol condensation of oxaloacetate (4 carbon) with two carbons from acetyl CoA to give citrate (6 carbon) in the TCA cycle (Akram, 2014). The source of acetyl CoA (which cannot cross the inner mitochondrial membrane) is pyruvate, which is usually generated via glycolysis and can cross the inner mitochondrial membrane. Pyruvate undergoes a reductive decarboxylation into acetate; the latter is then converted to acetyl CoA in the mitochondria. The citrate generated from oxaloacetate in the TCA cycle can cross the inner mitochondrial membrane to the cytosol via the mitochondrial citrate carrier (CIC, SLC25A1) where it can be broken down to oxaloacetate and acetyl CoA. The oxaloacetate can be converted to malate, via malate dehydrogenase, generating NADPH and malate can re-enter the mitochondria via the CIC. (Williams & O'Neill, 2018). The acetyl CoA in the cytosol can be converted to malonyl CoA with the enzyme ACC, which in turn can be catalyzed by fatty acid synthase (FASN) for the synthesis of fatty acids. Therefore, citrate can link glycolysis with fatty acid synthesis and increased citrate synthase activity can be indicative of fatty acid synthesis in the cell.

We examined the activity of the citrate synthase enzyme. For this, we incubated whole cell lysate from SNU423 cells expressing AKR1B10 or control with exogenous oxaloacetate and citrate synthase. The acetyl CoA needed for the reaction came from the cell. Thus, high citrate synthase activity would be indicative of the high availability of acetyl CoA and, therefore, citrate in the cell. Measurement of the change in absorbance at 412 nm indicated that the absorbance was modestly but consistently higher in SNU423 cells expressing AKR1B10 compared to control (EV) cells (**Figure 3.14**). Determination of the Kcat value suggested that the Kcat value of citrate synthase was 0.8 s^{-1} in the AKR1B10 expressing cells and 0.7 s^{-1} in the EV transfected cells. In the second biological

replication, the Kcat value for AKR1B10 expressing cells were 0.009 s^{-1} and 0.004 s^{-1} in EV cells (data not shown).

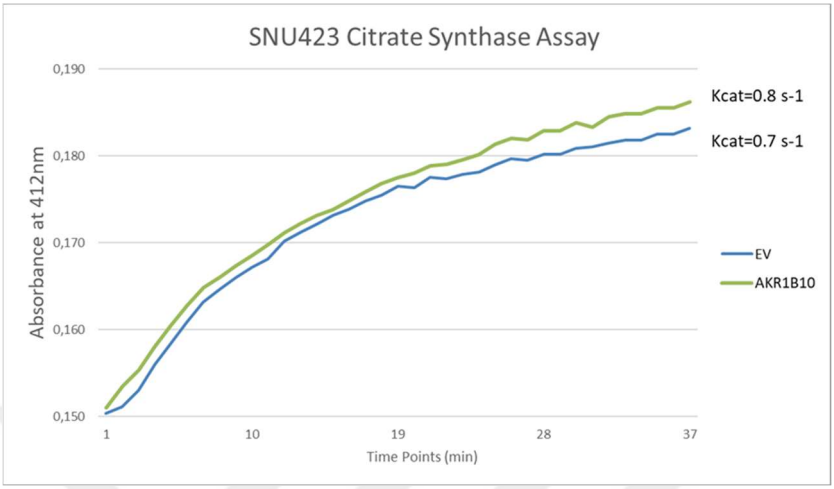

Figure 3.14 Citrate Synthase Assay in AKR1B10 expressing SNU423 cells.

1,000,000 SNU423 cells expressing AKR1B10 or transfected with the EV (control) were lysed. 10 µl of this lysate was incubated with 90 µl of a reaction mixture containing Ellman's reaction, oxaloacetate and citrate synthase as described in the Materials and Methods part. The endogenous acetyl CoA of the cell was used for the reaction. Absorbances at 412 nm were shown for 40 minutes. Two independent biological replicates were carried out, but only one replicate was shown.

3.2.1.10 Effect of AKR1B10 Expression on ROS Levels in SNU423 Cells Expressing AKR1B10

The high NADPH/NADP ratio and increased cell survival we observed in SNU423 cells expressing AKR1B10 and treated with 6-AN could be ascribed to an enhanced antioxidant response in the cells as well. Preliminary bioinformatics analyses carried out in our lab using differential expression analysis between $AKR1B10^{HIGH}$ and $AKR1B10^{LOW}$ LIHC samples from the TCGA database resulted in 100 oxidative stress related genes that were differentially expressed with statistical significance (FDR < 0.05, LFC > 0.5). The heatmap (**Figure 3.15**) shows

that the genes involved in oxidative stress response were consistently upregulated in AKR1B10^{HIGH} samples (most AKR1B10^{HIGH} samples were in the outlined cluster). These data were generated by Dr. Ilir Sheraj.

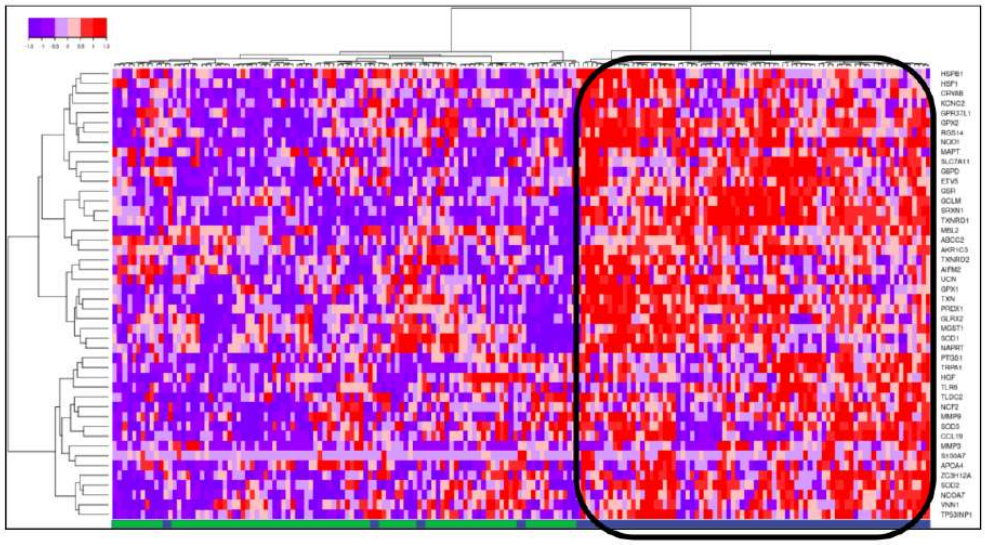

Figure 3.15 Heatmap showing genes upregulated in AKR1B10^{HIGH} LIHC tumors. *The bottom bar shows sample classification with blue representing AKR1B10^{HIGH} and green AKR1B10^{LOW} samples. The AKR1B10^{HIGH} samples with high expression of antioxidant genes were found in the outlined cluster. The heatmap was constructed using the heatmap.2 function from the gplot package in R with Euclidean distance and Ward.d2 linkage. This analysis and the figure were generated by Ilir Sheraj.*

We next examined whether the ROS levels were altered in AKR1B10 expressing or control SNU423 cells treated with 6-AN or vehicle. We observed significantly high ROS levels in AKR1B10 expressing cells compared to control (EV) (**Figure 3.16**). This high ROS level could be related to the consumption of cytosolic NADPH by the enzymatic function of AKR1B10, which can lead to decreased regeneration of reduced glutathione in the endogenous antioxidant pathway. It is also feasible to speculate that the upregulation of ROS mitigation genes in

AKR1B10^{HIGH} LIHC tumors (**Figure 3.15**) could be a response to high ROS levels in these cells. Of note, we did not observe any difference in the NADPH/NADP ratio between AKR1B10 and EV cells (**Figure 3.11**). However, the NADPH/NADP assay kit does not distinguish between mitochondrial and cytosolic NADPH. Therefore, it is possible that NADPH levels in the cytosol, where the AKR1B10 enzyme is localized, may be low but cannot be separately detected by the kit.

Both control and AKR1B10 expressing SNU423 cells showed an increase in ROS levels with increasing concentrations of 6-AN. This is expected since 6-AN is a strong inhibitor of the PPP, the primary NADPH generating pathway in the cells. Lower NADPH levels are generally associated with oxidative stress due to decreased regeneration of reduced glutathione in the endogenous antioxidant pathway. However, we did not observe any significant difference in the ROS levels between 6-AN treated AKR1B10 expressing cells versus controls.

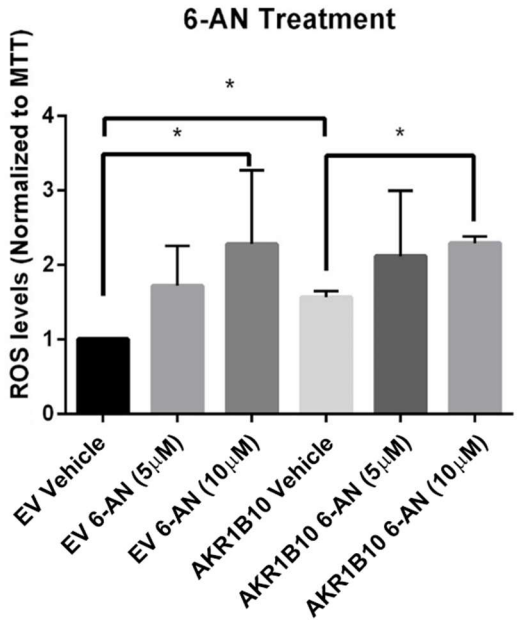

Figure 3.16 ROS levels in AKR1B10 expressing cells treated with 6-AN.

*AKR1B10 or empty vector (EV) transfected SNU423 cells were treated with 5 or 10 µM 6-aminonicotinamide (6-AN) or DMSO (vehicle control) for 24 hours. Dihydroethidium (DHE) assay was carried out in a fluorescent microplate reader. Results are represented as fold change with respect to the vehicle treated control (EV) cells. *p<0.05, t-test.*

Overall, my data suggest that AKR1B10 expression in a highly glycolytic cell line SNU423 did not lead to any remarkable alteration in proliferation. We did not observe any direct effect of AKR1B10 on the expression of the PPP enzymes. Rather, we observed unexpectedly that AKR1B10 expressing cells treated with 6-AN to inhibit the PPP resulted in a high NADPH/NADP ratio and high survival, hinting at the activation of alternative pathways for NADPH generation, ROS mitigation and survival and highlighting a strong metabolic plasticity in these cells. We have also observed a strong possibility of the activation of fatty acid synthesis in AKR1B10 expressing SNU423 cells, suggesting that biomass-generating pathways were enriched with AKR1B10 expression. Moreover, we observed high total ROS levels with AKR1B10 expression, which could be associated with the upregulation of ROS mitigation genes observed in $AKR1B10^{HIGH}$ LIHC tumors.

3.2.2 Evaluation of Metabolic Pathways in HuH-7 Cells Expressing AKR1B10

HuH-7 cells are highly oxidative cells that are not reliant on glucose as their primary source of energy (Ye et al., 2023). A colony formation assay carried out in our lab suggested a nearly complete loss of colonies when HuH-7 cells were grown in a medium containing high (4.5 g/L) glucose (data not shown). HuH-7 cells were also not sensitive to the loss of L-glutamine in the colony formation assay (data not shown). This suggests that HuH-7 cells may rely more on other nutrient sources, such as fatty acids and amino acids for energy generation and biomass production.

AKR1B10 expression in breast cancer cells was shown to activate fatty acid oxidation (FAO), which could lead to an increase in lung metastasis (van Weverwijk et al., 2019). Additionally, our data suggest the activation of lipid metabolism in SNU423 cells.

I hypothesized that AKR1B10 expression in HuH-7 cells enhanced their reliance on FAO. Since liver cells are metabolically highly active and plastic, simple inhibition of FAO in AKR1B10 expressing or control cells was unlikely to enhance any metabolic vulnerability of HuH-7 cells expressing AKR1B10. We, therefore, withdrew both glucose and L-glutamine from the culture medium. Glucose is a major source of energy in most cancer cells. Although HuH-7 cells are mainly oxidative, they do require glycolysis for the generation of metabolic intermediates. In fact, a long-term colony formation assay indicated that HuH-7 cells formed very few colonies when the cells were incubated in both low and high glucose-containing medium. Additionally, the colony formation assay also indicated that although the loss of L-glutamine alone from the medium did not affect cell viability, the withdrawal of both glucose and L-glutamine was highly detrimental to cell viability (data not shown). Therefore, we incubated HuH-7 cells stably expressing AKR1B10 or EV in glucose and L-glutamine free medium. In such cells, reliance on lipids is more likely for energy production and biomass generation for cell survival and proliferation.

Carnitine palmitoyl transferase 1 (CPT1) is an enzyme found in the outer membrane of the mitochondria to transport long-chain fatty acids by forming acylcarnitines (Guerra et al., 2022), which is required for fatty acid oxidation (FAO). Etomoxir is an irreversible CPT1 inhibitor that is widely used for the chemical inhibition of FAO. To further substantiate whether AKR1B10 expressing HuH7 cells were reliant on FAO, we treated the cells with etomoxir after long-term (72 hours) glucose and L-glutamine starvation.

3.2.2.1 Effects of Nutrient Restriction and Etomoxir Treatment on Cellular Proliferation

We first carried out an MTT assay to observe whether AKR1B10 expressing cells were more susceptible to the FAO inhibitor etomoxir after 72 hours of glucose and glutamine withdrawal. For this, cells were seeded in a 96-well plate and incubated with the glucose and glutamine free medium for 72 hours. This long duration of incubation was necessary to ensure that any glycogen stores in the cells are utilized via glycogenolysis. The cells were then incubated for an additional 48 hours in the presence of 5 μM etomoxir. At the end of the 120 hours of incubation, an MTT assay was carried out. Glucose and L-glutamine starved AKR1B10 expressing HuH-7 cells showed significantly less survival than EV cells. No further loss of survival, however, was observed with etomoxir treatment in AKR1B10 expressing cells compared to the corresponding control cells (**Figure 3.17**).

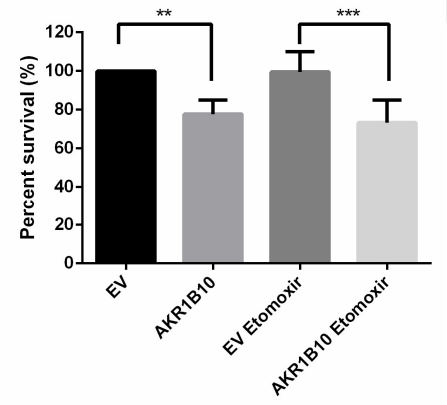

Figure 3.17 Effects of glucose and L-glutamine withdrawal and etomoxir treatment on cellular proliferation.

*The cells were incubated with 0 g/L glucose and 0 mM L-glutamine containing nutrient restriction medium for 72 hours, followed by 48 hours of 5 μM etomoxir treatment in the nutrient restriction medium. The survival of the samples was normalized to EV (empty vector) and percent survival is shown. Three independent biological replicates and two-way ANOVA were carried out. **p<0.01, ***p<0.001.*

3.2.2.2 Effects of Nutrient Restriction and Etomoxir Treatment on Energy-Sensing Pathways in AKR1B10 Expressing HuH-7 Cells

We next evaluated whether AKR1B10 expressing HuH-7 cells activated nutrient sensing pathways when nutrients were withdrawn. For this, AKR1B10 expressing cells and control cells were incubated with no glucose medium for 72 hours or no glucose medium for 48 hours and for an additional 24 hours with no glucose and no L-glutamine medium. After 72 hours of nutrient withdrawal, the cells were incubated with 100 μM etomoxir for 30 minutes and collected for western blotting (**Figure 3.18**). AKR1B10 expressing cells showed an increase in the phosphorylation of both AMPK and its downstream target ACC with glucose withdrawal, glucose withdrawal +etomoxir and glucose + L-glutamine withdrawal, compared to corresponding EV cells (**Figure 3.18 Lane 4, 6 and 8**). In addition, only AMPK phosphorylation was observed in etomoxir treated AKR1B10 expressing cells after 48 hours of glucose and 24 hours of glucose and L-glutamine starvation (**Figure 3.18 Lane 10**). These data suggest the activation of nutrient sensing with AKR1B10 expression in HuH-7 cells.

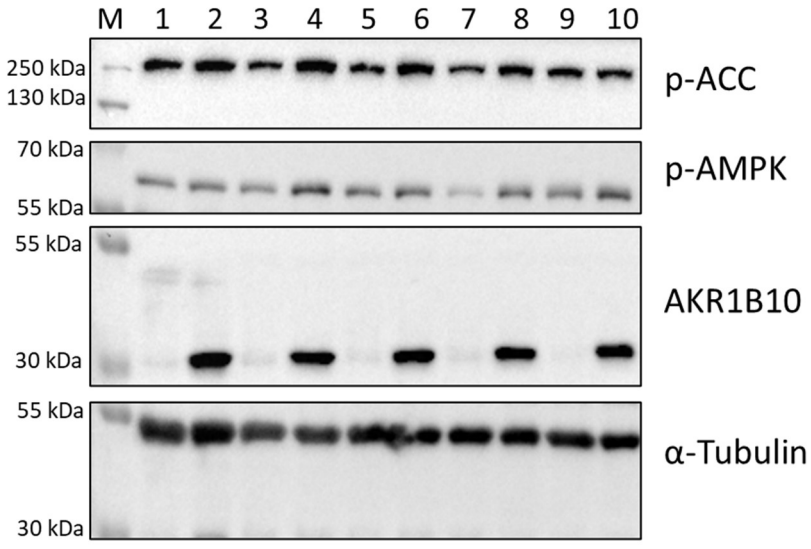

Figure 3.18 Phosphorylation of AMPK and ACC in AKR1B10 expressing HuH-7 cells after glucose and/or L-glutamine starvation.

M represents the protein ladder. Lanes 1-2 correspond to Empty Vector (EV) and AKR1B10 expressing cells incubated in a complete medium for 72 hours, respectively. Lane 3 corresponds to EV and lane 4 corresponds to AKR1B10 expressing cells incubated with 0 g/L glucose-containing medium for 72 hours. Lanes 5-6 represent EV and AKR1B10 expressing cells incubated with 100 µM etomoxir for 30 minutes after 72 hours of glucose withdrawal, respectively. Lanes 7 and 8 represent EV and AKR1B10 expressing cells incubated with 48 hours of 0 g/L glucose supplemented medium and 24 hours of 0 g/L glucose and 0 mM L-glutamine supplemented medium, respectively. Lane 9 (EV) and 10 (AKR1B10 expressing) represent cells incubated with 30 minutes of 100 µM etomoxir after 48 hours of 0 g/L glucose supplemented medium and 24 hours of 0 g/L glucose and 0 mM L-glutamine supplemented medium. 15 µg protein was loaded and α-Tubulin was used as a loading control. One biological replicate is shown here.

3.2.2.3 Untargeted Metabolomics in AKR1B10 Expressing HuH-7 Cells Under Nutrient Stress

The preferential phosphorylation of the nutrient-sensing protein AMPK and its downstream target ACC with AKR1B10 expression and withdrawal of various nutrients reaffirmed our hypothesis that metabolic pathways could be aberrantly regulated in these cells. To better substantiate our hypothesis, an untargeted metabolomics study was carried out with AKR1B10 expressing HuH-7 cells after 72 hours of glucose and glutamine starvation, followed by 30 minutes of treatment with 5 µM etomoxir. The analysis was carried out in collaboration with Dr. Emirhan Nemutlu and Dr. Cemil Can Eylem (Hacettepe University, Ankara). SIMCA Multivariate Data Analysis Software (Umetrics AB) and Metaboanalyst were used for the pathway analysis described in Materials and Methods.

3.2.2.3.1 Principal Component Analysis of Untargeted Metabolomics of All Samples

Principal component analysis (PCA) is a mathematical dimensionality reduction tool that can be used to reduce a large number of data sets. PCA is a widely used easy method in metabolomics analysis; however, it is not based on a statistical model (Nyamundanda et al., 2010). A graph was projected to cluster EV, AKR1B10 expressing cells, etomoxir treated EV, and etomoxir treated AKR1B10 expressing HuH-7 cells after 72 hours of glucose and L-glutamine starvation (**Figure 3.19**). At least five biological replicates were carried out for each untreated or treated sample. Each sample showed distinct and adjacent clusters, indicating minimal variation in the normalization of the raw data.

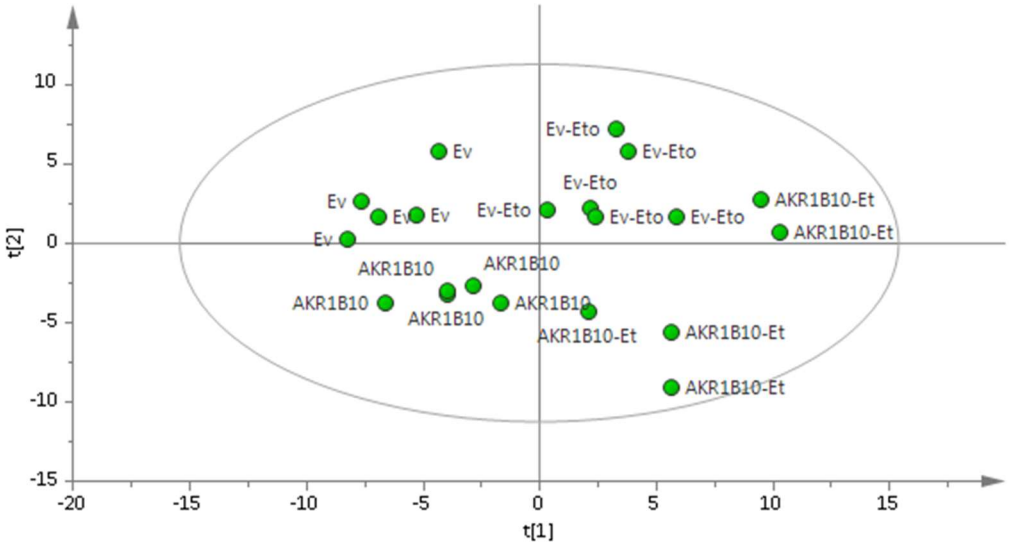

Figure 3.19 PCA score plot of untargeted metabolomics data of HuH-7 cells.

EV: Empty Vector cells, EV-Eto: EV cells were incubated with 5 µM etomoxir treatment for 30 minutes, AKR1B10: AKR1B10 expressing cells, AKR1B10-Et: AKR1B10 expressing cells were incubated with 5 µM etomoxir for 30 minutes. All cells were incubated with 0 g/L glucose and 0 mM L-glutamine for 72 hours before etomoxir or vehicle (water) treatment.

3.2.2.3.2 Partial Least Squares-Discriminant Analysis (PLS-DA) of Untargeted Metabolomics of All Samples

Partial least squares-discriminant analysis (PLS-DA) is a supervised machine learning tool and a method similar to the PCA for categorizing high throughput data. PLS-DA is one of the standard methods used in omics data analysis for better data projection (Ruiz-Perez et al., 2020). R^2 is the coefficient of determination and Q^2 is the model's predictability (Özen, 2019). A higher value of R^2 and Q^2 suggests that the model is predictable and fitted (high-quality separation) (Westerhuis et al., 2008). The model is significant and accurate if the R^2 and Q^2 values are higher than 0.5 (Eylem, 2022). The PLS-DA plot for the untargeted metabolomics data obtained from the HuH-7 cells showed an R^2= 0.973 and Q^2= 0.846 (**Figure 3.20**), suggesting a valid model.

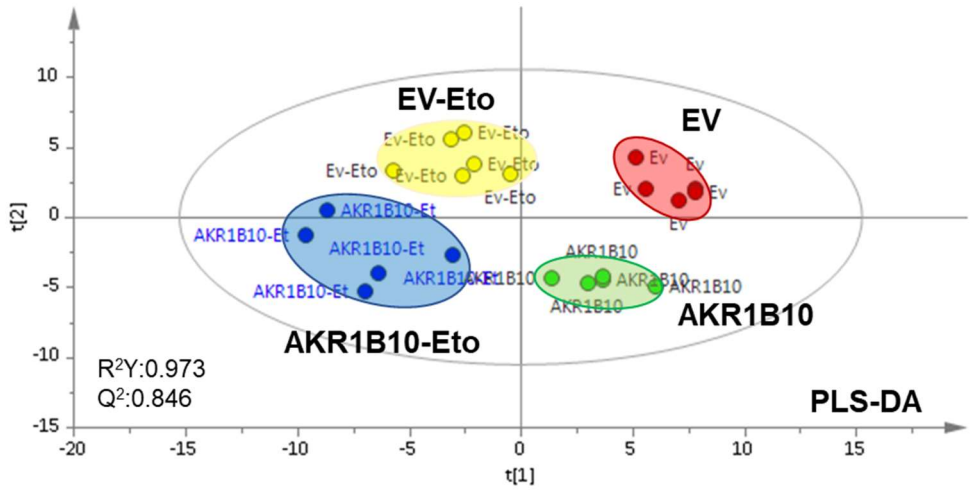

Figure 3.20 PLS-DA score plot of untargeted metabolomics data of HuH-7 cells.

EV (red cluster): Empty Vector cells, EV Eto (yellow cluster): EV cells were treated with 5 µM etomoxir for 30 minutes, AKR1B10 (green cluster): AKR1B10 expressing cells, AKR1B10-Eto (blue cluster): AKR1B10 expressing cells were treated with 5µM etomoxir for 30 minutes. All cells were incubated with 0 g/L glucose and 0 mM L-glutamine for 72 hours before etomoxir or vehicle (water) treatment. R^2Y and Q^2 values are represented in the plot.

3.2.2.3.3 Variable Important in Projection (VIP) in All Untargeted Metabolomics Samples

To investigate single metabolites that are changing between samples, variable important in projection (VIP) plots were generated by PLS-DA regression analysis. The most elevated VIP value of metabolite was determined as having the highest impact on the separation. Notably, the cut-off of the VIP plots exceeded 1.0, suggesting significant alterations in the metabolite profile (Eylem, 2022; Eylem et al., 2021). Among the top 25 significant metabolites, N-acetyl-L-aspartic acid showed the highest VIP score across all samples. In addition, levels of TCA (tricarboxylic acid) cycle metabolites and several different amino acids showed overall significant alterations in all samples (**Figure 3.21**).

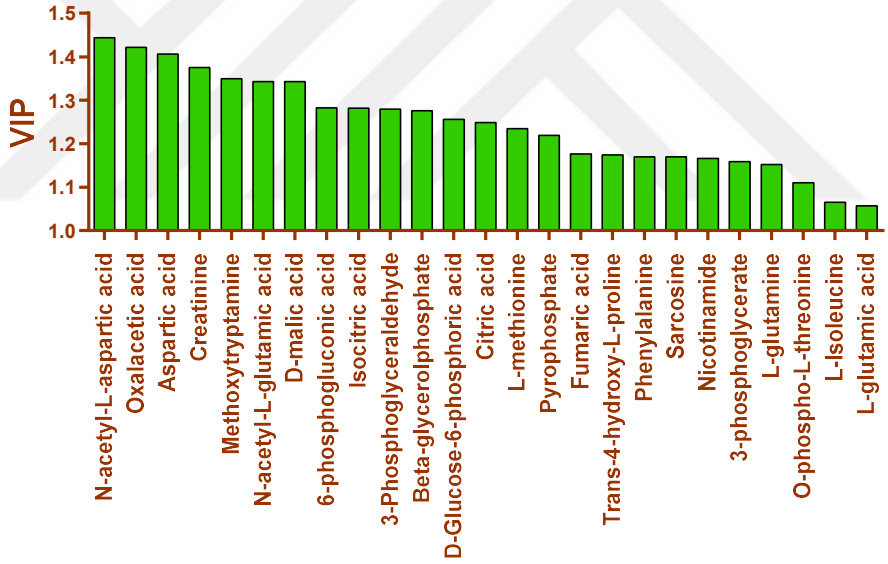

Figure 3.21 VIP plot between all samples.

VIP plot shows the levels of the most altered metabolites among all samples: AKR1B10 expressing cells, AKR1B10 expressing cells with etomoxir treatment, EV control cells and EV cells with etomoxir treatment. The top 25 metabolites are shown in the graph. All metabolites were altered significantly (>1.0 VIP).

3.2.2.3.4 Comparison of Metabolites in EV and AKR1B10 Expressing Cells

First, PLS-DA analysis was conducted between AKR1B10 expressing cells and EV control cells (**Figure 3.22 A**). R^2=0.998 and Q^2=0.940 values showed high accuracy of the model and better separation. In order to find the altering metabolites, a VIP plot was generated. Among 25 significant metabolites, TCA cycle metabolites and amino acids were altered compared to AKR1B10 expressing cells and EV cells (**Figure 3.22 B**). N-acetyl-L-aspartic acid and citric acid showed the highest VIP score. Following the identification of the crucial metabolites through VIP plots, coefficient graphs were also generated from regression analysis of PLS-DA to determine the direction of the alterations in the concentration of metabolites within specific subgroups. The coefficient graph revealed that oxalacetic acid, creatinine and N-acetyl-L-aspartic acid were the top three metabolites that were increased in AKR1B10 expressing cells compared to EV cells. Moreover, citric acid and L-methionine were the top two metabolites showing a decrease in AKR1B10-expressing cells (**Figure 3.22 C**). Glucogenic amino acids such as L-serine and L-alanine also showed increases in the AKR1B10-expressing cells compared to control cells.

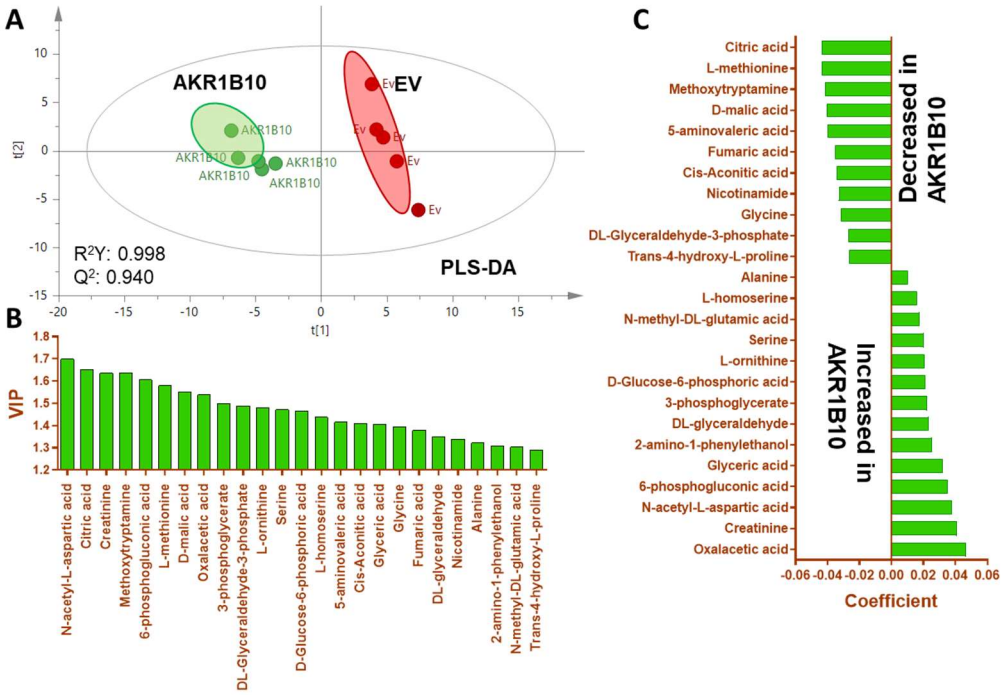

Figure 3.22 Comparison of metabolite levels in AKR1B10 expressing cells.

(A) PLS-DA was shown with R^2=0.998 and Q^2=0.940. (B) VIP plot of AKR1B10 expressing cells and EV cells were incubated with 0 g/L glucose and 0 mM L-glutamine for 72 hours. (C) The coefficient graph shows that metabolites were significantly increased in AKR1B10 expressing cells and decreased in the EV cells. "Decreased in AKR1B10" means that the metabolites in the graphs reduced in the AKR1B10 expressing cells and increased in EV cells or vice versa.

Significantly altered metabolites were determined by using a t-test according to EV cells incubated with 0 g/L glucose and 0 mM L-glutamine for 72 hours. The mean and standard error (SE) values were computed for each group. Datasets were integrated and transferred to the MetaboAnalyst platform. Consequently, the common Kyoto Encyclopedia of Genes and Genome (KEGG) pathways exhibiting the most significant alterations were identified and presented on the graphs. Glyoxylate and dicarboxylate metabolism, amino acid metabolism (alanine-

aspartate and glutamate metabolism) and TCA cycle were the top pathways that were differentially altered between AKR1B10 and control cells (**Figure 3.23**).

A

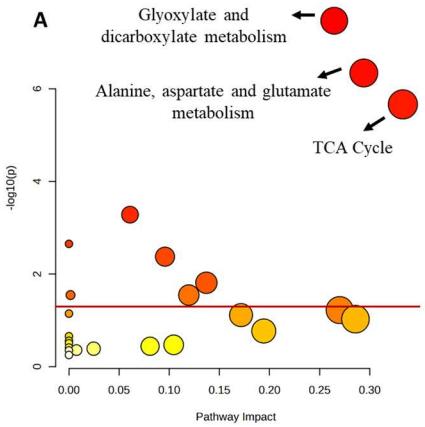

B

Pathway Name	Match Status	p	-log(p)	FDR
Glyoxylate and dicarboxylate metabolism	7/32	3.40E-08	7.4691	2.85E-06
Alanine, aspartate and glutamate metabolism	6/28	4.57E-07	6.3404	1.92E-05
Citrate cycle (TCA cycle)	5/20	2.17E-06	5.6632	6.08E-05
Arginine biosynthesis	3/14	5.23E-04	3.2818	0.010976
Aminoacyl-tRNA biosynthesis	4/48	0.002231	2.6515	0.037481
Glutathione metabolism	3/28	0.004218	2.3749	0.059056
Glycerolipid metabolism	2/16	0.015427	1.8117	0.18512
Pyruvate metabolism	2/22	0.028425	1.5463	0.2653
Pentose phosphate pathway	2/22	0.028425	1.5463	0.2653

Figure 3.23 Pathway analysis of altered metabolites in AKR1B10 expressing cells compared to EV cells.

Analysis was carried out in the MetabolAnalyst platform. A threshold is shown with a red line, indicating that the pathways above the threshold were significantly altered in EV vs. AKR1B10 expressing cells (A). The table represents significant pathways with match status, p, -log(p) and FDR (False Discovery Rate) values (B).

3.2.2.3.5 Comparison of Metabolites in Etomoxir Treated EV and AKR1B10 Expressing Cells

The metabolite levels in the AKR1B10 expressing cells were compared to the control (EV) cells incubated with 0 g/L glucose and 0 mM L-glutamine for 72 hours, followed by 30 minutes of treatment with 5 µM etomoxir. R^2 was calculated as 0.945 and Q^2 was calculated as 0.748 in PLS-DA, shown in **Figure 3.24 A**. VIP analysis again showed significant alteration in N-acetyl-L-aspartic acid and creatinine levels between etomoxir treated AKR1B10 expressing cells and EV cells (**Figure 3.24 B**).

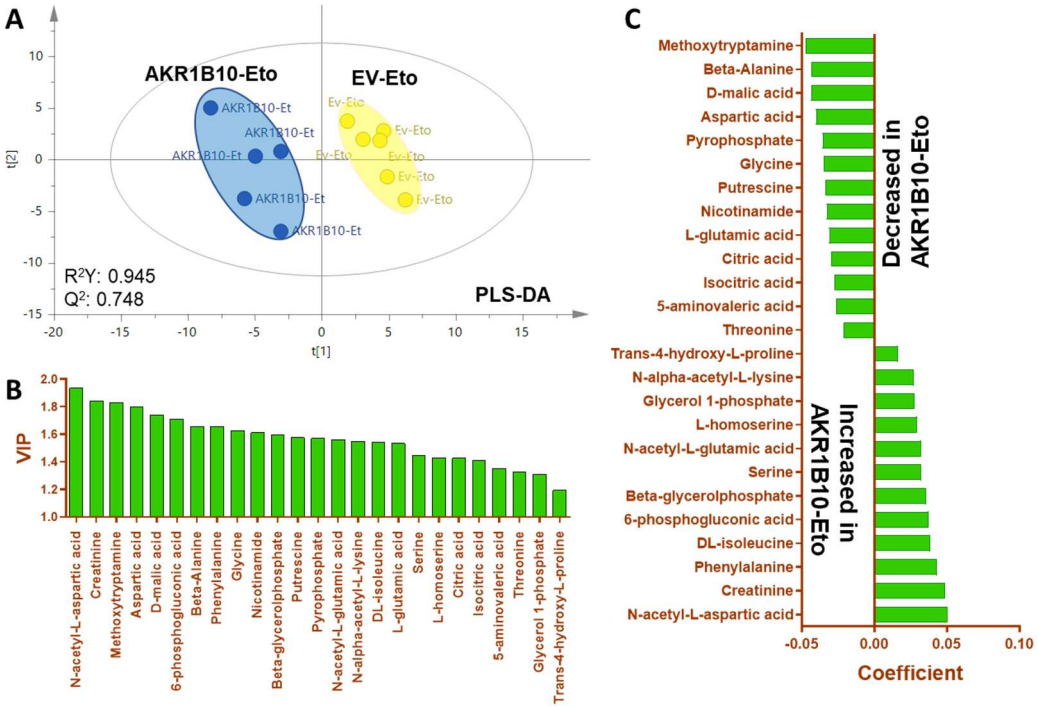

Figure 3.24 Comparison of metabolite levels of etomoxir treated AKR1B10 expressing cells.

(A) PLS-DA was shown with R2=0.945 and Q2=0.748. (B) The VIP plot of AKR1B10 expressing cells and EV cells was incubated with 0 g/L glucose and 0 mM L-glutamine for 72 hours before 5 µM etomoxir treatment for 30 minutes. (C) The coefficient graph shows that metabolites were significantly increased in etomoxir treated AKR1B10 expressing cells and decreased in the EV cells. "Decreased in AKR1B10-Eto" means that the metabolites in the graphs reduced in the AKR1B10 expressing cells and increased in EV cells or vice versa.

KEGG pathway analysis carried out in the etomoxir treated samples indicated significant enrichment of aminoacyl-tRNA biosynthesis, alanine-aspartate and glutamate metabolism, glyoxylate and dicarboxylate metabolism and arginine biosynthesis in etomoxir treated AKR1B10 expressing cells compared to etomoxir treated EV cells (**Figure 3.25**).

A

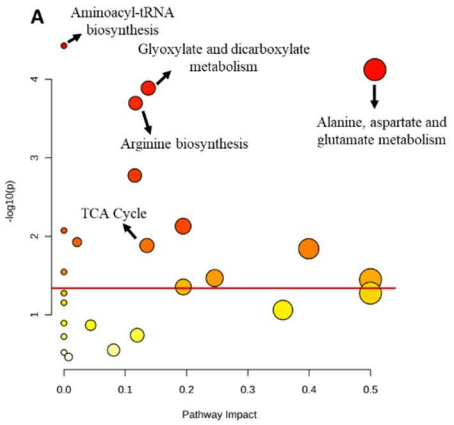

B

Pathway Name	Match Status	p	-log(p)	FDR
Aminoacyl-tRNA biosynthesis	5/48	3.75E-05	4.4263	0.003148
Alanine, aspartate and glutamate metabolism	4/28	7.55E-05	4.1221	0.003171
Glyoxylate and dicarboxylate metabolism	4/32	0.00013	3.8865	0.003636
Arginine biosynthesis	3/14	0.000202	3.6954	0.004235
Glutathione metabolism	3/28	0.001684	2.7737	0.028287
Nicotinate and nicotinamide metabolism	2/15	0.007441	2.1283	0.10153
Histidine metabolism	2/16	0.008461	2.0726	0.10153
Pantothenate and CoA biosynthesis	2/19	0.011871	1.9255	0.1212
Citrate cycle (TCA cycle)	2/20	0.013122	1.882	0.1212
beta-Alanine metabolism	2/21	0.014428	1.8408	0.1212
Porphyrin and chlorophyll metabolism	2/30	0.028532	1.5447	0.21788
Glycine, serine and threonine metabolism	2/33	0.0341	1.4672	0.23053
Phenylalanine, tyrosine and tryptophan biosynthesis	1/4	0.035677	1.4476	0.23053
Arginine and proline metabolism	2/38	0.044248	1.3541	0.26549

Figure 3.25 Pathway analysis of etomoxir treatment in AKR1B10 expressing cells compared to EV cells.

Analysis carried out in the MetabolAnalyst platform. A threshold is shown with a red line, indicating that pathways shown above the threshold were significantly altered in etomoxir treated EV vs. AKR1B10 expressing cells (A). The table represents significant pathways with match status, p, -log(p) and FDR (False Discovery Rate) values (B).

3.2.2.3.6 Overall Comparison of Untargeted Metabolomic Samples in the Context of Metabolic Pathways

To better understand the untargeted metabolomics data, we compared untreated EV and AKR1B10 expressing cells with etomoxir treated EV and AKR1B10 expressing cells. Of note, all cells were grown under glucose and glutamine withdrawal for 72 hours. We observed significant alteration in metabolite levels of glycolysis, tricarboxylic acid (TCA) cycle, gluconeogenesis and mitochondrial shuttles.

3.2.2.3.6.1 Altered Metabolites in Glycolysis

Glucose is converted to glucose 6-phosphate (G6P) by hexokinase in the preparatory phase of glycolysis (Nelson & Cox, 2017). Glyceraldehyde 3-phosphate (G3P), the first product of the payoff phase of glycolysis, is oxidized and phosphorylated to generate NADH. Dihydroxyacetone phosphate (DHAP) and G3P are cleaved by aldolase into triose phosphates. G3P enters subsequent glycolysis reaction steps, while DHAP is converted to G3P. In addition, 3-phosphoglycerate is another intermediate in the payoff phase of glycolysis following the first ATP generation (Nelson & Cox, 2017). A significant increase in the levels of D-glucose-6-phosphoric acid (G6P) and 3-phosphoglycerate was observed with AKR1B10 expression and with etomoxir treatment in both EV and AKR1B10 expressing cells compared to EV (**Figure 3.26**). However, G3P levels showed a significant decrease in untreated AKR1B10 expressing cells compared to untreated EV cells. With the etomoxir treatment, no difference was observed in glyceraldehyde-3-phosphate levels in the EV cells. The AKR1B10 expressing cells treated with etomoxir showed an increase in glyceraldehyde-3-phosphate levels, reaching to the same level as the EV cells. A feeder metabolite, glyceraldehyde, can be converted to glyceraldehyde 3-phosphate to enter glycolysis. An increment of glyceraldehyde levels was observed in AKR1B10 expressing cells as well as AKR1B10 expressing and EV cells treated with etomoxir. In animal tissues, lactic acid fermentation may support aerobic pyruvate oxidation (Nelson & Cox, 2017). We also observed no major difference in lactic acid levels between AKR1B10 expressing or EV cells. However, treatment with etomoxir resulted in a dramatic increase in lactic acid levels in both AKR1B10 and EV cells.

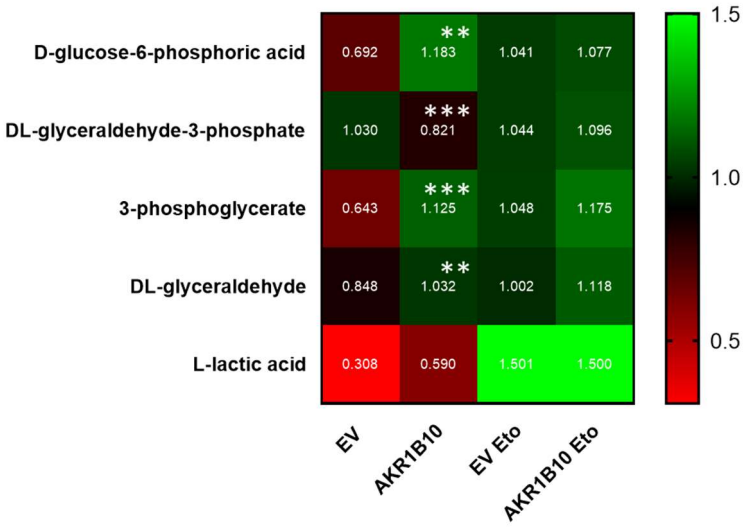

Figure 3.26 Altered metabolites in glycolysis compared to EV cells.

*Mean values are shown in the heatmap according to color code provided to the right of the figure. Red and green colors indicate low and high levels of indicated metabolites, respectively. For statistical analyses, AKR1B10 expressing cells were compared with EV cells and AKR1B10-Eto cells was compared with EV-Eto cells with Student's t-test. **p<0.01 and ***p<0.001. EV: Empty Vector, AKR1B10: AKR1B10 expressing cells, EV-Eto: EV cells treated with etomoxir, AKR1B10-Eto: AKR1B10 expressing cells.*

Overall, our data indicates a higher level of glycolytic intermediates in AKR1B10 expressing cells compared to EV. Many of the same metabolites increased with etomoxir treatment in the control (EV) cells. Etomoxir treatment of AKR1B10 cells did not show any further increase in these metabolites. Since the cells were cultured for 72 hours in the absence of any glucose, an increase in the rate of glycolysis is difficult to envisage. The liver and kidney are two of the major gluconeogenic organs of the body that can generate glucose from non-glucose sources such as amino acids (but not from lipids). The generated glucose is not used in the organ per se; rather, it is released into the circulation for use in other glucose utilizing organs. It has also been shown that liver cancer cells can undergo

gluconeogenesis; however, very often, the end product is not glucose, suggesting the activation of incomplete gluconeogenesis (Grasmann et al., 2019). Such a pathway would lead to the formation of several intermediates of glycolysis that can be utilized for biomass generation. It is feasible to speculate that the high levels of glycolytic intermediates observed in glucose/glutamine starved AKR1B10 expressing HuH-7 cells are actually intermediates of incomplete gluconeogenesis that are necessary to continue cell proliferation despite the lack of nutrients. The high lactic acid levels observed with etomoxir treatment, however, may be indicative of increased anaerobic oxidation.

3.2.2.3.6.2 Altered Metabolites in the TCA Cycle

The tricarboxylic acid (TCA) cycle is an important pathway for energy production along with the production of biosynthetic intermediates. Examination of the TCA cycle intermediates suggested remarkable alterations with the expression of AKR1B10. The first metabolite of the cycle, citrate, showed a significant decrease in AKR1B10 expressing cells compared to EV. With etomoxir treatment, we did not observe any further change in the AKR1B10 expressing cells; however, the EV cells showed a significant increase (**Figure 3.27**). Lower levels of the subsequent metabolites of the cycle, such as cis-aconitate and isocitrate levels, were observed in the AKR1B10 expressing cells compared to controls. Etomoxir treatment resulted in no significant change in these metabolites in the AKR1B10 expressing cells, while the EV cells continued to reveal elevated levels compared to untreated counterparts. No significant change in α-ketoglutarate levels was observed in any of the cells tested, while only etomoxir treated AKR1B10 expressing cells showed a significant decrease in succinate levels compared to untreated EV. The levels of fumarate and malate were again decreased significantly in AKR1B10 expressing cells, while etomoxir treatment did not lead to any further change in succinate levels. Malate levels were low in AKR1B10 cells and remained low in the etomoxir treated counterpart. Interestingly, the level of oxaloacetate (OAA) was

remarkably and significantly increased in AKR1B10 expressing cells. Etomoxir treatment of EV cells resulted in an increase in OAA, as also seen with other TCA cycle intermediates such as citrate, cis-aconitate and isocitrate. However, etomoxir treated AKR1B10 expressing cells showed a decrease in OAA levels, although the levels were still higher than the control EV cells. The TCA cycle is closely regulated and one of the primary regulators is the level of acetyl CoA coming from pyruvate (from glycolysis) or from the β-oxidation of fatty acids. The metabolomics analysis did not provide us with the levels of acetyl CoA in the cell and the high levels of oxaloacetate should suggest a robust TCA cycle. However, the decrease in levels of nearly every metabolite of the TCA cycle in AKR1B10 expressing cells suggests a slowing down of the cycle with glucose and glutamine starvation with the majority (4/8) metabolites staying low upon further inhibition of FAO with etomoxir.

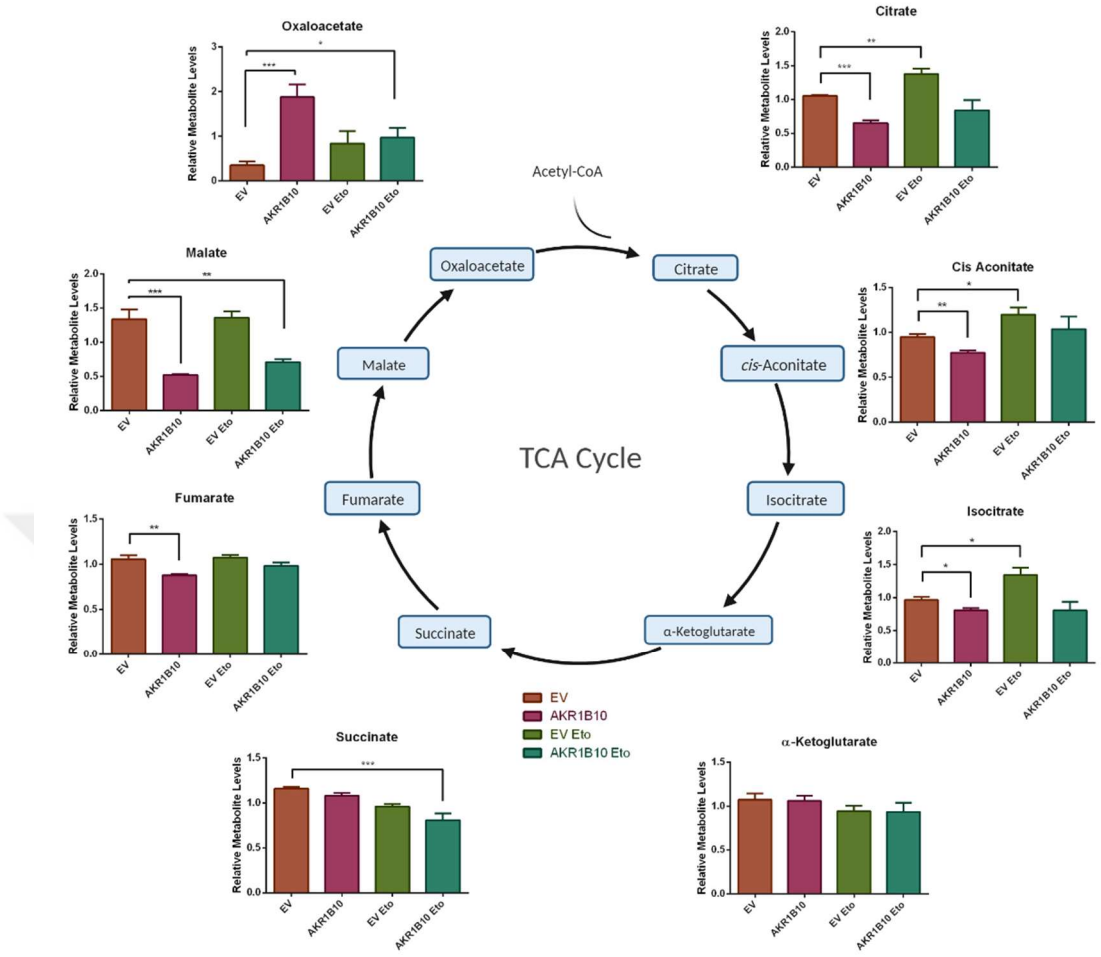

Figure 3.27 Alteration in TCA cycle metabolites across all samples.

*EV: Empty Vector (orange), AKR1B10: AKR1B10 expressing cells (purple), EV-Eto: EV cells treated with etomoxir (green), AKR1B10-Eto: AKR1B10 expressing cells treated with etomoxir (blue). The figure was created with Biorender. All groups were compared with EV cells for statistical analyses using Student's t-test, *p<0.05, **p<0.01 and ***p<0.001.*

I also determined the extracellular oxygen consumption rate (OCR) under nutrient restrictions in AKR1B10 expressing cells to measure cellular respiration and mitochondrial function according to the manufacturer's protocol. AKR1B10

expressing cells showed a very modest increase in OCR compared to EV cells. However, the AKR1B10 expressing cells showed a significantly mitochondrial low spare reserve capacity (SRC) compared to the control cells (**Figure 3.28**). High spare reserve capacity indicates high adaptation to stress conditions and the presence of healthy mitochondria (Marchetti et al., 2020). A spare reserve capacity suggests that under glucose and glutamine restriction, AKR1B10 expressing cells may not be able to adapt to stress conditions.

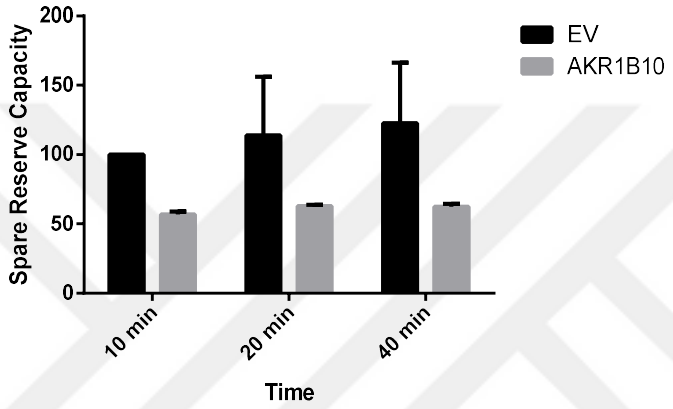

Figure 3.28 SRC of AKR1B10 expressing HuH-7 cells.

*AKR1B10 expressing and EV cells were treated with an uncoupling agent FCCP (Carbonyl cyanide-p-trifluoromethoxyphenylhydrazone) to measure maximal oxygen consumption rate (OCR^{max}). OCR of untreated cells was considered as basal OCR (OCR^{basal}). Spare Reserve Capacity (SRC) was calculated with the formula OCR^{max}/OCR^{basal}*100 at 10, 20 and 40 minutes.*

The remarkably high concentration of OAA in AKR1B10 expressing cells compared to EV cells was of particular interest to us. There are several pathways for the synthesis of OAA in the cells.

1. Conversion of malate to OAA (progression of the TCA cycle). Glucose and glutamine starved AKR1B10 expressing cells showed a decrease in malate levels compared to EV cells (**Figure 3.29**). This decrease in malate levels in

AKR1B10 expressing cells suggests that the high levels of OAA may not be synthesized from malate. It is likely that despite the low levels of TCA cycle intermediates in glucose and glutamine starved AKR1B10 expressing cells, FAO can provide the necessary mitochondrial acetyl-CoA necessary to sustain the TCA cycle in cancer cells that rely on OXPHOS (Icard et al., 2021). When FAO was inhibited with etomoxir, the level of malate did not differ in EV cells treated or untreated with etomoxir, while AKR1B10 expressing cells (AKR1B10-Eto) showed an increase in malate levels compared to untreated cells (from 0.521 to 0.711). The levels of OAA in EV and etomoxir treated EV cells also did not differ significantly. However, AKR1B10 expressing cells also showed a significant and remarkable decrease in OAA levels upon treatment with etomoxir.

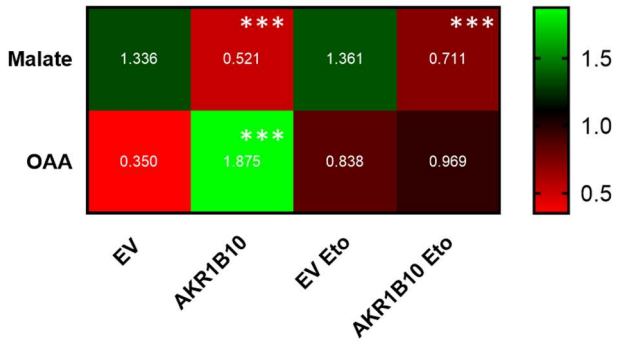

Figure 3.29 Malate and oxaloacetate levels metabolomics samples.

*Mean values are shown in the heatmap according to the color code where red and green colors indicate low and high levels of indicated metabolites, respectively. For statistical analyses AKR1B10 expressing cells were compared with EV cells and AKR1B10-Eto cells were compared with EV-Eto cells with Student's t-test. ***p<0.001. EV: Empty Vector, AKR1B10: AKR1B10 expressing cells, EV-Eto: EV cells treated with etomoxir, AKR1B10-Eto: AKR1B10 expressing cells.*

2. A second source of OAA in the cell is aspartate. Glutamic-oxaloacetic transaminase 1 (GOT1) and GOT2 catalyze a reversible reaction for the

conversion of aspartate (Asp) and α-ketoglutarate (α-KG) to OAA and glutamate in the cytoplasm or mitochondria of eukaryotic cells (Song et al., 2022). In these reactions, Asp and α-KG from the mitochondrial matrix can move to the cytosol and undergo a GOT1-catalyzed reaction to generate OAA and glutamate. This cytosolic OAA can be used for the generation of malate in the presence of malate dehydrogenase 1 (MDH1) with the synthesis of NADPH, which is followed by the conversion of malate to pyruvate. The same set of reactions for the synthesis of OAA can also occur in the mitochondrial matrix; however, the reaction is catalyzed by GOT2. The levels of α-KG, aspartate or glutamate did not differ between AKR1B10 or EV cells (**Figure 3.30**), suggesting that OAA may not have been synthesized from aspartate α-KG in these cells. Of note, etomoxir treatment decreased the levels of glutamate in EV and AKR1B10 expressing cells, with a more dramatic decrease observed in AKR1B10 expressing cells, while the α-KG levels remained largely unchanged. These data suggest glutamate was not used for the synthesis of OAA. Etomoxir treatment also led to a decrease in OAA levels in AKR1B10 expressing cells, suggesting that β-oxidation may be necessary for the generation of high OAA levels by supplying mitochondrial acetyl CoA.

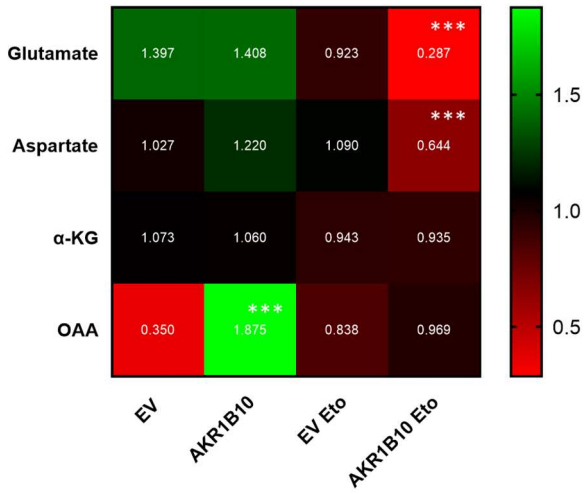

Figure 3.30 Metabolites for the synthesis of OAA from aspartate and α-KG.

*Mean values are shown in the heatmap according to color code where red and green colors indicate low and high levels of indicated metabolites, respectively. For statistical analyses, AKR1B10 expressing cells were compared to EV cells while AKR1B10-Eto cells were compared to EV-Eto cells using Student's t-test. ***p<0.001. EV: Empty Vector, AKR1B10: AKR1B10 expressing cells, EV-Eto: EV cells treated with etomoxir, AKR1B10-Eto: AKR1B10 expressing cells.*

3. The third source of OAA in AKR1B10 cells is from citrate in the cytosol. Citrate strongly inhibits citrate synthase activity (Martínez-Reyes & Chandel, 2020), while the availability of acetyl-CoA and OAA along with NADH and succinyl CoA can also partly regulate citrate synthase activity (Iacobazzi & Infantino, 2014). Since citrate levels were low in AKR1B10 cells (**Figure 3.27**) and OAA levels were high, it is highly likely that citrate synthase activity was not inhibited in these cells. However, the equilibrium for the conversion of OAA to citrate is far towards citrate formation with a highly negative ΔG value (-9 kcal/mol). This suggests that in the mitochondria, OAA and acetyl CoA can be converted to citrate, but citrate cannot be converted to OAA and acetate. However, citrate can move from the mitochondrion to the cytosol, where in the presence of ATP-citrate lyase (ACLY), it can be converted to OAA and acetyl CoA (Icard et al., 2021). The synthesis of OAA from citrate in the cytoplasm is, therefore, highly feasible in AKR1B10 expressing cells. The etomoxir treated AKR1B10 cells showed a decrease in the levels of OAA, suggesting that the less mitochondrial acetyl CoA due to the inhibition of β-oxidation can lead to a decrease in the synthesis of citrate and subsequently OAA.

3.2.2.3.6.3 Altered Metabolites in Gluconeogenesis

One of the major metabolic pathways for the utilization of cytosolic OAA is by conversion to phosphoenolpyruvate (PEP) to generate glucose via gluconeogenesis, primarily in the liver and kidneys. Additionally, OAA can be converted to aspartate

and then used for the synthesis of nucleotides and polyamine. Citrate is, therefore, a very critical gauge of for the balance between biomass generation and ATP synthesis via OXPHOS. In humans, short-term fasting (3-12 hours) in liver cells was shown to generate glucose by glycogenolysis and gluconeogenesis, whereas with long-term fasting (68 hours or longer), glucose is synthesized almost exclusively from gluconeogenesis (Rothman et al., 1991). We assumed that in an *in vitro* setup where glucose may not be available from the microenvironment, 72 hours of glucose withdrawal in HuH-7 cells would be sufficient to deplete all glycogen sources, leaving the cells to rely on gluconeogenesis. The remarkably high level of the metabolite OAA and low levels of citrate pointed towards the possibility of preferential activation of FAO-coupled gluconeogenesis in AKR1B10 expressing cells. Here, we assume that the acetyl CoA generated from FAO would be necessary for the synthesis of citrate and, thereby, OAA in the AKR1B10 expressing HuH7 cells.

The major sources of carbon for gluconeogenesis are lactate, glycerol, and amino acids (Shah & Wondisford, 2020). Two amino acids are the most relevant for gluconeogenesis: alanine in the liver and glutamine in the kidney. AKR1B10 cells showed a significantly higher amount of alanine compared to EV (1.4 fold increase). A trend for an increase in lactate levels (1.9 fold increase) in the AKR1B10 was also seen. Therefore, the cells may be carrying out gluconeogenesis from alanine and lactate for survival.

Alanine can be converted to pyruvate, which can undergo gluconeogenesis to glucose (Shah & Wondisford, 2020). An intermediary in this conversion is PEP, that is generated by coupling two high energy reactions utilizing ATP and GTP, one catalyzed by pyruvate carboxylase and the next by the enzyme phosphoenol pyruvate carboxykinase (PEPCK).

OAA is an intermediate in gluconeogenesis since pyruvate (generated from alanine in this case) is readily converted to OAA via pyruvate carboxylase in the mitochondria. Additionally, we assume that in the absence of glucose and

glutamine, a net synthesis of TCA cycle intermediates can occur from acetyl CoA generated from FAO in the AKR1B10 cells, leading to the synthesis of OAA.

The extracellular oxygen consumption rate assay (OCR) is a kinetic analysis to determine cellular respiration rate. We also observed increased oxygen consumption in AKR1B10 expressing cells after 72 hours of nutrient restriction (**Figure 3.31**). This may suggest that AKR1B10 expressing cells have more FAO compared to EV cells. Additionally, increased mitochondrial levels of acetyl CoA from FAO can activate pyruvate carboxylase, which converts pyruvate to OAA.

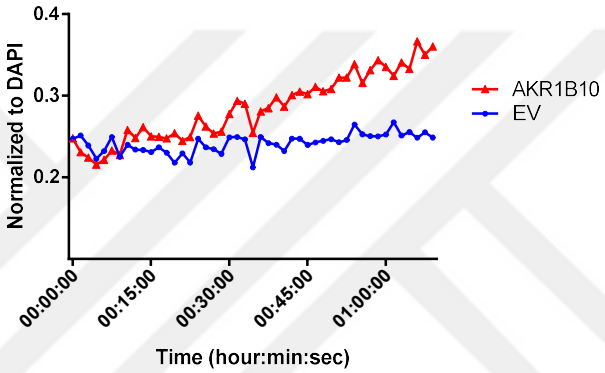

Figure 3.31 The extracellular oxygen consumption assay in AKR1B10 expressing HuH-7 cells.

The medium and reagent were incubated at 37 °C prior to the experiment. 30,000 cells were seeded in a tissue culture opaque plate and starved with glucose and glutamine for 72 hours. Abcam ab197243 kit's instructions were followed. Measured OCR values were normalized to the corresponding group's DAPI values.

OAA cannot be directly transported to the cytosol since the inner mitochondrial membrane is impermeable to OAA. However, it can be converted to aspartate, which can leave the mitochondrion via the glutamate-aspartate antiporter. We observed high levels of aspartate in AKR1B10 expressing cells (although the levels were not different between AKR1B10 and control cells, **Figure 3.30**). Alternately, citrate can be converted to OAA in the cytosol. Cytosolic OAA can be converted to

phosphoenol pyruvate via PEPCK-C or PEPCK-1. A comparable reaction can also be catalyzed in the mitochondria through the enzyme PEPCK-2 (Grasmann et al., 2019).

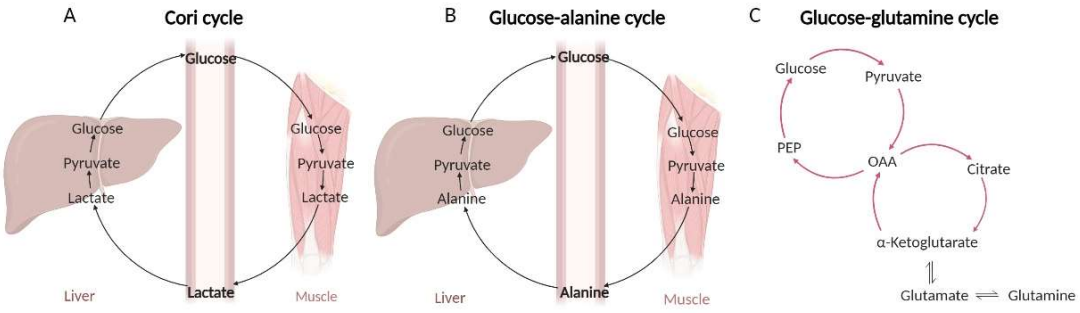

Figure 3.32 The carbon flux in the Cori cycle, glucose-alanine cycle and glucose-glutamine cycle.

PEP: Phosphoenolpyruvate, OAA: Oxaloacetate. This figure was generated by BioRender and adapted from Shah et al., 2020.

Lactate can also be used for the synthesis of glucose via the Cori cycle. In this, lactate is converted to pyruvate via lactate dehydrogenase, generating NADPH. Pyruvate is then converted to phosphoenol pyruvate and then to glucose as described earlier.

The purpose for the activation of gluconeogenesis in AKR1B10 cells is likely to be the availability of glycolytic intermediates (rather than glucose synthesis) since gluconeogenesis is more or less a reversal of the steps of glycolysis with some exceptions. In fact, the levels of D-glucose were similar between AKR1B10 and control cells (Mean±SEM; 0.796 ±0.069 in EV cells vs 0.739 ± 0.029 in AKR1B10 expressing cells). The intermediates of glycolysis were found to be higher in AKR1B10 expressing cells; however, in the absence of any glucose in the culture medium, it is very likely that these intermediates were generated from gluconeogenesis. Glycolytic intermediates are essential for biosynthetic reactions, specifically ribose-5-phosphate and NADPH for nucleotide biosynthesis (NADPH

levels were high in AKR1B10 expressing SNU423 cells) for the production of glycerol-1-phosphate for the synthesis of lipids (glycerol-1-phosphate levels were significantly higher in AKR1B10 expressing cells; mean±SEM; 0.820±0.040 in EV vs 1.125±0.096 in AKR1B10 expressing cells, $p<0.05$) or for the synthesis of serine and glycine and hexosamines. The levels of most gluconeogenic amino acids was higher in AKR1B10 cells (**Figure 3.33**).

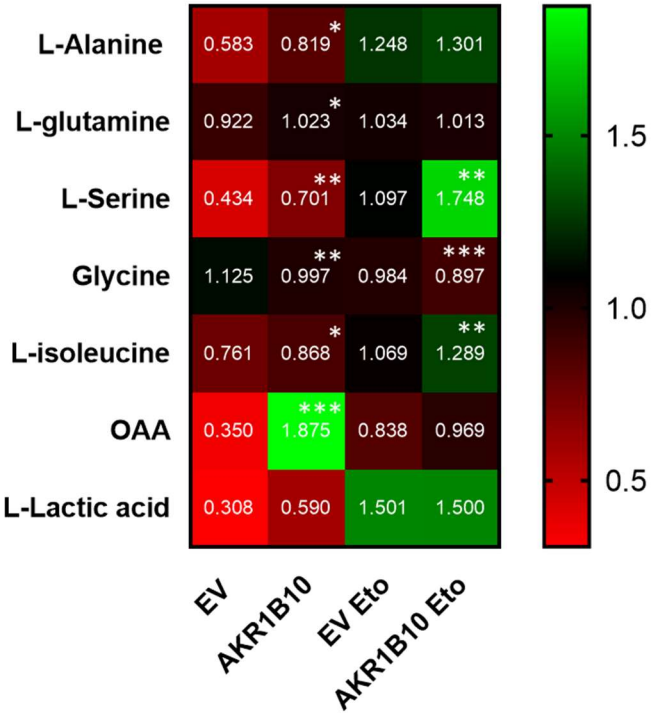

Figure 3.33 Metabolites for gluconeogenesis.

*Mean values are shown in the heatmap according to color code with red and green colors indicating low and high levels of the indicated metabolites, respectively. For statistical analyses, AKR1B10 expressing cells were compared to EV cells while AKR1B10-Eto cells were compared to EV-Eto cells using Student's t-test. *p<0.05, **p>0.01, ***p<0.001. EV: Empty Vector, AKR1B10: AKR1B10 expressing cells, EV-Eto: EV cells treated with etomoxir, AKR1B10-Eto: AKR1B10 expressing cells.*

When the AKR1B10 expressing HuH-7 cells were treated with etomoxir, an important source of mitochondrial acetyl CoA was lost. This may have resulted in the decrease of synthesis of OAA in AKR1B10 cells treated with etomoxir, such that the levels were OAA were similar between etomoxir treated AKR1B10 and control cells. Considering the levels of the glucogenic amino acids, both alanine and lactic acid levels were higher upon treatment with etomoxir; however, the levels were similar between AKR1B10 and controls. Therefore, these cells may rely on alternative glucogenic amino acids, such as serine and isoleucine levels, which were significantly higher in the AKR1B10 cells treated with etomoxir. 3-phosphoglycerate, an intermediate in both glycolysis and gluconeogenesis, can be converted to serine. The levels of both serine and 3-phosphoglycerate were higher in control cells (EV) treated with etomoxir compared to untreated control cells (**Figures 3.26 and 3.33**), suggesting that this pathway may be functional in cells with etomoxir treatment. In fact, serine levels remained high in AKR1B10 cells treated with etomoxir compared to control cells treated with etomoxir, suggesting that the synthesis of serine may be associated with AKR1B10 expression, both in FAO proficient and deficient cells. The levels of 3-phosphoglycerate also remained high in AKR1B10 cells treated with etomoxir, but the levels were not significantly different.

Serine and glycine can be utilized to generate many macromolecules, such as proteins, nucleic acids, and lipids (Amelio et al., 2014). Serine is synthesized from the glycolytic/gluconeogenic intermediate 3-phosphoglycerate via 3-phosphoglycerate dehydrogenase (PHGDH) and NAD^+ to give 3-phosphohydroxypyruvate. Next, a transamination reaction with the enzyme phosphoserine aminotransferase (PSAT1) and phosphate ester hydrolysis via the enzyme phosphoserine phosphatase (PSPH) leads to the conversion of 3-phosphohydroxypyruvate to serine. Serine can also be converted to glycine, catalyzed by the enzyme serine hydroxymethyltransferase (SHMT). This reaction is one of the major sources of CH3 groups for one-carbon metabolism that is

required for both nucleotide biosynthesis, NADPH generation and regulation of gene expression via DNA methylation (Amelio et al., 2014).

Overall, these data suggest that several gluconeogenic metabolites are highly enriched in AKR1B10 expressing cells grown in the absence of glucose and glutamine. We suggest that the cells can utilize acetyl CoA from FAO to generate OAA, which can then be used for the generation of gluconeogenic intermediates rather than the generation of glucose. These intermediates are essential for the synthesis of biomolecules that are necessary to sustain proliferation under nutrient stress.

3.2.2.3.6.4 Bioenergetics in AKR1B10 Expressing HuH-7 Cells

In addition to the transfer of metabolites from the mitochondrion to the cytosol, the malate aspartate shuttle is also responsible for the movement of reducing electrons from the cytoplasm to the mitochondrion (but not the reverse). A second shuttle, the glycerol-3-phosphate shuttle, is responsible for the movement of electrons from NADH (cytosolic) to FADH2 in the mitochondria. The malate aspartate shuttle is generally more functional in the liver. Since NADH or FADH2 cannot cross the inner mitochondrial membrane, the electrons from these electron carriers that are generated from glycolysis or gluconeogenesis are transported via such shuttles across the inner mitochondrial membrane.

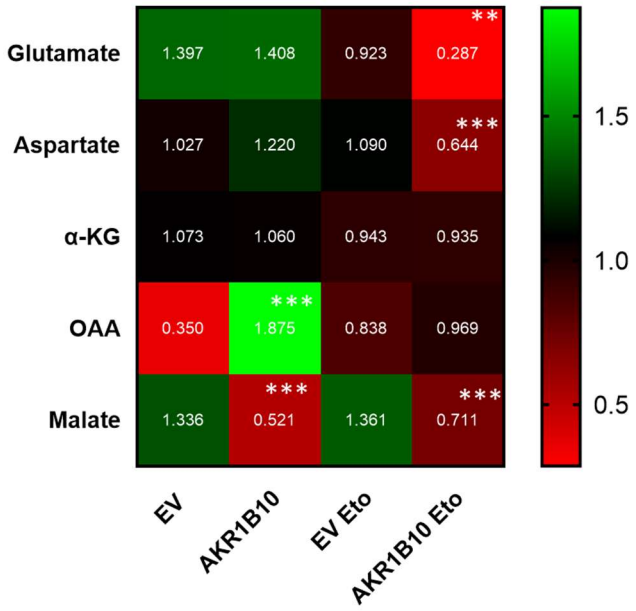

Figure 3.34 Levels of shuttle metabolites.

*Mean values are shown in the heatmap according to color code in which red and green colors indicate low and high levels of the indicated metabolites, respectively. For statistical analyses, AKR1B10 expressing cells were compared to EV cells while AKR1B10-Eto cells were compared to EV-Eto cells using Student's t-test. **p<0.01, ***p<0.001. EV: Empty Vector, AKR1B10: AKR1B10 expressing cells, EV-Eto: EV cells treated with etomoxir, AKR1B10-Eto: AKR1B10 expressing cells.*

We observed high levels of the shuttle metabolites in both EV and AKR1B10 expressing cells. However, when FAO was inhibited with etomoxir, the levels of many of these transporters decreased more in the AKR1B10 cells. This suggests that FAO inhibition may prevent the AKR1B10 expressing cells from utilizing reducing electrons from the cytosol and may reflect less ATP synthesis from the electron transport chain. FAO inhibition may also lead to a loss of gluconeogenesis, suggesting that its inhibition may be a metabolic vulnerability in AKR1B10 cells. We did not observe any overt loss of proliferation in AKR1B10 cells treated with etomoxir (**Figure 3.17**); nonetheless, it is possible that other

cellular characteristics, such as migration and metastatic capacity, may be altered with the loss of FAO. In fact, breast cancer cells showing AKR1B10 expression and high FAO were associated with enhanced metastasis to the lung with no alteration in the primary tumor size (van Weverwijk et al., 2019).

CHAPTER 4

DISCUSSION

Colorectal cancer and hepatocellular carcinoma, classified as gastrointestinal (GI) tract cancers, have the highest mortality rate after lung cancer in both sexes (Sung et al., 2021). Although the genetic changes (mutations) associated with GI cancers have been described extensively, such knowledge has not resulted in novel therapeutics or dramatic improvement in mortality, mainly due to poor prognosis and late diagnosis. Reprogramming cellular metabolism is accepted as one of the main hallmarks of cancer (Hanahan, 2022). Metabolic studies in GI cancers suggest that glucose, glutamine and lipid metabolism may alter during cancer progression. Therefore, the focus has shifted in recent years to better understand how the metabolome supports the progression of cancer in order to identify vulnerabilities of the tumor, new biomarkers and novel therapeutic approaches (Nannini et al., 2020; Pal et al., 2022).

The main focus of my thesis was to understand the role of the metabolic enzymes AKR1B1 and AKR1B10 in GI cancers where both proteins are highly expressed. Although they belong to the same family (AKR1B), their substrate specificity differs considerably (Banerjee, 2021). AKR1B1 is a rate-limiting enzyme in the polyol pathway, which reduces excess glucose to sorbitol (**Figure 1.1**). AKR1B10 can reduce retinals, isoprenyls and cytotoxic aldehydes (Matsunaga et al., 2012) but is a poor reductant of glucose. AKR1B1 is ubiquitously expressed in most human tissues; however, AKR1B10 is highly expressed in the GI tract. Although AKRs have been reported extensively in diabetic complications, the enzymes AKR1B1 and AKR1B10 have been gaining attention in human cancers such as liver, colon, lung and breast tumors (Banerjee, 2021).

The expression of AKR1B10 was reported to be very low in CRC (Shen et al., 2015; Taskoparan et al., 2017), and high (with a high variation) in HCC and lung cancer (Banerjee, 2021). Along with its expression, the role of AKR1B10 can vary between different tumor types. AKR1B10 expression was shown to be associated with tumor node metastasis and decreased response to chemotherapy in gastric cancer (S. M. U. Ahmed et al., 2019). AKR1B10 was suggested as a potential biomarker in the early stages of HCC (Z. Wang et al., 2022); however, the prognostic value and underlying mechanism of AKR1B10 in HCC need further investigations (Distefano & Davis, 2019).

4.1 AKR Signature in Colorectal Cancer

Previously, we have reported functional differences in the expression of AKR1B1 and AKR1B10 in colorectal cancer (Taskoparan et al., 2017). The expression of AKR1B1 enhanced cellular motility, proliferation and inflammation, while the expression of AKR1B10 reduced motility and inflammation in CRC (Taskoparan et al., 2017). Next, we evaluated whether a combination of the expression of AKR1B1 and AKR1B10 (AKR-Signature) can predict prognosis. Indeed, we observed that $AKR1B1^{HIGH}$ and $AKR1B10^{LOW}$ tumors were associated with significantly poor DFS (disease-free survival) and RFS (recurrence-free survival) (Demirkol-Canlı et al., 2020). This supports the four-gene signature, including AKR1B10, which was shown to predict better OS in CRC patients (Dai et al., 2020).

A study with Cancer Cell Line Encyclopedia (CCLE) and NCI-60 (human tumor cell lines) panel analysis indicated higher expression of AKR1B1 in mesenchymal cell lines, whereas AKR1B10 did not exhibit a similar pattern (Schwab et al., 2018). In this thesis, using *ex vivo* samples (Ankara cohort), I have shown that $AKR1B1^{HIGH}$ and $AKR1B10^{LOW}$ tumors were more mesenchymal (**Figure 3.1 and 3.2**) whereas $AKR1B1^{LOW}$ and $AKR1B10^{HIGH}$ tumors were more epithelial. Supporting our findings, analysis of the publicly available CRC dataset GSE39582

(Marisa et al., 2013), we observed that patients with AKR1B1^{HIGH} and AKR1B10^{LOW} tumors were associated with a mesenchymal CMS4 phenotype while AKR1B1^{LOW} and AKR1B10^{HIGH} patients were associated with CMS3 phenotype, which includes metabolism of sugars, glutamine and fatty acids (Guinney et al., 2015).

We next aimed to understand mechanistically why the AKR1B10^{HIGH} samples were enriched for metabolic pathways. We evaluated reverse phase protein array (RPPA) data from the Cancer Genome Atlas (TCGA) colon adenocarcinoma (COAD) patient samples and CRC cell lines from Cancer Cell Line Encyclopedia (CCLE) and observed significant changes in the activation of nutrient-sensing pathways. Western blot of colon cancer cell lines ectopically expressing AKR1B10 (mimicking the AKR1B1^{LOW} and AKR1B10^{HIGH} phenotype), but not ectopically expressing AKR1B1, showed a decrease in phosphorylation of p70S6K (T308). Phosphorylation of p70S6K, an mTOR downstream target, regulates protein synthesis, cellular proliferation and motility (Manning, 2004). Active p70S6K phosphorylates PDCD4 (at S67), leading to proteasomal degradation of the latter (Dorrello et al., 2006). PDCD4, a tumor suppressor, is a well-known checkpoint protein at the G1-S phase (Haas et al., 2020; Hwang et al., 2010). AKR1B10 expression showed a significant increase in total PDCD4 protein levels in two different cell lines.

Previous studies have shown that treatment with the AKR inhibitor fidarestat increased PCDC4 levels via the downregulation of miR-21, which regulates PDCD4 post-transcriptionally (Saxena et al., 2013). An RPPA assay carried out with the Ankara cohort indicated that the phosphorylation of GSK3β (S9) was significantly high in AKR1B1^{LOW} and AKR1B10^{HIGH} samples. S9 phosphorylation of GSK3β is inhibitory phosphorylation via IRS1 (Eldar-Finkelman & Krebs, 1997) and Akt (T308); however, we were unable to identify a similar increase in phosphorylation of GSK3β in CRC cell lines ectopically expressing AKR1B10. Tumors collected from patients consist of both epithelial and stromal cells and may also harbor considerable heterogeneity compared to cell lines that are relatively

more homogeneous. Therefore, it is possible that stromal-epithelial interactions may be needed to achieve the full spectrum of phosphorylations we observed with the *ex vivo* samples.

4.2 AKR1B10 Signaling and Metabolic Evaluation in Hepatocellular Carcinoma

Our data with CRC cell lines and patient material suggested a strong association of AKR1B10 with metabolism. The liver is the primary metabolic organ of the body; moreover, AKR1B10 expression was shown to be elevated in liver cancer compared to normal tissues (Banerjee, 2021). Therefore, we attempted to establish mechanistically the function of AKR1B10 in HCC using transcriptome analysis of HCC tumors and metabolomics analysis of HCC cell lines expressing AKR1B10. Overall, our data suggest that the AKR1B10 expression leads to alterations in NADPH metabolism and oxidative stress in SNU423 cells and FAO and gluconeogenesis in HuH-7 cells, all of which may contribute to poor survival in patients. Another study in our group suggested that AKR1B10 expression showed an increase in cirrhosis, followed by liver cell dysplasia (Sheraj et al., 2021).

Ye et al. classified HCC tumors and cell lines according to their expression of metabolic genes (Ye et al., 2023). Cluster 1 cell lines were associated with reliance on glycolysis and PPP for survival with resistance to sorafenib (Raf/MEK inhibitor) compared to the cluster 2 cells, which rely on glutaminolysis and FAO (Ye et al., 2023). SNU423 and HuH-7 cells were classified under cluster 1 and cluster 2, respectively. These cell lines, therefore, have highly divergent metabolic profiles and do not express AKR1B10 within the detection limits of western blot. Therefore, we selected these two cell lines to stably ectopically express AKR1B10 and evaluate which metabolic pathways were differentially activated in comparison to the empty vector (control) cells.

4.2.1 Evaluation of Metabolic Pathways in SNU423 Cells Expressing AKR1B10

SNU423 cells were shown to be more reliant on glycolysis and PPP (Ye et al., 2023). A colony formation assay indicated that SNU423 cells underwent extensive cell death when grown in the absence of glucose for eight days (data not shown). The enzymatic activity of AKR1B10 relies on the presence of NADPH as a donor of reducing electrons. The primary source of NADPH in cells is the Pentose Phosphate Pathway (PPP), a shunt that uses glucose-6-phosphate to generate riboses as well as NADPH (Ghanem et al., 2021). NADPH generated from the PPP is also used to maintain low oxidative stress in cells via the regeneration of reduced glutathione (GSH). Therefore, cancer cells are often known to activate the PPP for survival (Ghanem et al., 2021). We hypothesized that AKR1B10 expression may modulate the NADPH levels in SNU423 cells via activation of the PPP.

Incubation of SNU423 cells with the PPP inhibitor 6-AN (5 μM) led to extensive cell death in a clonogenic assay, confirming the reliance of these cells on the PPP for survival. Interestingly, treatment of AKR1B10 expressing SNU423 cells with 2 μM 6-AN led to greater survival compared to the control EV cells (**Figure 3.9**), along with a higher ratio of NADPH/NADH (**Figure 3.11),** suggesting that these cells could be highly plastic and activate alternative pathways for the synthesis of NADPH. Increased cellular levels of NADPH could be associated with increased biosynthesis (anabolic reactions). The enzyme acetyl CoA carboxylase (ACC1, localized in the cytosol and ACC2, localized in the mitochondria) catalyzes the carboxylation of acetyl-CoA to produce malonyl-CoA, which can be utilized by the enzyme FASN for fatty acid synthesis (FAS). At the same time, the malonyl CoA generated from the enzymatic activity of ACC1 can inhibit carnitine palmitoyltransferase-1 (CPT1), an enzyme of the outer mitochondrial membrane that catalyzes the transfer of the acyl group from acyl-coenzyme A to carnitine. This is the first step in FAO. The phosphorylation of ACC is closely regulated

primarily by the kinase AMPK, the nutrient sensor that can sense the low energy state of the cell. Upon phosphorylation, the enzymatic activity of ACC is inhibited, leading to a loss of malonyl CoA and thereby loss of its inhibition on FAO. ACC therefore is a nodal enzyme that aids in the decision of the cell to activate anabolic pathways such as FAS or catabolic pathways such as FAO, depending on the energy requirements of the cell (Y. Wang et al., 2022). We observed that AKR1B10 expression in SNU423 cells was associated with reduced ACC phosphorylation compared to the control cells, which might result in elevated FAS. FAS relies on the availability of acetyl-CoA, which is primarily generated from citrate in the TCA cycle in the mitochondria (Fang & Lowenstein, 1967). Citrate can cross the inner mitochondrial membrane and be converted to acetyl CoA via the enzyme ACLY, which, along with cytosolic NADPH, can be used for FAS in the cytosol. Lipids are high energy sources; therefore, increased lipid synthesis by tumor cells may contribute to cellular processes linked with tumor progression (Röhrig & Schulze, 2016). Since we observed high survival of AKR1B10 expressing cells treated with the PPP inhibitor, along with increased NADPH/NADP ratio, we speculate that AKR1B10 cells may be associated with FAS in HCC cells that are generally reliant on glucose for energy. Of note, increased FAS should also be associated with increased FAO when cells require energy. The Randle cycle, initially described in skeletal muscles and later also demonstrated in the liver, entails the activation of FAO at the cost of glycolysis when fatty acids are available. An increase in the [acetyl-CoA]/[CoA] ratio as well as [NADH]/[NAD^+] ratio with increased FAO, can inhibit the enzyme pyruvate dehydrogenase (PDH), which catalyzes the conversion of pyruvate to acetyl CoA and CO_2, thereby inhibiting the later stages of glycolysis, with modest inhibitory effect on the uptake of glucose (Hue & Taegtmeyer, 2009). The increased levels of acetyl CoA from FAO can also increase the levels of citrate that can be further utilized for FAS. Further studies using lipidomics analyses are currently underway in our lab to better establish whether AKR1B10 expression can actually lead to enhanced FAS and thereby FAO on SNU423 cells.

FAO is associated with the activation of oxidative phosphorylation in the mitochondria for the synthesis of ATP, which in turn can be associated with increased oxidative stress, particularly in the mitochondria. SNU423 cells are KEAP1 mutated, which allows NRF2 to remain constitutively active to relieve oxidative stress (Gong et al., 2020). *In silico* analysis of the TCGA liver hepatocellular carcinoma (LIHC) data by our group showed a remarkable increase in the expression of several different antioxidant genes in AKR1B10^{HIGH} LIHC tumors compared to AKR1B10^{LOW} tumors (**Figure 3.15**). We observed higher ROS levels in SNU423 cells expressing AKR1B10 compared to controls (**Figure 3.16**). Such an increase in ROS levels in a highly glycolytic cell line allows us to speculate that increased FAO in AKR1B10 expressing cells may have led to increased ROS levels; however, further evaluation of whether this ROS is cytosolic or mitochondrial needs to be established.

4.2.2 Evaluation of Metabolic Pathways in HuH-7 Cells Expressing AKR1B10

According to Ye et al., HuH-7 cells are highly dependent on glutaminolysis and FAO for their energy requirement (cluster 2, Ye et al., 2023). We observed that treatment of HuH-7 cells with 6-AN showed a difference in the number of colonies formed compared to the vehicle treated cells, suggesting that these cells were not reliant on the PPP for their survival (Tuğral, 2022). HuH-7 cells also showed a decrease in the number of colonies formed when grown in the presence of high glucose (data not shown). Withdrawal of glutamine also did not affect colony formation in HuH-7 cells, but the loss of both glucose and glutamine was highly detrimental to cell survival (data not shown). This demonstrates lower reliance of HuH-7 cells on glycolysis and greater reliance on FAO followed by OXPHOS for energy generation. To establish whether AKR1B10 expression in HuH-7 cells led to any alteration in energy sensing and metabolism, we withdrew glucose and glutamine from the culture medium for a period of 72 hours. In a parallel set of

experiments, we treated the glucose and glutamine withdrawn cells with the CPT1 inhibitor etomoxir. Glucose/glutamine withdrawal led to a decrease in viability of AKR1B10 expressing HuH-7 cells compared to controls, which was not decreased any further with FAO inhibition. These data suggest a particular vulnerability of AKR1B10 expressing cells to glucose and glutamine withdrawal.

An untargeted metabolomics assay revealed that upon glucose and glutamine withdrawal, HuH-7 cells expressing AKR1B10 showed a remarkable increase in the levels of the metabolite OAA. In general, high OAA levels are associated with the continuation of the TCA cycle; however, we observed a decrease in the level of most of the metabolites of the TCA cycle. A very recent study on brain metastasis of lung cancer cells showed that AKR1B10 expression could promote the Warburg effect by regulating the expression of LDHA (lactate dehydrogenase A) (Duan et al., 2023). Increased lactate production stimulated histone lactylation and *CCNB1* transcription was activated to promote the cell cycle. In the same study, an untargeted metabolomics assay showed significant alterations in the TCA cycle, glyoxylate and dicarboxylate metabolism, PPP, alanine-aspartate and glutamate metabolism metabolites in AKR1B10 overexpressing lung cancer brain-metastatic cells compared to control. The same pathways were also activated in glucose/glutamine starved HuH-7 cells (**Figure 3.23**), re-emphasizing a role of AKR1B10 in the metabolic rewiring of cancer cells.

Glucose/glutamine starved HuH-7 cells expressing AKR1B10 also showed significantly decreased levels of citrate compared to controls. In fact, citrate levels are generally suppressed in cancer cells since citrate can carry out feedback inhibition of the glycolytic enzymes (PFK1 and PFK2). Low citrate levels can, therefore, promote the Warburg effect. Additionally, high FAO can also lead to high synthesis of citrate, which is rapidly converted to acetyl CoA and OAA (Icard et al., 2021). Previously, data generated in our laboratory revealed increased ACC phosphorylation in AKR1B10 expressing HuH-7 cells grown in a complete medium (Tuğral, 2022), suggesting the possibility of high FAO in these cells.

Since the metabolomics analysis was carried out with HuH-7 cells cultured for 72 hours in glucose/glutamine free culture medium, we can assume that glycolysis was less efficient, if not absent in these cells. Therefore, the likelihood of the occurrence of the Warburg effect in these cells is also low. During fasting, approximately 80% of endogenous glucose is produced by the liver through gluconeogenesis (Tian et al., 2020). The combination of low citrate levels and high OAA levels in AKR1B10 expressing HuH-7 cells also suggests a strong possibility of activation of gluconeogenesis. Gluconeogenesis includes many steps that are the reversal of glycolysis; in fact, activation of gluconeogenic enzymes such as phosphoenolpyruvate carboxykinase 1 (PCK1) and fructose-1,6-bisphosphatase 1 (FBP1) can inhibit glycolysis (Hirata et al., 2016). The possibility of incomplete gluconeogenesis has been suggested in cancer cells (Grasmann et al., 2019). In this, the ultimate aim is not to generate glucose for other glucose utilizing organs; rather, activation of gluconeogenesis generates some of the intermediates of glycolysis that are needed for biomass generation.

The high OAA levels in AKR1B10 expressing cells may also be explained by increased activity of the enzyme pyruvate carboxylase (PC). Pyruvate is converted to OAA by PC to prevent oxidative stress and to produce non-essential amino acids (Kiesel et al., 2021). In malignancies, PC activity can enable tumor growth by suppressing oxidative stress in the cells (Kiesel et al., 2021).

It is, however, currently unclear whether the activation of gluconeogenesis in LIHC in the presence of AKR1B10 would have any prognostic significance. We have observed in bioinformatics analyses that AKR1B10 expression in LIHC is associated with poor prognosis; additionally, AKR1B10 was expressed very early in the transformation of liver epithelial cells from cirrhosis to HCC (Sheraj, 2021). However, the inhibition of the Warburg effect has been suggested as a means for therapy in HCC. The primary enzymes of gluconeogenesis, PCK1 and FBP1, were shown to be expressed less in liver cancer compared to normal and low expression of these proteins was associated with poor prognosis (M.-X. Liu et al., 2018). Overexpression of PCK1 in HCC cells under glucose starvation led to the energy

crisis and oxidative stress, along with cataplerosis from the TCA cycle (M.-X. Liu et al., 2018). We have observed that glucose/glutamine starved HuH-7 cells expressing AKR1B10 showed lower viability than control cells. Therefore, it is important to establish whether the low viability resulted from the activation of gluconeogenesis in AKR1B10 expressing cells.

CHAPTER 5

CONCLUSION AND FUTURE STUDIES

The aim of my thesis was to better understand the role of the enzymes aldo keto reductases (AKR1B1 and AKR1B10) in gastrointestinal cancers. These enzymes catalyze the reduction of glucose along with a wide variety of other substrates, such as retinol, chemotherapy drugs etc., using reducing electrons from NADPH. A role of AKR1B1 in diabetes has been established very well, primarily in the context of diabetic retinopathy; however, a role of these enzymes in various different cancers has been emerging in the last decade. The primary findings of my thesis can be divided into two parts: 1. Establishment of a role of AKR1B1 in mediating an EMT phenotype in colorectal cancer and 2. Understanding the role of AKR1B10 in mediating metabolic deregulation in liver cancer.

5.1 AKR Signature in Colorectal Cancer

The primary findings with regards to the establishment of an AKR signature in colorectal cancer can be summarized as follows:

1. The mRNA expression of *AKR1B1* was evaluated by RT-qPCR in *ex vivo* colon and rectal tumor patient samples (Ankara cohort, n=51) for which survival data were also available. AKR1B1 expression was positively and significantly correlated with the expression of the mesenchymal marker *VIM* and negatively correlated with the transcript levels of the epithelial marker *CDH1*. On the other hand, *AKR1B10* expression was significantly and positively correlated with the expression of *CDH1* and significantly negatively correlated with the expression of *VIM*.
2. The EMT score of patients in the Ankara cohort was positively correlated with AKR1B1 expression confirming a more mesenchymal phenotype in

AKR1B1^{HIGH} tumors. AKR1B10^{HIGH} tumors were significantly and negatively correlated with the EMT score suggesting more epithelial phenotype. We observed that AKR1B1^{HIGH} and AKR1B10^{LOW} tumors in the GSE39582 dataset (Marisa et al., 2013) were primarily in the Consensus Molecular Subtype (CMS) 4 category (Demirkol-Canlı et al., 2020). CMS4 tumors are more prone to distant metastases, have a high content of stromal fibroblasts and also show more expression of mesenchymal genes. A follow-up and currently ongoing study that has emerged from my research has established for the first time the high expression of AKR1B1 in the stromal rather than epithelial cells in CRC.

3. Colon cancer cell lines (RKO and SW480) ectopically expressing AKR1B10 showed low phosphorylation of p70S6K (T389) and an increase in total PDCD4 protein levels compared to control cells. Other experiments, such as *in silico* evaluation of publicly available RPPA data, along with RPPA data from the Ankara cohort carried out by other members of our group, supported an aberrant activation of metabolic pathways. In fact, AKR1B1^{LOW} and AKR1B10^{HIGH} tumors in the GSE39582 dataset (Marisa et al., 2013) were primarily assigned to CMS3 (Demirkol-Canlı et al., 2020). These tumors are epithelial, have evident metabolic dysregulation and tend to rely on glutaminolysis and lipidogenesis (Thanki et al., 2017).

Overall, my findings suggest that the AKR1B1^{HIGH} and AKR1B10^{LOW} (AKR signature) is associated with mesenchymal phenotype and poor survival; therefore, the AKR signature may be considered as a novel prognostic marker in colon cancer. This work, where I served as a joint first author, has been published (Demirkol-Canlı et al., 2020).

Recent data generated from our laboratory showed that upon overnight serum starvation followed by refeed, AKR1B10 expressing CRC cell lines showed slower reactivation of the mTOR pathway. These data support my finding of lower activation of p70S6K in AKR1B10 expressing cells. However, exactly how AKR1B10 can crosstalk with the mTOR pathway is currently unclear and needs to

be established. Moreover, treatment of AKR1B10 expressing CRC cell lines with the mTOR inhibitor AZD8055 (Selleckchem) followed by expression of nutrient-sensing pathways and functional changes will be examined to better understand whether AKR1B10 mediates its tumor suppressive properties in part via the inhibition of mTOR signaling.

5.2 AKR1B10 Signaling and Metabolic Deregulation in Hepatocellular Carcinoma (HCC)

5.2.1 Role of AKR1B10 Expression in the Glycolytic Cell Line SNU423

My primary hypothesis was that AKR1B10 expression in HCC cell lines that are dependent on glycolysis can lead to aberrant activation of the Pentose Phosphate Pathway (PPP). This hypothesis stemmed from the fact that the enzymatic activity of AKR1B10 relies on the availability of NADPH and the PPP is the primary source of NADPH in cells. I did not observe any change in the mRNA or protein expression of the rate-limiting enzymes of the PPP. Nonetheless, some of the major findings from these experiments can be summarized as follows:

1. Blockage of PPP with the inhibitor 6-aminonicotinamide (6-AN) in AKR1B10 expressing or control SNU423 cells resulted in enhanced survival of the AKR1B10 expressing cells in a long-term clonogenic assay. The AKR1B10 expressing cells also showed an increased NADPH/NADP ratio when the PPP was blocked. These data suggested that expression of AKR1B10 in SNU423 cells could render the cells to be highly plastic such that the cells could use alternate NADPH generating pathways, perhaps in the mitochondria, which helped maintain cell viability even when a critical pathway such as the PPP was inhibited.
2. Tumors often grow under the stress of hypoxia, along with nutrient stress, and are known to activate survival mechanisms. Since AKR1B10 expressing cells appeared to be highly plastic, we therefore examined

whether the inhibition of PPP and hypoxia could lead to the differential activation of metabolic pathways. We observed that when the PPP was inhibited under hypoxia, the control cells (EV) cells showed very high phosphorylation of acetyl CoA carboxylase (ACC), an enzyme that activates fatty acid synthesis (FAS) when hypophosphorylated and fatty acid oxidation (FAO) when hyperphosphorylated. The activation of ACC in the AKR1B10 expressing cells was also high with hypoxia, but the protein was relatively less phosphorylated compared to the control cells.

3. AKR1B10 expressing cells also showed hypophosphorylation of ACC compared to EV cells in normoxia. These data suggest the possibility of elevated FAS in AKR1B10 expressing cells.
4. FAS relies on the availability of acetyl CoA, particularly from citrate via the enzyme ACLY (Röhrig & Schulze, 2016). We observed that AKR1B10 expressing cells showed elevated citrate synthase activity compared to EV cells, indicating that these cells may have increased availability of citrate and therefore acetyl CoA for FAS.
5. SNU423 cells have a KEAP1 mutation, suggesting constitutive activation of NRF2 and oxidative stress mitigation. Since our data hinted at the possibility of increased FAS, we surmised that the synthesized lipids may also be utilized via FAO. FAO relies on oxidative phosphorylation in the mitochondria and may generate reactive oxygen species. *In silico* analysis carried out with TCGA LIHC data set in our lab showed that oxidative stress-related genes are significantly upregulated in AKR1B10^{HIGH} LIHC tumors compared to AKR1B10^{LOW} tumors. We also observed significantly higher ROS levels in stably AKR1B10 expressing cells compared to EV cells, which was exacerbated when the PPP was inhibited. The elevated NADPH/NADP ratio and better survival under PPP inhibition might be explained by better ROS mitigation in AKR1B10 expressing cells.

In the future, we will carry out a targeted lipidomics analysis in collaboration with Dr. Mehmet Gümüştaş (Ankara University), Dr. Ezel Boyacı (METU) and Dr.

Yeliz Akpınar (Ahi Evran University) to determine the lipid profile of the AKR1B10 expressing cells. Fatty acid methyl esters (FAME) will be extracted from HCC cell lines expressing AKR1B10 using solid phase microextraction (SPME) followed by gas chromatography-flame ion detection (GC-FID). We will determine the differential levels of 37 FAME in HCC cell lines (SNU423 and HuH-7) with AKR1B10 expression. Initial optimization studies on SPME have been completed and a novel protocol for the extraction of lipid samples from cultured epithelial cells has been established.

Another important finding of the current study was the high ROS levels in AKR1B10 expressing SNU423 cells. We currently do not know whether the ROS is generated from the mitochondria. Therefore, using MitoSOX (Invitrogen), we will establish whether AKR1B10 expression in SNU423 cells led to an increase in mitochondrial ROS levels. If we observe increased mitochondrial ROS, we will determine the expression of oxidative stress-related genes via Qiagen RT^2 Profiler PCR Array Human Oxidative Stress Pathway Plus along with the GSSG/GSH ratio in AKR1B10 expressing SNU423 cells.

5.2.2 Evaluation of Metabolic Pathways in HuH-7 Cells Expressing AKR1B10

Based on our finding of a potential increase in FAS upon the expression of AKR1B10 in a highly glycolytic cell line (SNU423), we next wanted to determine whether the expression of the enzyme in a cell line reliant on FAO (but not glucose metabolism) would lead to aberrant activation of metabolic pathways. We withdrew glucose and glutamine from the culture medium for 72 hours to ensure that the cells had no access to glucose from glycogenolysis and therefore would rely mostly on FAO. We carried out an untargeted metabolomics analysis in these cells and compared the changes in the metabolome in cells that also underwent FAO inhibition with the CPT1 inhibitor etomoxir. My main findings are as follows:

1. Glucose and glutamine starved AKR1B10 expressing HuH7 cells showed less viability compared to the control cells. FAO inhibition did not lead to any further decrease in viability. The withdrawal of glucose and glutamine also led to increased activation of the nutrient-sensing protein AMPK and its downstream protein ACC in AKR1B10 expressing cells compared to the control cells.
2. An untargeted metabolomics analysis showed a good and significant separation in PCA and PLS-DA analysis. VIP analysis was carried out to observe the changes in metabolite levels across the four different groups. We mainly observed significant alterations in TCA cycle metabolites and amino acid levels. In the KEGG pathway analysis, TCA cycle, alanine-aspartate and glutamate metabolism and glyoxylate-dicarboxylate pathways showed significant enrichment in comparison between EV and AKR1B10 expressing cells or Etomoxir treated EV and AKR1B10 expressing HuH-7 cells.
3. The metabolomics analysis showed significant alteration in overall metabolite levels of glycolysis, TCA cycle, gluconeogenesis and mitochondrial shuttles. Since HuH-7 cells are mainly oxidative, we first focused on the TCA cycle. We observed that except oxaloacetate (OAA), most of the TCA cycle intermediates were decreased in AKR1B10 expressing cells after glucose and glutamine starvation. OAA has multiple roles in cellular metabolism, one of which is to participate in gluconeogenesis, especially when glucose levels are scarce in a gluconeogenic organ like the liver. We also observed significantly high levels of glucogenic amino acids and glycolytic intermediates in AKR1B10 expressing cells. Since the cells were glucose starved, we can speculate that the increased levels of glycolytic intermediates could also have resulted from enhanced gluconeogenesis. One reason for carrying out gluconeogenesis in cancer cells is to generate intermediates of glycolysis/gluconeogenesis that can be used for biomass generation rather

than the generation of glucose that can be used in other organs. In fact, we also observed high levels of serine, which can be synthesized from the glycolytic intermediate 3-phospho-glycerate in AKR1B10 cells.

4. From our data, it is also feasible to speculate that energy generation in AKR1B10 cells was low since the TCA cycle was slower, along with a decrease in the spare reserve capacity of the mitochondrial electron transport chain. To compensate for this loss, the AKR1B10 expressing cells may have enhanced the shunting of electrons from cytosolic NADPH to the mitochondria. However, since glycolysis was also inhibited due to a lack of glucose in the culture medium, the energy generation may not have been sufficient, causing both loss of viability and increased activation of AMPK.

In future studies, we would like to validate the activation of gluconeogenesis in HuH-7 cells expressing AKR1B10. We will assess the expression of the major gluconeogenic enzymes, such as PEPCK or pyruvate carboxylase (PC), at the transcript level. We can also carry out RNAi-mediated inhibition of a differentially expressed enzyme, followed by functional and metabolomics analysis to determine the fate of AKR1B10 expressing cells when gluconeogenesis is abrogated. Pyruvate is also one of the major metabolites in gluconeogenesis or glycolysis. An increase in the pyruvate levels in AKR1B10 expressing cells would also validate whether gluconeogenesis was active in these cells. Metformin is an approved drug for the treatment of type 2 diabetes, suppressing hepatic gluconeogenesis (Madiraju et al., 2018). 3-Mercaptopicolinic acid hydrochloride (3-MPA) is a chemical inhibitor of PEPCK. Glucose and glutamine starved AKR1B10 expressing HuH-7 cells will be treated with metformin or 3-MPA and functional changes such as proliferation and cellular motility will be examined. If we observe significant changes *in vitro*, we will also examine the tumor forming ability of HuH-7 cells in a chorioallantoic membrane (CAM) assay *in vivo*.

Treatment of glucose and glutamine starved HuH7 cells with etomoxir led to a decrease in the levels of gluconeogenic metabolites in AKR1B10 expressing cells. We speculate that this could be due to the lack of mitochondria derived acetyl CoA

from FAO. Therefore, it is possible that AKR1B10 expressing HuH-7 cells rely on FAO for biomass generation. Therefore, a targeted lipidomics analysis will be carried out to address the FAO dependence of AKR1B10 expressing cells.

REFERENCES

Ahmed, M. M. E., Wang, T., Luo, Y., Ye, S., Wu, Q., Guo, Z., Roebuck, B. D., Sutter, T. R., & Yang, J. Y. (2011). Aldo-keto reductase-7A protects liver cells and tissues from acetaminophen-induced oxidative stress and hepatotoxicity. *Hepatology (Baltimore, Md.)*, *54*(4), 1322–1332. https://doi.org/10.1002/hep.24493

Ahmed, S. M. U., Jiang, Z. N., Zheng, Z. H., Li, Y., Wang, X. J., & Tang, X. (2019). AKR1B10 expression predicts response of gastric cancer to neoadjuvant chemotherapy. *Oncology Letters*, *17*(1), 773–780. https://doi.org/10.3892/ol.2018.9705

Akram, M. (2014). Citric acid cycle and role of its intermediates in metabolism. *Cell Biochemistry and Biophysics*, *68*(3), 475–478. https://doi.org/10.1007/s12013-013-9750-1

Amelio, I., Cutruzzolá, F., Antonov, A., Agostini, M., & Melino, G. (2014). Serine and glycine metabolism in cancer. *Trends in Biochemical Sciences*, *39*(4), 191–198. https://doi.org/10.1016/j.tibs.2014.02.004

Ballinger, A. B., & Anggiansah, C. (2007). Colorectal cancer. *British Medical Journal*, *335*(7622), 715–718. https://doi.org/10.1136/bmj.39321.527384.BE

Banerjee, S. (2021). Aldo Keto Reductases AKR1B1 and AKR1B10 in Cancer: Molecular Mechanisms and Signaling Networks. *Advances in Experimental Medicine and Biology*, *1347*, 65–82. https://doi.org/10.1007/5584_2021_634

Boros, L. G., Lee, P. W. N., Brandes, J. L., Cascante, M., Muscarella, P., Schirmer, W. J., Melvin, W. S., & Ellison, E. C. (1998). Nonoxidative pentose phosphate pathways and their direct role in ribose synthesis in tumors: Is

cancer a disease of cellular glucose metabolism? *Medical Hypotheses*, *50*(1), 55–59. https://doi.org/10.1016/S0306-9877(98)90178-5

Busuioc, C., Ciocan-Cartita, C. A., Braicu, C., Zanoaga, O., Raduly, L., Trif, M., Muresan, M.-S., Ionescu, C., Stefan, C., Crivii, C., Al Hajjar, N., Mărgărit, S., & Berindan-Neagoe, I. (2021). Epithelial-Mesenchymal Transition Gene Signature Related to Prognostic in Colon Adenocarcinoma. *Journal of Personalized Medicine*, *11*(6). https://doi.org/10.3390/jpm11060476

Cairns, R., Harris, I., & Mak, T. (2011). Regulation of cancer cell metabolism. *Nature Reviews Cancer*, *11*(2), 85–95. https://doi.org/10.1038/nrc2981

Cassim, S., Raymond, V.-A., Dehbidi-Assadzadeh, L., Lapierre, P., & Bilodeau, M. (2018). Metabolic reprogramming enables hepatocarcinoma cells to efficiently adapt and survive to a nutrient-restricted microenvironment. *Cell Cycle (Georgetown, Tex.)*, *17*(7), 903–916. https://doi.org/10.1080/15384101.2018.1460023

Chaffer, C. L., San Juan, B. P., Lim, E., & Weinberg, R. A. (2016). EMT, cell plasticity and metastasis. *Cancer and Metastasis Reviews*, *35*(4), 645–654. https://doi.org/10.1007/s10555-016-9648-7

Chawla, A., Barak, Y., Nagy, L., Liao, D., Tontonoz, P., & Evans, R. M. (2001). PPAR-gamma dependent and independent effects on macrophage-gene expression in lipid metabolism and inflammation. *Nature Medicine*, *7*(1), 48–52. https://doi.org/10.1038/83336

Chen, S., Hu, Q., Tao, X., Xia, J., Wu, T., Cheng, B., & Wang, J. (2022). Retinoids in cancer chemoprevention and therapy: Meta-analysis of randomized controlled trials. In *Frontiers in genetics* (Vol. 13, p. 1065320). https://doi.org/10.3389/fgene.2022.1065320

Chen, W. D., & Zhang, Y. (2012). Regulation of aldo-keto reductases in human diseases. *Frontiers in Pharmacology*, *3 MAR*. https://doi.org/10.3389/fphar.2012.00035

Chu, C., Xin, A., Zhou, Y., & Zhang, Y. (2013). A simple protocol for producing high-titer lentivirus. *Acta Biochimica et Biophysica Sinica*, *45*(12), 1079–1082. https://doi.org/10.1093/abbs/gmt112

Chung, Y. T., Matkowskyj, K. A., Li, H., Bai, H., Zhang, W., Tsao, M. S., Liao, J., & Yang, G. Y. (2012). Overexpression and oncogenic function of aldo-keto reductase family 1B10 (AKR1B10) in pancreatic carcinoma. *Modern Pathology*, *25*(5), 758–766. https://doi.org/10.1038/modpathol.2011.191

Clark, T., Maximin, S., Meier, J., Pokharel, S., & Bhargava, P. (2015). Hepatocellular Carcinoma: Review of Epidemiology, Screening, Imaging Diagnosis, Response Assessment, and Treatment. *Current Problems in Diagnostic Radiology*, *44*(6), 479–486. https://doi.org/10.1067/j.cpradiol.2015.04.004

Dai, G.-P., Wang, L.-P., Wen, Y.-Q., Ren, X.-Q., & Zuo, S.-G. (2020). Identification of key genes for predicting colorectal cancer prognosis by integrated bioinformatics analysis. *Oncology Letters*, *19*(1), 388–398. https://doi.org/10.3892/ol.2019.11068

DeBerardinis, R. J., & Chandel, N. S. (2016). Fundamentals of cancer metabolism. *Science Advances*, *2*(5), e1600200. https://doi.org/10.1126/sciadv.1600200

Demirkol-Canlı, S., Seza, E. G., Sheraj, I., Gömçeli, I., Turhan, N., Carberry, S., Prehn, J. H. M., Güre, A. O., & Banerjee, S. (2020). Evaluation of an aldo-keto reductase gene signature with prognostic significance in colon cancer via activation of epithelial to mesenchymal transition and the p70S6K pathway. *Carcinogenesis*, 1–10. https://doi.org/10.1093/carcin/bgaa072

Demirkol, S. (2018). *Prediction of prognosis and chemosensitivity in gastrointestinal cancers*. *December*.

Demirkol, S., Gomceli, I., Isbilen, M., Dayanc, B. E., Tez, M., Bostanci, E. B., Turhan, N., Akoglu, M., Ozyerli, E., Durdu, S., Konu, O., Nissan, A., Gonen, M., & Gure, A. O. (2017). A combined ULBP2 and SEMA5A expression signature as a prognostic and predictive biomarker for colon cancer. *Journal of Cancer*, *8*(7), 1113–1122. https://doi.org/10.7150/jca.17872

Distefano, J. K., & Davis, B. (2019). Diagnostic and prognostic potential of akr1b10 in human hepatocellular carcinoma. *Cancers*, *11*(4), 1–13. https://doi.org/10.3390/cancers11040486

Dorrello, N. V., Peschiaroli, A., Guardavaccaro, D., Colburn, N. H., Sherman, N. E., & Pagano, M. (2006). S6k1- and βTRCP-mediated degradation of PDCD4 promotes protein translation and cell growth. *Science*, *314*(5798), 467–471. https://doi.org/10.1126/science.1130276

Duan, W., Liu, W., Xia, S., Zhou, Y., Tang, M., Xu, M., Lin, M., Li, X., & Wang, Q. (2023). Warburg effect enhanced by AKR1B10 promotes acquired resistance to pemetrexed in lung cancer-derived brain metastasis. *Journal of Translational Medicine*, *21*(1), 547. https://doi.org/10.1186/s12967-023-04403-0

Eldar-Finkelman, H., & Krebs, E. G. (1997). Phosphorylation of insulin receptor substrate 1 by glycogen synthase kinase 3 impairs insulin action. *Proceedings of the National Academy of Sciences of the United States of America*, *94*(18), 9660–9664. https://doi.org/10.1073/pnas.94.18.9660

Eylem, C. C. (2022). *Glioblastoma Multiforme, Menenjiyom (Birincil) ve Metastaz (İkincil) Beyin Tümörlerine ait Fenotiplerin Belirlenmesinde Kullanılacak Bütünleşik Omiks Analizler için Analitik Yöntem Geliştirilmesi ve Uygulanması*.

Eylem, C. C., Baysal, İ., Erikci, A., Yabanoglu-Ciftci, S., Zhang, S., Kır, S., Terzic, A., Dzeja, P., & Nemutlu, E. (2021). Gas chromatography-mass spectrometry based (18)O stable isotope labeling of Krebs cycle intermediates. *Analytica Chimica Acta*, *1154*, 338325. https://doi.org/10.1016/j.aca.2021.338325

Fan, J., Ye, J., Kamphorst, J. J., Shlomi, T., Thompson, C. B., & Rabinowitz, J. D. (2014). Quantitative flux analysis reveals folate-dependent NADPH production. *Nature*, *510*(7504), 298–302. https://doi.org/10.1038/nature13236

Fang, M., & Lowenstein, J. M. (1967). Citrate and the conversion of carbohydrate into fat. The regulation of fatty acid synthesis by rat liver extracts. *The Biochemical Journal*, *105*(2), 803–811. https://doi.org/10.1042/bj1050803

Feoktistova, M., Geserick, P., & Leverkus, M. (2016). Crystal Violet Assay for Determining Viability of Cultured Cells. *Cold Spring Harbor Protocols*, *2016*(4), pdb.prot087379. https://doi.org/10.1101/pdb.prot087379

Fhu, C. W., & Ali, A. (2020). Fatty Acid Synthase: An Emerging Target in Cancer. In *Molecules* (Vol. 25, Issue 17). https://doi.org/10.3390/molecules25173935

Frezza, C., Zheng, L., Tennant, D. A., Papkovsky, D. B., Hedley, B. A., Kalna, G., Watson, D. G., & Gottlieb, E. (2011). Metabolic profiling of hypoxic cells revealed a catabolic signature required for cell survival. *PloS One*, *6*(9), e24411. https://doi.org/10.1371/journal.pone.0024411

Fukumoto, S. I., Yamauchi, N., Moriguchi, H., Hippo, Y., Watanabe, A., Shibahara, J., Taniguchi, H., Ishikawa, S., Ito, H., Yamamoto, S., Iwanari, H., Hironaka, M., Ishikawa, Y., Niki, T., Sohara, Y., Kodama, T., Nishimura, M., Fukayama, M., Dosaka-Akita, H., & Aburatani, H. (2005). Overexpression of the aldo-keto reductase family protein AKR1B10 is highly correlated with smokers' non-small cell lung carcinomas. *Clinical Cancer Research*, *11*(5), 1776–1785. https://doi.org/10.1158/1078-0432.CCR-04-1238

Galic, S., Loh, K., Murray-Segal, L., Steinberg, G. R., Andrews, Z. B., & Kemp, B. E. (2018). AMPK signaling to acetyl-CoA carboxylase is required for fasting- and cold-induced appetite but not thermogenesis. *ELife*, *7*, 1–22. https://doi.org/10.7554/eLife.32656

Garcia, D., & Shaw, R. J. (2017). Review AMPK : Mechanisms of Cellular Energy Sensing and Restoration of Metabolic Balance. *Molecular Cell*, *66*(6), 789–800. https://doi.org/10.1016/j.molcel.2017.05.032

Ghanem, N., El-Baba, C., Araji, K., El-Khoury, R., Usta, J., & Darwiche, N. (2021). The Pentose Phosphate Pathway in Cancer: Regulation and Therapeutic Opportunities. In *Chemotherapy* (Vol. 66, Issues 5–6, pp. 179–191). https://doi.org/10.1159/000519784

Gong, M., Li, Y., Ye, X., Zhang, L., Wang, Z., Xu, X., Shen, Y., & Zheng, C. (2020). Loss-of-function mutations in KEAP1 drive lung cancer progression via KEAP1/NRF2 pathway activation. *Cell Communication and Signaling : CCS*, *18*(1), 98. https://doi.org/10.1186/s12964-020-00568-z

Grasmann, G., Smolle, E., Olschewski, H., & Leithner, K. (2019). Gluconeogenesis in cancer cells - Repurposing of a starvation-induced metabolic pathway? *Biochimica et Biophysica Acta. Reviews on Cancer*, *1872*(1), 24–36. https://doi.org/10.1016/j.bbcan.2019.05.006

Güderer, İ. (2021). *Evaluation of Funtional Changes in AKR1B1 and AKR1B10 Overexpressing Colorectal Cancer Cell Lines*.

Guerra, I. M. S., Ferreira, H. B., Melo, T., Rocha, H., Moreira, S., Diogo, L., Domingues, M. R., & Moreira, A. S. P. (2022). Mitochondrial Fatty Acid β-Oxidation Disorders: From Disease to Lipidomic Studies-A Critical Review. *International Journal of Molecular Sciences*, *23*(22). https://doi.org/10.3390/ijms232213933

Guinney, J., Dienstmann, R., Wang, X., De Reyniès, A., Schlicker, A., Soneson, C., Marisa, L., Roepman, P., Nyamundanda, G., Angelino, P., Bot, B. M., Morris, J. S., Simon, I. M., Gerster, S., Fessler, E., De Sousa .E Melo, F., Missiaglia, E., Ramay, H., Barras, D., … Tejpar, S. (2015). The consensus molecular subtypes of colorectal cancer. *Nature Medicine*, *21*(11), 1350–1356. https://doi.org/10.1038/nm.3967

Haas, A., Nilges, B. S., Leidel, S. A., & Klempnauer, K. H. (2020). PDCD4 controls the G1/S-phase transition in a telomerase-immortalized epithelial cell line and affects the expression level and translation of multiple mRNAs. *Scientific Reports*, *10*(1), 1–12. https://doi.org/10.1038/s41598-020-59678-w

Hanahan, D. (2022). *Hallmarks of Cancer : New Dimensions*. *January*, 31–46. https://doi.org/10.1158/2159-8290.CD-21-1059

Hanahan, D., & Weinberg, R. A. (2011). Hallmarks of cancer: The next generation. In *Cell* (Vol. 144, Issue 5, pp. 646–674). https://doi.org/10.1016/j.cell.2011.02.013

Hardie, D. G. (2015). Molecular pathways: Is AMPK a friend or a foe in cancer? *Clinical Cancer Research*, *21*(17), 3836–3840. https://doi.org/10.1158/1078-0432.CCR-14-3300

Herzig, S., & Shaw, R. J. (2018). AMPK: Guardian of metabolism and mitochondrial homeostasis. *Nature Reviews Molecular Cell Biology*, *19*(2), 121–135. https://doi.org/10.1038/nrm.2017.95

Hirata, H., Sugimachi, K., Komatsu, H., Ueda, M., Masuda, T., Uchi, R., Sakimura, S., Nambara, S., Saito, T., Shinden, Y., Iguchi, T., Eguchi, H., Ito, S., Terashima, K., Sakamoto, K., Hirakawa, M., Honda, H., & Mimori, K. (2016). Decreased Expression of Fructose-1,6-bisphosphatase Associates with Glucose Metabolism and Tumor Progression in Hepatocellular Carcinoma. *Cancer Research*, *76*(11), 3265–3276. https://doi.org/10.1158/0008-

5472.CAN-15-2601

Hsu, N. Y., Ho, H. C., Chow, K. C., Lin, T. Y., Shih, C. S., Wang, L. S., & Tsai, C. M. (2001). Overexpression of dihydrodiol dehydrogenase as a prognostic marker of non-small cell lung cancer. *Cancer Research*, *61*(6), 2727–2731.

Hue, L., & Taegtmeyer, H. (2009). The Randle cycle revisited: a new head for an old hat. *American Journal of Physiology. Endocrinology and Metabolism*, *297*(3), E578-91. https://doi.org/10.1152/ajpendo.00093.2009

Hwang, S.-K., Minai-Tehrani, A., Lim, H.-T., Shin, J.-Y., An, G.-H., Lee, K.-H., Park, K.-R., Kim, Y.-S., Beck, G. R. J., Yang, H.-S., & Cho, M.-H. (2010). Decreased level of PDCD4 (programmed cell death 4) protein activated cell proliferation in the lung of A/J mouse. *Journal of Aerosol Medicine and Pulmonary Drug Delivery*, *23*(5), 285–293. https://doi.org/10.1089/jamp.2009.0778

Iacobazzi, V., & Infantino, V. (2014). *Citrate – new functions for an old metabolite*. *395*(4), 387–399. https://doi.org/doi:10.1515/hsz-2013-0271

Icard, P., Coquerel, A., Wu, Z., Gligorov, J., Fuks, D., Fournel, L., Lincet, H., & Simula, L. (2021). Understanding the Central Role of Citrate in the Metabolism of Cancer Cells and Tumors: An Update. *International Journal of Molecular Sciences*, *22*(12). https://doi.org/10.3390/ijms22126587

Jez, J. M., Flynn, T. G., & Penning, T. M. (1997). A new nomenclature for the aldo-keto reductase superfamily. *Biochemical Pharmacology*, *54*(6), 639–647. https://doi.org/10.1016/s0006-2952(97)84253-0

Jiang, P., Du, W., & Wu, M. (2014). Regulation of the pentose phosphate pathway in cancer. *Protein and Cell*. https://doi.org/10.1007/s13238-014-0082-8

Jin, Jonghwa, Byun, J.-K., Choi, Y.-K., & Park, K.-G. (2023). Targeting glutamine metabolism as a therapeutic strategy for cancer. *Experimental & Molecular Medicine*, *55*(4), 706–715. https://doi.org/10.1038/s12276-023-00971-9

Jin, Junfei, Liao, W., Yao, W., Zhu, R., Li, Y., He, S., Ferlay, J., Altekruse, S. F., McGlynn, K. A., Reichman, M. E., Cao, D., Fan, S. T., Chung, S. S., Laffin, B., Petrash, J. M., Matkowskyj, K. A., Heringlake, S., Woenckhaus, M., Fukumoto, S., … Liao, W. (2016). Aldo-keto Reductase Family 1 Member B 10 Mediates Liver Cancer Cell Proliferation through Sphingosine-1-Phosphate. *Scientific Reports*, *6*(October 2015), 22746. https://doi.org/10.1038/srep22746

Kang, H., Kim, H., Lee, S., Youn, H., & Youn, B. (2019). Role of metabolic reprogramming in epithelial–mesenchymal transition (EMT). *International Journal of Molecular Sciences*, *20*(8). https://doi.org/10.3390/ijms20082042

Ke, R., Xu, Q., Li, C., Luo, L., & Huang, D. (2018). Mechanisms of AMPK in the maintenance of ATP balance during energy metabolism. *Cell Biology International*, *42*(4), 384–392. https://doi.org/10.1002/cbin.10915

Kiesel, V. A., Sheeley, M. P., Coleman, M. F., Cotul, E. K., Donkin, S. S., Hursting, S. D., Wendt, M. K., & Teegarden, D. (2021). Pyruvate carboxylase and cancer progression. *Cancer & Metabolism*, *9*(1), 20. https://doi.org/10.1186/s40170-021-00256-7

Kim, N. H., Cha, Y. H., Lee, J., Lee, S. H., Yang, J. H., Yun, J. S., Cho, E. S., Zhang, X., Nam, M., Kim, N., Yuk, Y. S., Cha, S. Y., Lee, Y., Ryu, J. K., Park, S., Cheong, J. H., Kang, S. W., Kim, S. Y., Hwang, G. S., … Kim, H. S. (2017). Snail reprograms glucose metabolism by repressing phosphofructokinase PFKP allowing cancer cell survival under metabolic stress. *Nature Communications*, *8*(May 2016). https://doi.org/10.1038/ncomms14374

Korge, P., Calmettes, G., & Weiss, J. N. (2015). Increased Reactive Oxygen Species Production During Reductive Stress: The Roles of Mitochondrial Glutathione and Thioredoxin Reductases. *Physiology & Behavior*, *1847*(0), 514–524. https://doi.org/10.1016/j.physbeh.2017.03.040

Koundouros, N., & Poulogiannis, G. (2020). Reprogramming of fatty acid metabolism in cancer. *British Journal of Cancer*, *122*(1), 4–22. https://doi.org/10.1038/s41416-019-0650-z

Kovac, S., Angelova, P. R., Holmström, K. M., Zhang, Y., Dinkova-Kostova, A. T., & Abramov, A. Y. (2015). Nrf2 regulates ROS production by mitochondria and NADPH oxidase. *Biochimica et Biophysica Acta (BBA) - General Subjects*, *1850*(4), 794–801. https://doi.org/10.1016/j.bbagen.2014.11.021

Kuipers, E. J., Grady, W. M., Lieberman, D., Seufferlein, T., Sung, J. J., Boelens, P. G., Van De Velde, C. J. H., & Watanabe, T. (2015). Colorectal cancer. *Nature Reviews Disease Primers*, *1*, 1–25. https://doi.org/10.1038/nrdp.2015.65

Lai, X., Li, Q., Wu, F., Lin, J., Chen, J., Zheng, H., & Guo, L. (2020). Epithelial-Mesenchymal Transition and Metabolic Switching in Cancer: Lessons From Somatic Cell Reprogramming. *Frontiers in Cell and Developmental Biology*, *8*. https://doi.org/10.3389/fcell.2020.00760

Laplante, M., & Sabatini, D. M. (2012). mTOR signaling in growth control and disease. *Cell*, *149*(2), 274–293. https://doi.org/10.1016/j.cell.2012.03.017

Lemonde, H. A., Custard, E. J., Bouquet, J., Duran, M., Overmars, H., Scambler, P. J., & Clayton, P. T. (2003). Mutations in SRD5B1 (AKR1D1), the gene encoding delta(4)-3-oxosteroid 5beta-reductase, in hepatitis and liver failure in infancy. *Gut*, *52*(10), 1494–1499. https://doi.org/10.1136/gut.52.10.1494

Liu, G. Y., & Sabatini, D. M. (2020). mTOR at the nexus of nutrition, growth, ageing and disease. In *Nature Reviews Molecular Cell Biology* (Vol. 21, Issue 4, pp. 183–203). Nature Research. https://doi.org/10.1038/s41580-019-0199-y

Liu, M.-X., Jin, L., Sun, S.-J., Liu, P., Feng, X., Cheng, Z.-L., Liu, W.-R., Guan, K.-L., Shi, Y.-H., Yuan, H.-X., & Xiong, Y. (2018). Metabolic reprogramming by PCK1 promotes TCA cataplerosis, oxidative stress and apoptosis in liver cancer cells and suppresses hepatocellular carcinoma. *Oncogene*, *37*(12), 1637–1653. https://doi.org/10.1038/s41388-017-0070-6

Ma, J., Yan, R., Zu, X., Cheng, J. M., Rao, K., Liao, D. F., & Cao, D. (2008). Aldo-keto reductase family 1 B10 affects fatty acid synthesis by regulating the stability of acetyl-CoA carboxylase-α in breast cancer cells. *Journal of Biological Chemistry*, *283*(6), 3418–3423. https://doi.org/10.1074/jbc.M707650200

Macleod, A. K., Acosta-Jimenez, L., Coates, P. J., McMahon, M., Carey, F. A., Honda, T., Henderson, C. J., & Roland Wolf, C. (2016). Aldo-keto reductases are biomarkers of NRF2 activity and are co-ordinately overexpressed in non-small cell lung cancer. *British Journal of Cancer*, *115*(12), 1530–1539. https://doi.org/10.1038/bjc.2016.363

Madiraju, A. K., Qiu, Y., Perry, R. J., Rahimi, Y., Zhang, X.-M., Zhang, D., Camporez, J.-P. G., Cline, G. W., Butrico, G. M., Kemp, B. E., Casals, G., Steinberg, G. R., Vatner, D. F., Petersen, K. F., & Shulman, G. I. (2018). Metformin inhibits gluconeogenesis via a redox-dependent mechanism in vivo. *Nature Medicine*, *24*(9), 1384–1394. https://doi.org/10.1038/s41591-018-0125-4

Manning, B. D. (2004). Balancing Akt with S6K: implications for both metabolic diseases and tumorigenesis. *The Journal of Cell Biology*, *167*(3), 399–403. https://doi.org/10.1083/jcb.200408161

Marchetti, P., Fovez, Q., Germain, N., Khamari, R., & Kluza, J. (2020). Mitochondrial spare respiratory capacity: Mechanisms, regulation, and significance in non-transformed and cancer cells. *FASEB Journal : Official Publication of the Federation of American Societies for Experimental Biology*, *34*(10), 13106–13124. https://doi.org/10.1096/fj.202000767R

Marisa, L., de Reyniès, A., Duval, A., Selves, J., Gaub, M. P., Vescovo, L., Etienne-Grimaldi, M. C., Schiappa, R., Guenot, D., Ayadi, M., Kirzin, S., Chazal, M., Fléjou, J. F., Benchimol, D., Berger, A., Lagarde, A., Pencreach, E., Piard, F., Elias, D., … Boige, V. (2013). Gene Expression Classification of Colon Cancer into Molecular Subtypes: Characterization, Validation, and Prognostic Value. *PLoS Medicine*, *10*(5). https://doi.org/10.1371/journal.pmed.1001453

Martínez-Reyes, I., & Chandel, N. S. (2020). Mitochondrial TCA cycle metabolites control physiology and disease. *Nature Communications*, *11*(1), 102. https://doi.org/10.1038/s41467-019-13668-3

Matsunaga, T., Wada, Y., Endo, S., Soda, M., El-Kabbani, O., & Hara, A. (2012). Aldo-keto reductase 1B10 and its role in proliferation capacity of drug-resistant cancers. *Frontiers in Pharmacology*, *3*(5). https://doi.org/10.3389/fphar.2012.00005

Matsunaga, T., Yamane, Y., Iida, K., Endo, S., Banno, Y., El-Kabbani, O., & Hara, A. (2011). Involvement of the aldo-keto reductase, AKR1B10, in mitomycin-c resistance through reactive oxygen species-dependent mechanisms. *Anti-Cancer Drugs*, *22*(5), 402–408. https://doi.org/10.1097/CAD.0b013e3283448df0

Mindnich, R. D., & Penning, T. M. (2009). Aldo-keto reductase (AKR) superfamily: genomics and annotation. *Hum.Genomics*, *3*(4), 362–370. https://doi.org/10.1186/1479-7364-3-4-362

Mori, M., Genda, T., Ichida, T., Murata, A., Kamei, M., Tsuzura, H., Sato, S., Narita, Y., Kanemitsu, Y., Ishikawa, S., Kikuchi, T., Shimada, Y., Hirano, K., Iijima, K., Sugimoto, K., Wada, R., Nagahara, A., & Watanabe, S. (2017). Aldo-keto reductase family 1 member B10 is associated with hepatitis B virus-related hepatocellular carcinoma risk. *Hepatology Research : The Official Journal of the Japan Society of Hepatology*, *47*(3), E85–E93. https://doi.org/10.1111/hepr.12725

Murata, A., Genda, T., Ichida, T., Amano, N., Sato, S., Tsuzura, H., Sato, S., Narita, Y., Kanemitsu, Y., Shimada, Y., Hirano, K., Iijima, K., Wada, R., Nagahara, A., & Watanabe, S. (2016). Pretreatment AKR1B10 expression predicts the risk of hepatocellular carcinoma development after hepatitis C virus eradication. *World Journal of Gastroenterology*, *22*(33), 7569–7578. https://doi.org/10.3748/wjg.v22.i33.7569

Nannini, G., Meoni, G., Amedei, A., & Tenori, L. (2020). Metabolomics profile in gastrointestinal cancers: Update and future perspectives. *World Journal of Gastroenterology*, *26*(20), 2514–2532. https://doi.org/10.3748/wjg.v26.i20.2514

Nelson, D. L., & Cox, M. M. (2017). Lehninger principles of biochemistry (7th ed.). W.H. Freeman.

Nieto, M. A., Huang, R. Y.-J., Jackson, R. A., & Thiery, J. P. (2016). EMT: 2016. *Cell*, *166*(1), 21–45. https://doi.org/10.1016/j.cell.2016.06.028

Nyamundanda, G., Brennan, L., & Gormley, I. C. (2010). Probabilistic principal component analysis for metabolomic data. *BMC Bioinformatics*, *11*(1), 571. https://doi.org/10.1186/1471-2105-11-571

Özen, G. (2019). *Metabolomik ve fluksomik çalişmalar ile kolon kanserinde kemoterapötiklere karşi direncin in vitro değerlendirilmesi*.

Pal, S., Sharma, A., Mathew, S. P., & Jaganathan, B. G. (2022). Targeting cancer-specific metabolic pathways for developing novel cancer therapeutics. *Frontiers in Immunology*, *13*, 955476. https://doi.org/10.3389/fimmu.2022.955476

Patra, K. C., & Hay, N. (2014). The pentose phosphate pathway and cancer. In *Trends in Biochemical Sciences* (Vol. 39, Issue 8, pp. 347–354). https://doi.org/10.1016/j.tibs.2014.06.005

Pavlova, N. N., & Thompson, C. B. (2016). The Emerging Hallmarks of Cancer Metabolism. *Cell Metabolism*, *23*(1), 27–47. https://doi.org/10.1016/j.cmet.2015.12.006

Pavlova, N. N., Zhu, J., & Thompson, C. B. (2022). The hallmarks of cancer metabolism: Still emerging. *Cell Metabolism*, *34*(3), 355–377. https://doi.org/https://doi.org/10.1016/j.cmet.2022.01.007

Penning, T. M. (2005). AKR1B10: A new diagnostic marker of non-small cell lung carcinoma in smokers. *Clinical Cancer Research*, *11*(5), 1687–1690. https://doi.org/10.1158/1078-0432.CCR-05-0071

Penning, T. M. (2015). The aldo-keto reductases (AKRs): Overview. *Chemico-Biological Interactions*. https://doi.org/10.1016/j.cbi.2014.09.024

Penning, T. M. (2017). Aldo-keto reductase regulation by the Nrf2 system: Implications for stress response, chemotherapy drug resistance, and carcinogenesis. In *Chemical Research in Toxicology* (Vol. 30, Issue 1, pp. 162–176). American Chemical Society. https://doi.org/10.1021/acs.chemrestox.6b00319

Penning, T. M., & Drury, J. E. (2007). *Human ALdo-Keto Reductases: Function,*

Gene Regulation, and Single Nucleotide Polymorphisms. *464*(2), 241–250.

Pfaffl, M. W. (2001). A new mathematical model for relative quantification in real-time RT-PCR. *Nucleic Acids Research*. https://doi.org/10.1093/nar/29.9.e45

Pope, E. D., Kimbrough, E. O., Vemireddy, L. P., Surapaneni, P. K., Copland, J. A., & Mody, K. (2019). Aberrant lipid metabolism as a therapeutic target in liver cancer. *Expert Opinion on Therapeutic Targets*, *23*(6), 473–483. https://doi.org/10.1080/14728222.2019.1615883

Ramana, K. V. (2011). Aldose reductase: New insights for an old enzyme. In *Biomolecular Concepts* (Vol. 2, Issues 1–2, pp. 103–114). https://doi.org/10.1515/bmc.2011.002

Ramana, K. V., Tammali, R., & Srivastava, S. K. (2010). Inhibition of Aldose Reductase Prevents Growth Factor–Induced G1-S Phase Transition through the AKT/Phosphoinositide 3-Kinase/E2F-1 Pathway in Human Colon Cancer Cells. *Molecular Cancer Therapeutics*, *9*(4).

Röhrig, F., & Schulze, A. (2016). The multifaceted roles of fatty acid synthesis in cancer. *Nature Reviews Cancer*, *16*(11), 732–749. https://doi.org/10.1038/nrc.2016.89

Rothman, D. L., Magnusson, I., Katz, L. D., Shulman, R. G., & Shulman, G. I. (1991). Quantitation of hepatic glycogenolysis and gluconeogenesis in fasting humans with 13C NMR. *Science (New York, N.Y.)*, *254*(5031), 573–576. https://doi.org/10.1126/science.1948033

Ruiz-Perez, D., Guan, H., Madhivanan, P., Mathee, K., & Narasimhan, G. (2020). So you think you can PLS-DA? *BMC Bioinformatics*, *21*(1), 2. https://doi.org/10.1186/s12859-019-3310-7

Sato, S., Genda, T., Hirano, K., Tsuzura, H., Narita, Y., Kanemitsu, Y., Kikuchi, T., Iijima, K., Wada, R., & Ichida, T. (2012). Up-regulated aldo-keto reductase family 1 member B10 in chronic hepatitis C: association with serum alpha-fetoprotein and hepatocellular carcinoma. *Liver International : Official Journal of the International Association for the Study of the Liver*, *32*(9), 1382–1390. https://doi.org/10.1111/j.1478-3231.2012.02827.x

Saxena, A., Shoeb, M., Ramana, K. V., & Srivastava, S. K. (2013). Aldose reductase inhibition suppresses colon cancer cell viability by modulating microRNA-21 mediated programmed cell death 4 (PDCD4) expression. *European Journal of Cancer*, *49*(15), 3311–3319. https://doi.org/10.1016/j.ejca.2013.05.031

Schwab, A., Siddiqui, A., Vazakidou, M. E., Napoli, F., Bottcher, M., Menchicchi, B., Raza, U., Saatci, O., Krebs, A. M., Ferrazzi, F., Rapa, I., Dettmer-Wilde, K., Waldner, M. J., Ekici, A. B., Rasheed, S. A. K., Mougiakakos, D., Oefner, P. J., Sahin, O., Volante, M., … Ceppi, P. (2018). Polyol pathway links glucose metabolism to the aggressiveness of cancer cells. *Cancer Research*, *78*(7), 1604–1618. https://doi.org/10.1158/0008-5472.CAN-17-2834

Shah, A. M., & Wondisford, F. E. (2020). Tracking the carbons supplying gluconeogenesis. *The Journal of Biological Chemistry*, *295*(42), 14419–14429. https://doi.org/10.1074/jbc.REV120.012758

Shen, Y., Ma, J., Yan, R., Ling, H., Li, X., Yang, W., Gao, J., Huang, C., Bu, Y., Cao, Y., He, Y., Wan, L., Zu, X., Liu, J., Huang, M. C., Stenson, W. F., Liao, D.-F., & Cao, D. (2015). Impaired self-renewal and increased colitis and dysplastic lesions in colonic mucosa of AKR1B8-deficient mice. *Clinical Cancer Research : An Official Journal of the American Association for Cancer Research*, *21*(6), 1466–1476. https://doi.org/10.1158/1078-0432.CCR-14-2072

Sheraj, I. (2021). *Analysis of Transcriptome Data for the Evaluation of Metabolic Deregulation in Cancer*.

Sheraj, I., Guray, N. T., & Banerjee, S. (2021). A pan-cancer transcriptomic study showing tumor specific alterations in central metabolism. *Scientific Reports*, *11*(1), 1–19. https://doi.org/10.1038/s41598-021-93003-3

Shi, J., Chen, L., Chen, Y., Lu, Y., Chen, X., & Yang, Z. (2019). Aldo-Keto reductase family 1 member B10 (AKR1B10) overexpression in tumors predicts worse overall survival in hepatocellular carcinoma. *Journal of Cancer*, *10*(20), 4892–4901. https://doi.org/10.7150/jca.32768

Sia, D., Villanueva, A., Friedman, S. L., & Llovet, J. M. (2017). Liver Cancer Cell of Origin, Molecular Class, and Effects on Patient Prognosis. *Gastroenterology*, *152*(4), 745–761. https://doi.org/10.1053/j.gastro.2016.11.048

Soliman, G. A. (2011). The integral role of mTOR in lipid metabolism. In *Cell cycle (Georgetown, Tex.)* (Vol. 10, Issue 6, pp. 861–862). https://doi.org/10.4161/cc.10.6.14930

Song, Z., Yang, Y., Wu, Y., Zheng, M., Sun, D., Li, H., & Chen, L. (2022). Glutamic oxaloacetic transaminase 1 as a potential target in human cancer. *European Journal of Pharmacology*, *917*, 174754. https://doi.org/https://doi.org/10.1016/j.ejphar.2022.174754

Srivastava, S. K., Yadav, U. C. S., Reddy, A. B. M., Saxena, A., Tammali, R., Shoeb, M., Ansari, N. H., Bhatnagar, A., Petrash, M. J., Srivastava, S., & Ramana, K. V. (2011). Aldose reductase inhibition suppresses oxidative stress-induced inflammatory disorders. *Chemico-Biological Interactions*, *191*(1–3), 330–338. https://doi.org/10.1016/j.cbi.2011.02.023

Steinberg, G. R., & Carling, D. (2019). AMP-activated protein kinase: the current landscape for drug development. *Nature Reviews. Drug Discovery*, *18*(7), 527–551. https://doi.org/10.1038/s41573-019-0019-2

Sung, H., Ferlay, J., Siegel, R. L., Laversanne, M., Soerjomataram, I., Jemal, A., & Bray, F. (2021). Global Cancer Statistics 2020: GLOBOCAN Estimates of Incidence and Mortality Worldwide for 36 Cancers in 185 Countries. *CA: A Cancer Journal for Clinicians*, *71*(3), 209–249. https://doi.org/10.3322/caac.21660

Tammali, R., Srivastava, S. K., & Ramana, K. V. (2011). Targeting aldose reductase for the treatment of cancer. *Current Cancer Drug Targets*, *11*(5), 560–571.

Taskoparan, B., Seza, E. G., Demirkol, S., Tuncer, S., Stefek, M., Gure, A. O., & Banerjee, S. (2017). Opposing roles of the aldo-keto reductases AKR1B1 and AKR1B10 in colorectal cancer. *Cellular Oncology*, *40*(6), 563–578. https://doi.org/10.1007/s13402-017-0351-7

Thanki, K., Nicholls, M. E., Gajjar, A., Senagore, A. J., Qiu, S., Szabo, C., Hellmich, M. R., & Chao, C. (2017). Consensus Molecular Subtypes of Colorectal Cancer and their Clinical Implications. *International Biological and Biomedical Journal*, *3*(3), 105–111.

Tian, H., Zhu, X., Lv, Y., Jiao, Y., & Wang, G. (2020). Glucometabolic Reprogramming in the Hepatocellular Carcinoma Microenvironment: Cause and Effect. *Cancer Management and Research*, *12*, 5957–5974. https://doi.org/10.2147/CMAR.S258196

Tuğral, H. (2022). *The Role of AKR1B10 in Oxidative Stress Response in Hepatocellular Carcinoma*.

Tunçer, S., Keşküş, A. G., Çolakoğlu, M., Çimen, I., Yener, C., Konu, Ö., & Banerjee, S. (2017). 15-Lipoxygenase-1 re-expression in colorectal cancer alters endothelial cell features through enhanced expression of TSP-1 and ICAM-1. *Cellular Signalling*, *39*. https://doi.org/10.1016/j.cellsig.2017.07.022

Ulusan, S., Sheraj, I., Stehling, S., Ivanov, I., Das, A., Kühn, H., & Banerjee, S. (2022). Structural and functional evaluation mammalian and plant lipoxygenases upon association with nanodics as membrane mimetics. *Biophysical Chemistry*, *288*, 106855. https://doi.org/https://doi.org/10.1016/j.bpc.2022.106855

van Weverwijk, A., Koundouros, N., Iravani, M., Ashenden, M., Gao, Q., Poulogiannis, G., Jungwirth, U., & Isacke, C. M. (2019). Metabolic adaptability in metastatic breast cancer by AKR1B10-dependent balancing of glycolysis and fatty acid oxidation. *Nature Communications*, *10*(1), 1–13. https://doi.org/10.1038/s41467-019-10592-4

Wang, C., Yan, R., Luo, D., Watabe, K., Liao, D. F., & Cao, D. (2009). Aldo-keto reductase family 1 member B10 promotes cell survival by regulating lipid synthesis and eliminating carbonyls. *Journal of Biological Chemistry*, *284*(39), 26742–26748. https://doi.org/10.1074/jbc.M109.022897

Wang, J., Zhou, Y., Fei, X., Chen, X., & Chen, Y. (2018). Biostatistics mining associated method identifies AKR1B10 enhancing hepatocellular carcinoma cell growth and degenerated by miR-383-5p. *Scientific Reports*, *8*(1). https://doi.org/10.1038/s41598-018-29271-3

Wang, Y., Yu, W., Li, S., Guo, D., He, J., & Wang, Y. (2022). Acetyl-CoA Carboxylases and Diseases. *Frontiers in Oncology*, *12*(March), 1–10. https://doi.org/10.3389/fonc.2022.836058

Wang, Z., Pei, Y., Li, W., Zhang, J., & Liu, J. (2022). Clinical value of AKR1B10 in hepatocellular carcinoma: A systematic review and meta-analysis. *PloS One*, *17*(12), e0279591. https://doi.org/10.1371/journal.pone.0279591

Warburg, O., Wind, F., & Negelein, E. (1927). THE METABOLISM OF TUMORS IN THE BODY. *The Journal of General Physiology*, *8*(6), 519–530. https://doi.org/10.1085/jgp.8.6.519

Westerhuis, J. A., Hoefsloot, H. C. J., Smit, S., Vis, D. J., Smilde, A. K., van Velzen, E. J. J., van Duijnhoven, J. P. M., & van Dorsten, F. A. (2008). Assessment of PLSDA cross validation. *Metabolomics*, *4*(1), 81–89. https://doi.org/10.1007/s11306-007-0099-6

Williams, N. C., & O'Neill, L. A. J. (2018). A Role for the Krebs Cycle Intermediate Citrate in Metabolic Reprogramming in Innate Immunity and Inflammation. *Frontiers in Immunology*, *9*, 141. https://doi.org/10.3389/fimmu.2018.00141

Xiao, W., Wang, R. S., Handy, D. E., & Loscalzo, J. (2018). NAD(H) and NADP(H) Redox Couples and Cellular Energy Metabolism. In *Antioxidants and Redox Signaling*. https://doi.org/10.1089/ars.2017.7216

Yan, R., Zu, X., Ma, J., Liu, Z., Adeyanju, M., & Cao, D. (2007). Aldo-keto reductase family 1 B10 gene silencing results in growth inhibition of colorectal cancer cells: Implication for cancer intervention. *International Journal of Cancer*, *121*(10), 2301–2306. https://doi.org/10.1002/ijc.22933

Ye, M., Li, X., Chen, L., Mo, S., Liu, J., Huang, T., Luo, F., & Zhang, J. (2023). A High-Throughput Sequencing Data-Based Classifier Reveals the Metabolic Heterogeneity of Hepatocellular Carcinoma. *Cancers*, *15*(3). https://doi.org/10.3390/cancers15030592

Yilmaz, N., Yilmaz, U. E., Suer, K., Goral, V., & Cakir, N. (2018). Screening for hepatocellular carcinoma: summary of current guidelines up to 2018. *Screening for Hepatocellular Carcinoma: Summary of Current Guidelines up to 2018*, *4*, 46. https://doi.org/10.20517/2394-5079.2018.49

Yoon, M.-S. (2017). mTOR as a Key Regulator in Maintaining Skeletal Muscle Mass. *Frontiers in Physiology*, *8*, 788. https://doi.org/10.3389/fphys.2017.00788

Young, L., Sung, J., & Masters, J. R. (2010). Detection of mycoplasma in cell cultures. *Nature Protocols*. https://doi.org/10.1038/nprot.2010.43

Zarrinpar, A. (2017). Metabolic Pathway Inhibition in Liver Cancer. *SLAS Technology*, *22*(3), 237–244. https://doi.org/10.1177/2472630317698683

Zhang, L., Lee, J. J., Tang, H., Fan, Y.-H., Xiao, L., Ren, H., Kurie, J., Morice, R. C., Hong, W. K., & Mao, L. (2008). Impact of smoking cessation on global gene expression in the bronchial epithelium of chronic smokers. *Cancer Prevention Research (Philadelphia, Pa.)*, *1*(2), 112–118. https://doi.org/10.1158/1940-6207.CAPR-07-0017

Zhang, Z., TeSlaa, T., Xu, X., Zeng, X., Yang, L., Xing, G., Tesz, G. J., Clasquin, M. F., & Rabinowitz, J. D. (2021). Serine catabolism generates liver NADPH and supports hepatic lipogenesis. *Nature Metabolism*, *3*(12), 1608–1620. https://doi.org/10.1038/s42255-021-00487-4

Zhou, L., Liu, J., & Luo, F. (2006). Serum tumor markers for detection of hepatocellular carcinoma. *World Journal of Gastroenterology*, *12*(8), 1175–1181. https://doi.org/10.3748/wjg.v12.i8.1175

Zhu, R., Xiao, J., Luo, D., Dong, M., Sun, T., & Jin, J. (2019). Serum AKR1B10 predicts the risk of hepatocellular carcinoma - A retrospective single-center study. *Gastroenterologia y Hepatologia*, *42*(10), 614–621. https://doi.org/10.1016/j.gastrohep.2019.06.007

APPENDICES

A. Maps of the Vectors Used in the Study

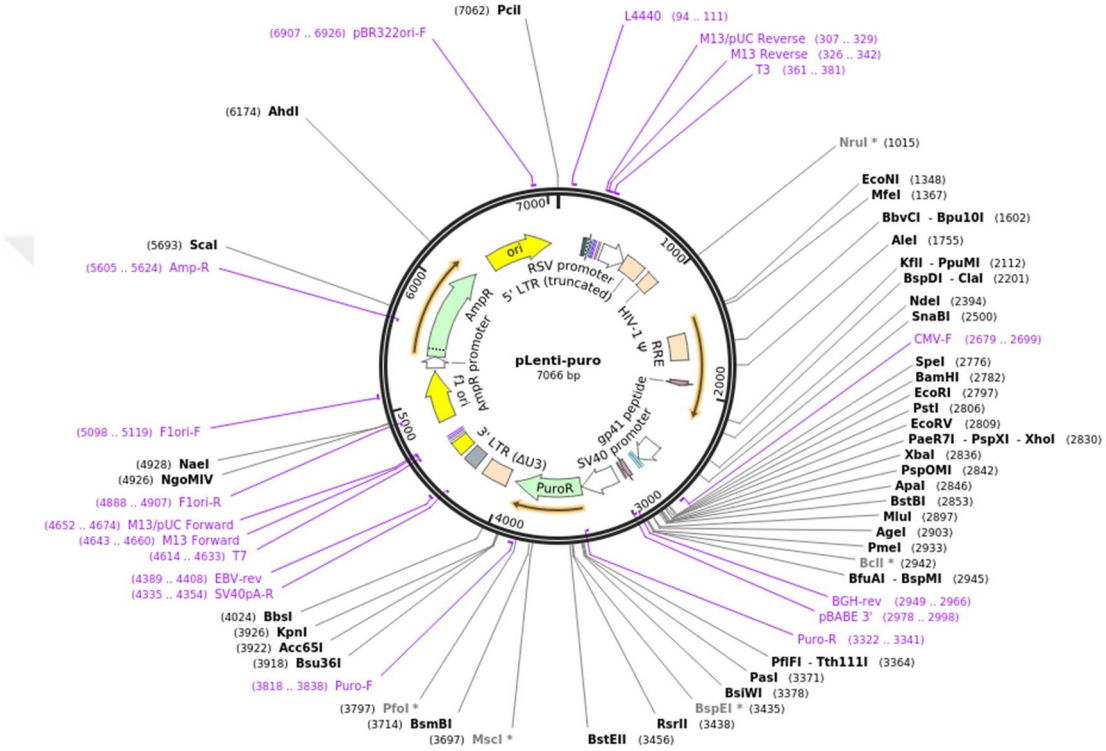

Figure A1. The empty backbone map of tetracycline inducible third generation lentiviral vector pLenti-puro (Addgene #39481). cDNA of AKR1B1 and AKR1B10 were cloned into the pLenti-puro vector.

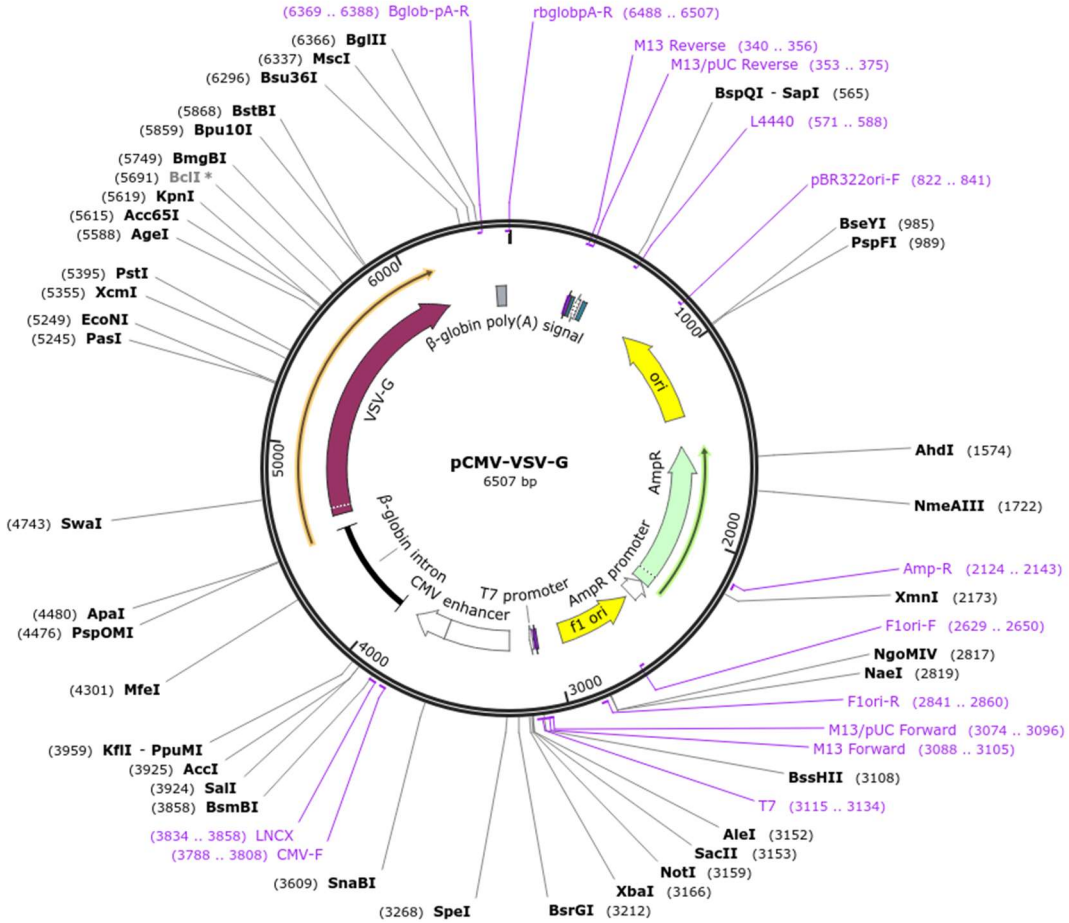

Figure A2. The empty backbone of pCMV-VSV-G (Addgene #8454) for envelope protein of the lentiviruses.

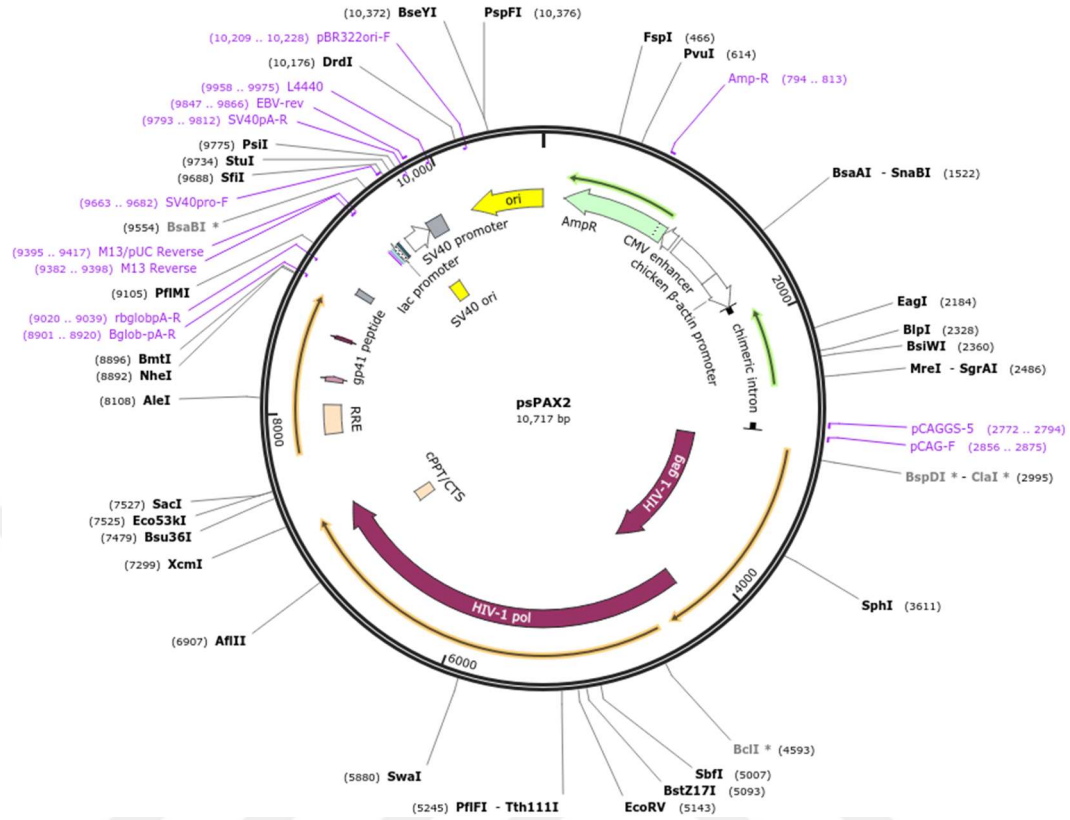

Figure A3. The empty backbone of psPAX2 (Addgene #12260) for the packaging of the lentiviruses.

B. Metabolomics Protein Measurement

Table 4. Absorbance values of the proteins used in the metabolomics.

Absorbances	Empty Vector (EV)	AKR1B10 expressing cells	EV Etomoxir treatment	AKR1B10 Etomoxir treatment
Replicate 1	0.558	0.509	0.544	0.483
Replicate 2	0.527	0.520	0.528	0.483
Replicate 3	0.562	0.502	0.545	0.494
Replicate 4	0.541	0.492	0.523	0.480
Replicate 5	0.521	0.491	0.554	0.532

The two replicates of each sample are shown in average in the Table.

CURRICULUM VITAE

Surname, Name: Seza, Esin Gülce

EDUCATION

Degree	Institution	Year of Graduation
MSc	METU Molecular Biology and Genetics	2017
BS	METU Biology	2015
High School	Atatürk Anadolu High School, Bolu	2010

FOREIGN LANGUAGES

Advanced English, Native Turkish

PUBLICATIONS

1. Demirkol Canlı S, Seza EG, Sheraj I, Gömçeli I, Turhan N, Carberry S, Prehn JHM, Güre AO, Banerjee S. "Evaluation of an aldo-keto reductase gene signature with prognostic significance in colon cancer via activation of epithelial to mesenchymal transition and the p70S6K pathway", Carcinogenesis, 41(9):1219-1228 (2020)
2. Seza EG, Guderer I, Ermis C, Banerjee S. "PRKAA1 (protein kinase AMP-activated catalytic subunit alpha 1)", Atlas Genet Cytogenet Oncol Haematol., (2018)
3. Taskoparan B, Seza EG, Demirkol S, Tuncer S, Stefek M, Gure AO, Banerjee S. "Opposing roles of the aldo-keto reductases AKR1B1 and AKR1B10 in colorectal cancer", Cell Oncol (Dordr), 40(6):563-578 (2017)